GKSS
FORSCHUNGSZENTRUM
in der HELMHOLTZ-GEMEINSCHAFT

Outstanding past decadal-scale climate events in the Greater Alpine Region analysed by 250 years data and model runs

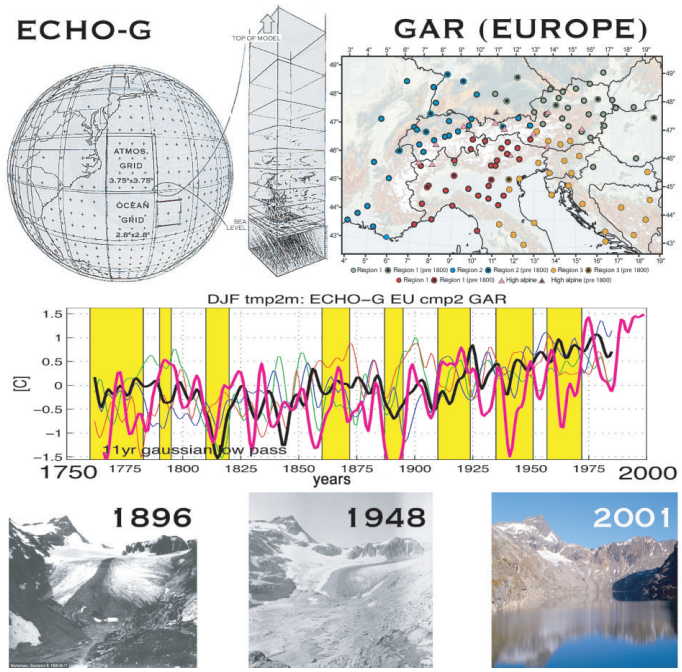

Authors:

C. Matulla
I. Auer
R. Böhm
M. Ungersböck
W. Schöner
S. Wagner
E. Zorita

ISSN 0344-9629

GKSS ist Mitglied der Hermann von Helmholtz-Gemeinschaft Deutscher Forschungszentren e.V.

GKSS 2005/4

GKSS 2005/4

Outstanding past decadal-scale climate events in the Greater Alpine Region analysed by 250 years data and model runs

Authors:

C. Matulla
I. Auer
R. Böhm
M. Ungersböck
W. Schöner

(Central Institute for Meteorology and Geodynamics, Vienna, Austria)

S. Wagner
E. Zorita

(Institute for Coastal Research, GKSS Research Centre, Geesthacht, Germany)

GKSS-Forschungszentrum Geesthacht GmbH • Geesthacht • 2005

Title figures:
the left sub-panel in the first row was taken from the Internet
(http://www.bom.gov.au/announcements/media_releases/ho/20030320e.jpg)
and modified to meet our needs.
Photos (third line) are from 'Photoarchiv Sonnblickverein' and other panels
are part of the present study.

Die Berichte der GKSS werden kostenlos abgegeben.
The delivery of the GKSS reports is free of charge.

Anforderungen/Requests:

GKSS-Forschungszentrum Geesthacht GmbH
Bibliothek/Library
Postfach 11 60
D-21494 Geesthacht
Germany
Fax.: (49) 04152/871717

Als Manuskript vervielfältigt.

ISSN 0344-9629

GKSS-Forschungszentrum Geesthacht GmbH · Telefon (04152)87-0
Max-Planck-Straße 1 · D-21502 Geesthacht / Postfach 11 60 · D-21494 Geesthacht

GKSS 2005/4

Outstanding past decadal-scale climate events in the Greater Alpine Region analysed by 250 years data and model runs

Christoph Matulla, Ingeborg Auer, Reinhard Böhm, Markus Ungersböck, Wolfgang Schöner, Sebastian Wagner and Eduardo Zorita

114 pages with 54 figures and 13 tables

Abstract

Detrended climatic time series are in general not white but show on a multi-annual to decadal timescale significant anomalies, hereafter called 'outstanding periods' (O.P.). Such O.P.s are the central subject/core of the study. Basis of the investigation are two datasets that cover the past 250 years and their consistencies at regional and multi-annual to decadal scales respectively. The first data set is representative at sub-European to European scale and consists of homogenized time series of several climate elements. This study contributes to its generation. The second dataset covers the whole globe at a rather coarse resolution and results from differently forced climate models imulations.

There is a set of goals achieved by this study. First, to comprehensively describe climate and its variability during the past 250 years with in the Greater Alpine Region. Second, the detection of 'outstanding temperature periods' from 1760 onward. Third, the investigation of the linkage/interplay between large scale circulation and regional scale temperature and thereby fourth, making a contribution to the understanding of the interrelation between external forcings and regional scale climate.

The first goal is achieved by creating a homogenized dataset (hereafter called HISTALP) of instrumental monthly series of air temperature, precipitation, air pressure, sunshine duration and cloudiness, that are of sufficient length. These series cover 'the Greater Alpine Region' (hereafter' GAR'), which extends from 43N4Eto49N19E and some of them start as early as1760. The HISTALP series have been quality improved in terms of detection and elimination of non climatic inhomogeneities and outliers.

Based on temperature 'outstanding periods', which are multi-annual to decadal sequences of years that exhibit large fractions of stations showing significantly higher or lower values than the detrended long-term course, are detected. The reality of these outstanding periods is shown to be supported by the temporal advancing and retreating of Alpine glacier records. Precipitation records are used to confirm the detection of outstanding periods and series of sunshine-duration and cloud cover help to formulate a hypothesis explaining some model-data mismatches.

During outstanding periods we investigate the synoptic scale behaviour as simulated by the atmosphere-ocean general circulation model ECHO-G. Atmospheric circulation is analysed by an objective decomposition of ECHO-G's SLP, which is done by rotated empirical orthogonal functions. This step helps to achieve the third goal.

The fourth goal is aimed for by the analysis of several ECHO-G model runs driven by dif-ferent external forcings. Although findings should not be overrated this approach seems to be appropriate for answering questions related to the regional scale impacts of different external forcings. Such comparisons between homogenized historical series and model simulations have the potential to enhance our knowledge about the interaction of the scales and the possible physical-dynamical background. For winter plus the whole year results, achieved by the comparison of large scale simulation and regional scale reaction, are some what promising. Results achieved for summer are more difficult to interpret mainly because of summer circulation and a reduced sample size of outstanding periods compared to winter and the whole year.

Untersuchung herausragender, dekadischer Klimaperioden in der Greater Alpine Region anhand von 250 Jahren historischer Daten und Klimamodellläufen

Zusammenfassung

Trendbereinigte Klimazeitreihen sind i.a. statistisch nicht weiß, sondern zeigen auf einer mehrjährigen bis dekadischen Zeitskala Anomalien, die Gegenstand dieser Studie sind und in der Folge 'outstanding periods' (O.P.) genannt werden. Herzstück dieser Studie sind zwei Datensätze, die sich über die letzten 250 Jahre erstrecken. Der erste ist repräsentativ für einen bedeutenden räumlichen Sektor Europas und umfasst eine Reihe von klimatischen Größen. Die Studie hat maßgeblich zur Erstellung dieses Datensatzes beigetragen. Der zweite Datensatz ist global und besteht aus verschieden angetriebenen Läufen des Klimamodels ECHO-G.

Diese Studie strebt eine Reihe von Zielen an: zuerst die Untersuchung des Klimas und seiner Variabilität während der letzten 250 Jahre in der Greater Alpine Region (GAR), zweitens, die Isolierung von Perioden mit herausragendem Temperaturverhalten. Dann wird das Zusammenspiel zwischen großräumiger Zirkulation und regionaler Temperaturentwicklung untersucht. Damit kann ein Beitrag zum Verständnis von externem Antrieb und regionaler Temperaturreaktion geleistet werden.

Das erstgenannte Ziel wird durch die neue HISTALP-Datenbank erreicht. HISTALP enthält monatliche Zeitreihen von Lufttemperatur, Niederschlag, Luftdruck, Sonnenscheindauer und Bewölkung, deren Qualität durch Homogenisierung und Outlier-Korrektur maximal möglich erhöht worden ist. Die Daten beginnen zum Teil 1760 und decken die Greater Alpine Region, die sich von 43N4E bis 49N19E erstreckt, ab.

Basierend auf den Temperaturdaten werden 'outstanding periods' detektiert. Das sind Zeitabschnitte, die sich über mehrere Jahre bis Jahrzehnte erstrecken und einen hohen Anteil an Stationen aufweisen, die signifikante Temperaturanomalien der trendbereinigten Daten haben. Diese O.P.s können auch in Aufzeichnungen über Gletscherschwankungen gefunden werden. Dabei wird auch der Niederschlags-Datensatz in Betracht gezogen. Die Reihen der Bewölkung werden für die Formulierung einer Hypothese herangezogen, die das Auseinanderklaffen von Simulationen und Beobachtungen in den drei letzten herausragenden Sommer-Perioden erklären kann.

Während der herausragenden Perioden wird die synoptikskalige Zirkulation, wie sie vom Klimamodell ECHO-G simuliert wird, untersucht. Das geschieht mit Hilfe von rotierten Orthogonalfunktionen. Mit diesem Schritt wird das dritte Ziel erreicht.

Das vierte Ziel wird zu erreichen versucht, indem verschieden angetriebene ECHO-G-Modellläufe hinsichtlich ihrer Zirkulation in den herausragenden Perioden untersucht und ausgewählt werden. Obwohl die Ergebnisse nicht überansprucht werden sollten, scheint dieser Zugang geeignet, Fragen bezüglich der regionalen Auswirkung verschiedener externer Antriebe zu beantworten. Derartige Vergleiche von homogenisierten Stationsreihen und Modellsimulationen haben das Potenzial, das Verständnis über die Interaktion zwischen den Skalen und den physikalisch-dynamischen Prozessen zu vertiefen. Die Ergebnisse für den Winter und das Gesamtjahr sind ermutigend, während die Resultate für den Sommer sehr unsicher sind und keine einfache Interpretation zulassen. Dieser Umstand kann mit der komplexeren Zirkulation und dem gegenüber dem Winter und Jahr verringerten Stichprobenumfang an 'outstanding periods' begründet werden.

Manuscript received / Manuskripteingang in TDB: 29. April 2005

Contents

List of Figures

List of Tables

Chapter 1

Introduction

The aim of this chapter is to briefly review some basics features of circulation and climate in 'the North Atlantic–EUropean' sector (hereafter NAEU) and 'the Greater Alpine Region' (hereafter GAR), respectively. NAEU represents the large scale for which the climate model, used in this study, provides simulations from 1756 to 1990. GAR stands for the regional scale where the HISTALP database provides homogenised historical time series for 1760–2003.

1.1 Large scale circulation

The panels in Figure 1.1 show Sea Level Pressure (SLP) above NAEU as simulated by ECHO-G averaged over 1756–1990. ECHO-G (Legutke and Voss 1999; see Chapter 3) is the acronymn for the Atmospheric-Ocean General Circulation Model (AOGCM) used in this study . Figure 1.1 is intended to give a very cursory impression about circulation conditions above NAEU, which is quite enough to meet the goal of this chapter. A somewhat closer look in terms of comparing ECHO-G and ERA40 SLP fields is taken in Chapter 6. ERA40 (Uppala 2003) is a reanalysis dataset, calculated at the European Center for Medium range Weather Forecasts (ECMWF), that starts in 1958.

The ECHO-G SLP pattern of January (first line, left column) expectedly indicates a pronounced zonal circulation with a southern component. Minimum pressure can be found south of Iceland, taking on values somewhat below 1000 hPa. Maximum pressure is located above the Iberian Peninsula and shows values of about 1025 hPa. This pressure-dipole is closely related to the North Atlantic Oszillation (NAO). The main orientation of the isobars is from South-West towards North-East, gradually taking on lower pressure values with increasing latitude. The 1020-Isobar shows a characteristic deflection to the south above the Balkans. This feature can be found in the ERA40 dataset too (cf. Matulla and Wagner 2004) and may be related to orography like the Alps and the Carpathians. If the January pattern is replaced by the winter (December to February) pattern this feature remains in case of ECHO-G but is weakened in the ERA40 dataset (see Chapter 6, Figure 6.1). The 1024- and 1012-Isobar, exhibit related runs, which could point to orography again – the Appennines and the mountain ranges along the Adriatic coast of the Balkans or Scandinavia. However, the latter two curvatures are not to be found in the ERA40 dataset (see Figure 6.1). Altogether, the circulatory situation reflects westerlies with a southern component and if the above mentioned NAO is in its positive phase it is more likely to obtain dry conditions in GAR than when NAO is in its negative mode, which is more related to wet GAR conditions (Hurrell 1995).

April shows a relative flat pressure distribution over most parts of NAEU. Highest values are

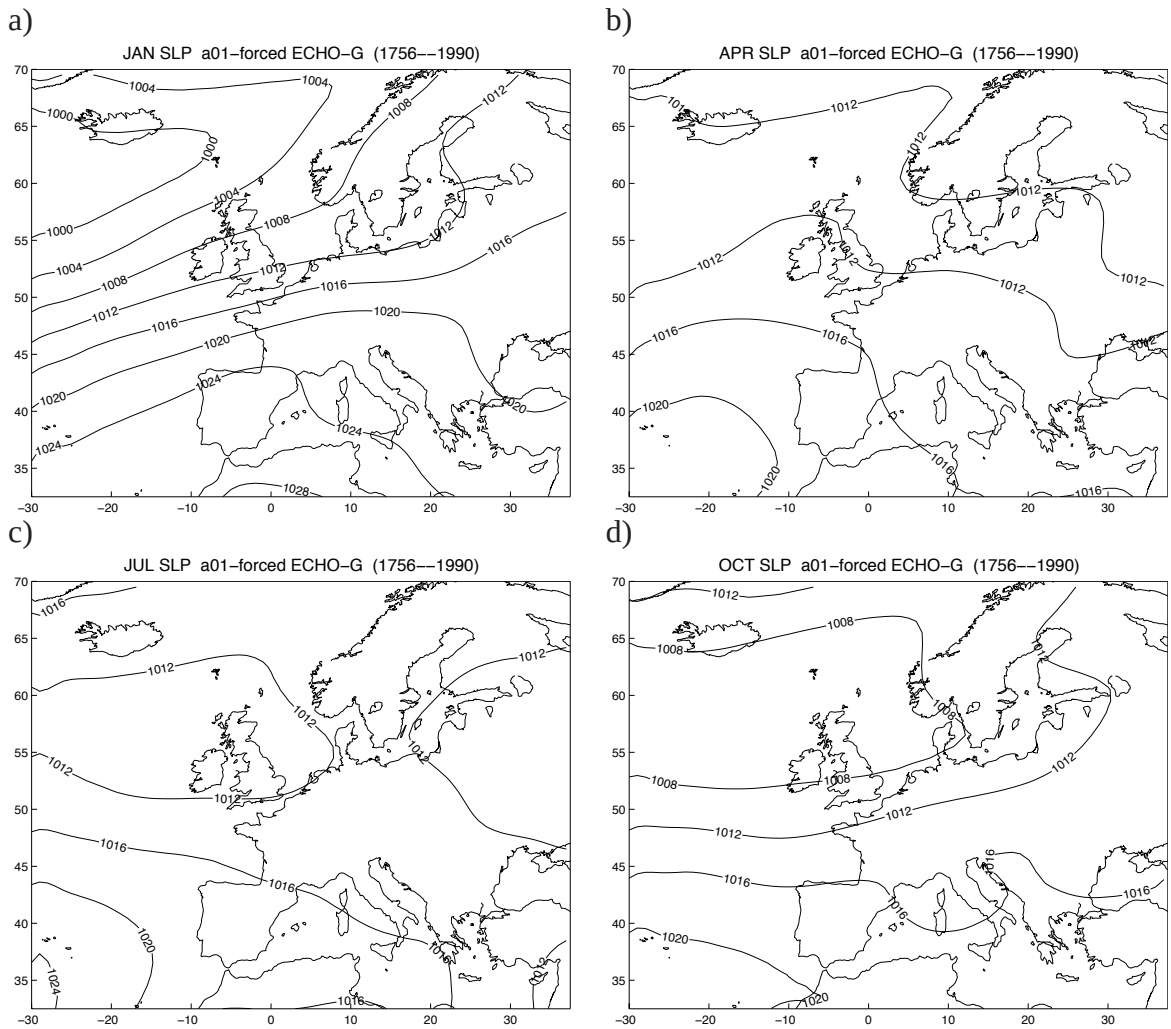

Figure 1.1: Mean (1756–1990) monthly SLP [hPa] over NAEU as simulated by ECHO-G (when forced acording to a0); a) January, b) April, c) July and d) October (ECHO-G and the different forcings are introduced in Chapter 3; a comparison with the ERA 40 reanalysis-data is given in Chapter 6)

around 1020 hPa, reached south-west of the Iberian Peninsula. Central Europe is covered by about 5 hPa lower pressure values. This distribution can stand for a mixed zonal-meridional air mass transport and fits present day conditions. ECHO-G SLP in July is related to the April situation, but is more different from present day conditions, as July's ECMWF-reanalysis shows a more differentiated pattern (cf. Matulla and Wagner 2004). In April (Figure 1.1b) the 1015 hPa-Isobar (not shown here) runs through France and somewhat west of the Alpine chain out to the Mediterranean. In July (Figure 1.1c) the 1015-Isobar is bent around the northern edge of the Alps and out to the Adriatic sea.

October shows, compared to January, a flat pressure distribution. The range of pressure is about 10 hPa, decreasing northward and the pattern indicates air mass transport from the Atlantic into Europe with a western component in the main. The low pressure over Italy appears as a remarkable feature.

Additionaly, we have calculated the corresponding mean patterns for different forced ECHO-G simulations (see Chapter 3) separately for the 19th and 20th century. There is not much

of a difference, indicating that, based on the investigated periods, mean circulatory features averaged over quite long periods of time are not much affected by different forcings. On shorter timescales however, the reaction of the climate model to different forcings can actually be quite different. This can be seen in Chapter 6 from the already mentioned Figures 6.1 and 6.2 but also from 6.4 and 6.5, which display the evolution of SLP time coefficients (von Storch and Zwiers 1999).

1.2 Regional scale climate

The instrumental based 'regional climate' part of the study is targeted to the 'Greater Alpine Region' (GAR). It icludes the European Alps and their greater suroundings. It spans a regions from Lorraine-Burgundy-Camargue in the West to the Hungarian Plains, the Slovak and Bosnian mountains in the East and from the Bavarian pre-alpine hills in the North to Toscana-Umbria-Marche in the South (compare Figures 2.5 and 2.6 in Chapter 2). In terms of climate, the region shares three of the principal European climates: Atlantic-maritime in the West and Northwest, the more continental East and the Mediterranean South of the GAR. These three domains border and interfere in the Alpine part of the GAR and are additionally modified here through vertical effects. The mountain chain of the Alps starts in the Southwest in meridional direction, then bends to the Northeast and East and has zonal extension for the greater part of its total length of aproximately 1000km. Therefore it has a more complicated influence than other big mountain chains (Rockies, Andes, Alps of New Zealand) which are perpendicular to the prevailing circulation and thus produce very clear windward and leeward climates. The European Alps mainly cause an intensification of the northern border of the Mediterranean versus the moderate westerlies part of the GAR. The Atlantic-Continental transition in the North of the GAR on the other hand is rather smooth and obviously not modified by the Alps. Only a small segment of the South-Western chain of the Alps has such an influence by suddenly increasing continentality on the path from Burgundy and Haute Savoye over the Alps to the Piemonte-Lombardian Po-Plain (more details in Chapter 2).

Different regionalisation attempts based on objective methods (for temperature described and referenced in Chapter 2) produce more or less similar results in good accordance with the above mentioned forcings. The horizontal north-south and west-east forcing gradients result in a splitting into four leading sub-regions identical with the NW, the NE, the SW and the SE of the GAR, having a common crossing point in the Austrian Central Alps near 47N/13E (compare Figures 2.5 and 2.6).

There are slight differences if temperature or precipitation is regionalised, but the leading features are identical. Only one major effect makes temperature regionalisation deviate from precipitation – the dominance of vertical effects. Figure 1.2 shows respective examples of the annual temperature courses of 19 selected sites in GAR in altitude steps of 500m. Annual mean temperature (not shown) decreases by 24 degrees C (+16 deg to -8 deg) at the given altitude increase of 3500m (represented by long-term instrumental datasets available in GAR). The respective summer (winter) values are 26 (22) degrees.

The shapes of the annual courses are similar but show some additional general tendencies and regional (local) effects. Among the former is a tendency for the minima to shift from January to February and the maxima from July to August with increasing altitude, as well as a general vertical decrease of the annual range (compare Figure 1.3). To the latter belong the increasing regional splitting with decreasing altitude (spanned by the arrows in Figure 1.2) and some more

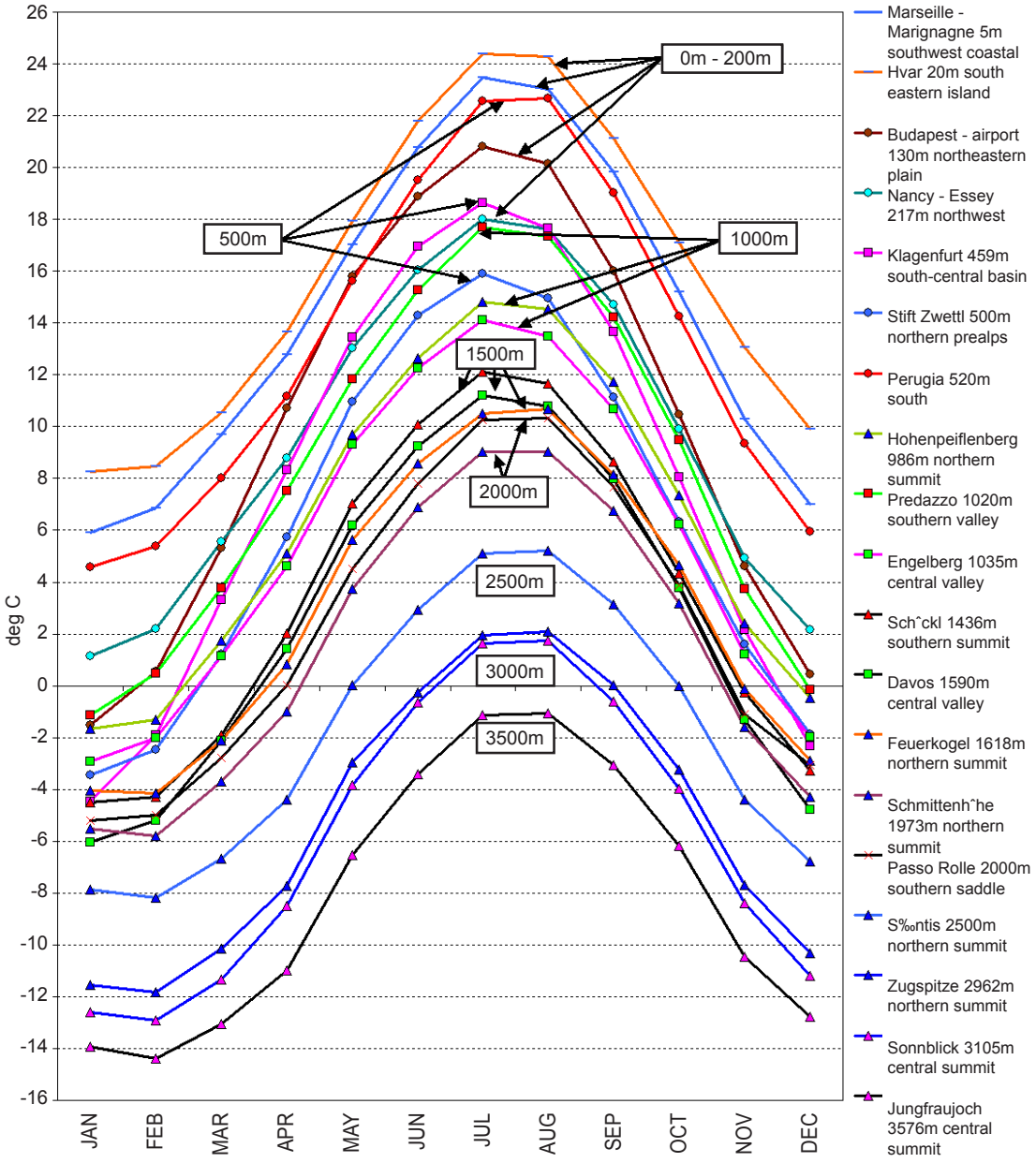

Figure 1.2: Selection of typical annual temperature cycles in the Greater Alpine Region (1 to 4 examples for each 500m altitude step) 19 station subsample of the 132 HISTALP temperature series, all means refer to 1901–2000.

local topographic effects that modify for example the mentioned vertical gradient of the annual range shown in Figure 1.3. The two maximum annual range values of the sample are caused by different forcings: A large scale increase of continentality from West to East produces the increase of the annual temperature range from less than 17 deg in the western (Nancy) to more than 22 deg in the eastern lowlands (Budapest). The absolute maximum annual range of more than 23 deg in Klagenfurt on the contrary is produced by the basin-situation there. At the other end of the spectrum, the decrease of annual temperature range with altiutude is additionally reduced by summit topography (reducing annual range) versus saddle, valley or basin position (increasing annual range).

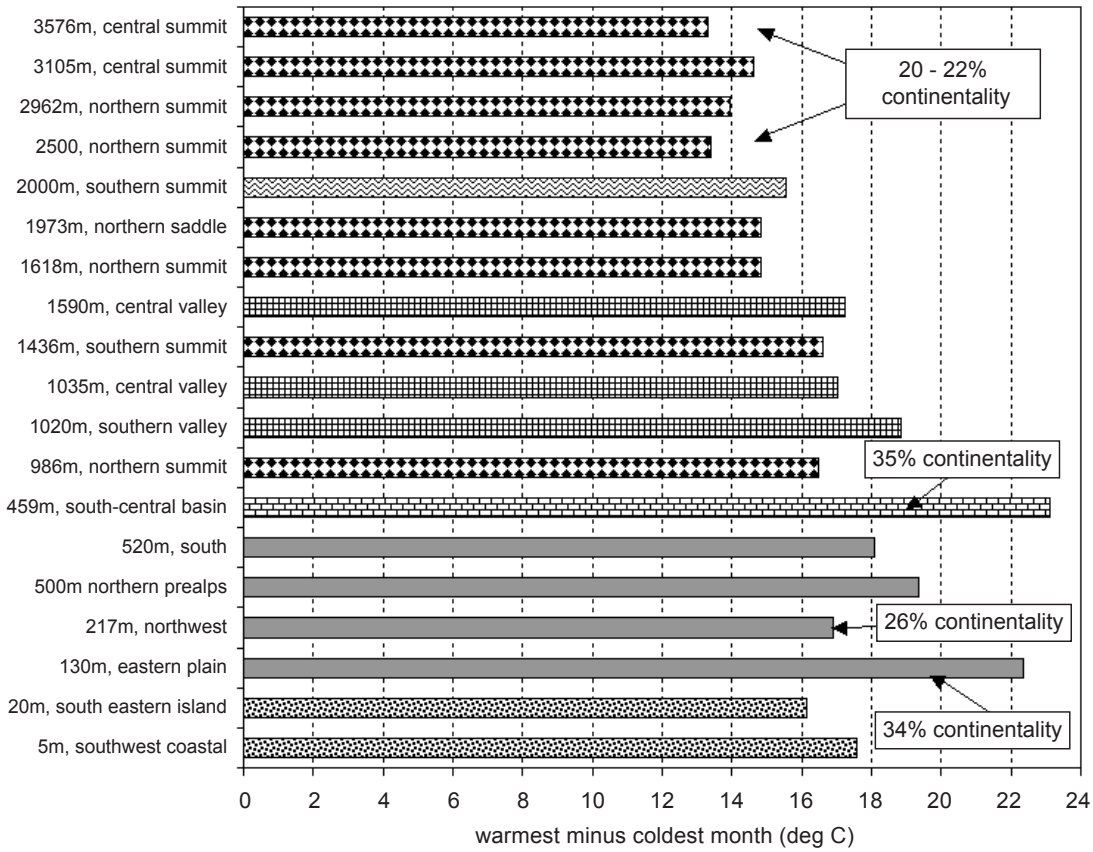

Figure 1.3: Selection of typical annual temperature ranges in the Greater Alpine Region (warmest minus coldest month) sorted according to altitude same HISTALP temperature subsample as for Figure 1.2; means refer to 1901–2000 continentality (thermal) in percent of the annual range of Werchojansk, Siberia.

A small but remarkably different subsample of the GAR (and the respective HISTALP sites) are the coastlines and their immediate hinterland. Here the annual range is also reduced mainly due to much warmer winters together with slightly cooler summers.

The precipitation climate of the study region varies not only in terms of absolute values (less than 500mm to more than 2500mm) and the annual range (less than 20mm to more than 150mm mean difference between maximum and minimum monthly totals) but shows also different to completely reverse shapes of the annual course. A recent (not yet finished) study on regional precipitation variability within the GAR based on the 192 long-term HISTALP precipitation series (the creation of the dataset is described in Auer et al. 2005) resulted in surprisingly distinct subregions with homogeneous shapes of annual courses. Figure 1.4 shows the six principal respective regimes in the GAR, all of them having in common only small intra-group variability bands (the range between the two thin lines framing the bold line of the mean subgroup annual course). It is clear to see that inter-group variability is significantly lower than the differences between the means of the six subgroups. The diagrams a, b and c show the three northern subregions. The western parts of GAR (a, mainly in France) are under Atlantic maritime influence and show only a marginal annual course. Proceeding further east towards the northern Alps and the Bavarian, Swiss, Austrian pre-alpine hills (b) a distinct summer precipitation maximum emerges. Here summer precipitation (maximum in July) is more than twice as strong

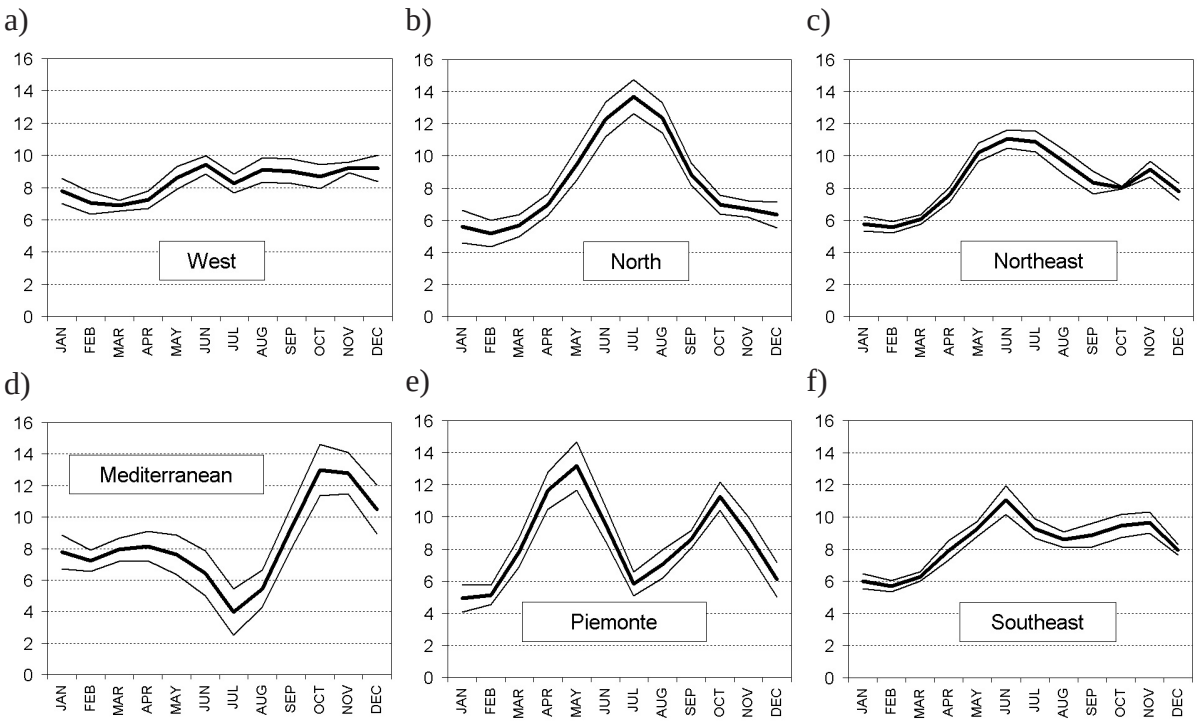

Figure 1.4: The dominating mean annual precipitation cycles in the Greater Alpine Region (monthly shares of the annual total in percent); bold: mean of all sites in the respective subregion, thin: plus/minus 1 standard deviation; database: 192 HISTALP precipitation series, sample 1901–2000; a) the Atlantic sector in the French part of GAR, b) central northern GAR (Swiss - S-German - Austrian), c) E-Austrian - Slowak - Hungarian GAR, d) most of the Mediterranean belt of the GAR except e) and the southernmost GAR (Figure 1.5 i), e) Piemonte and parts of western Lombardia and Swiss Ticino, f) the non coastal SE-GAR.

as in winter. The shape is clearly unimodal and similar to temperature. In the northeast (c, eastern Austria, Slovakia, Hungary) the curve becomes flatter again and an emerging secondary maximum in November makes the curve bimodal. The diagrams d, e and f describe the southern parts of GAR under Mediterranean influence. Although none of them shows the classic respective feature with a complete reverse of the shape of diagram b) to a summer minimum and a winter maximum. Only two of the 192 stations (one of them shown in Figure 1.5h) have that fully developed winter maximum, too few to create an own subgroup. The parallel-band roughly from 44° to 46°N, representing Mediterranean influences in GAR, is characterised by a strong bimodality with two precipitation maxima in spring and in autumn, a summer minimum between, but also a significant decrease in the core winter months. In the greater part of that latitude band (d) the autumn maximum is significantly stronger than the spring maximum. The time lag of the seasurface temperatures in the Tyrrhenian and the Adriatic seas with still high evaporative potential together with a simultaneous start of cyclonal activity in the air above explain the autumn maximum. The causes for the increase of the spring maximum in the inner part of the bow of the Western Alps (e), in Piemonte and parts of Swiss Ticino and Lombardia is less easy to understand. Several mechanisms, topographical-dynamical and thermodynamical ones are responsible for it (Rhone valley, Genova depression, the special shape of the Western Alpine mountain chain ...). The type f annual course, predominant in the non-coastal parts of Slowenia, Croatia, Bosnia-Herzegovina and southern Hungary is the slightly Mediterranean in-

fluenced version of the continental type c. In both subregions of the GAR the topography of the Alps plays only a minor role. Thus the transition between c) and f) is rather smooth.

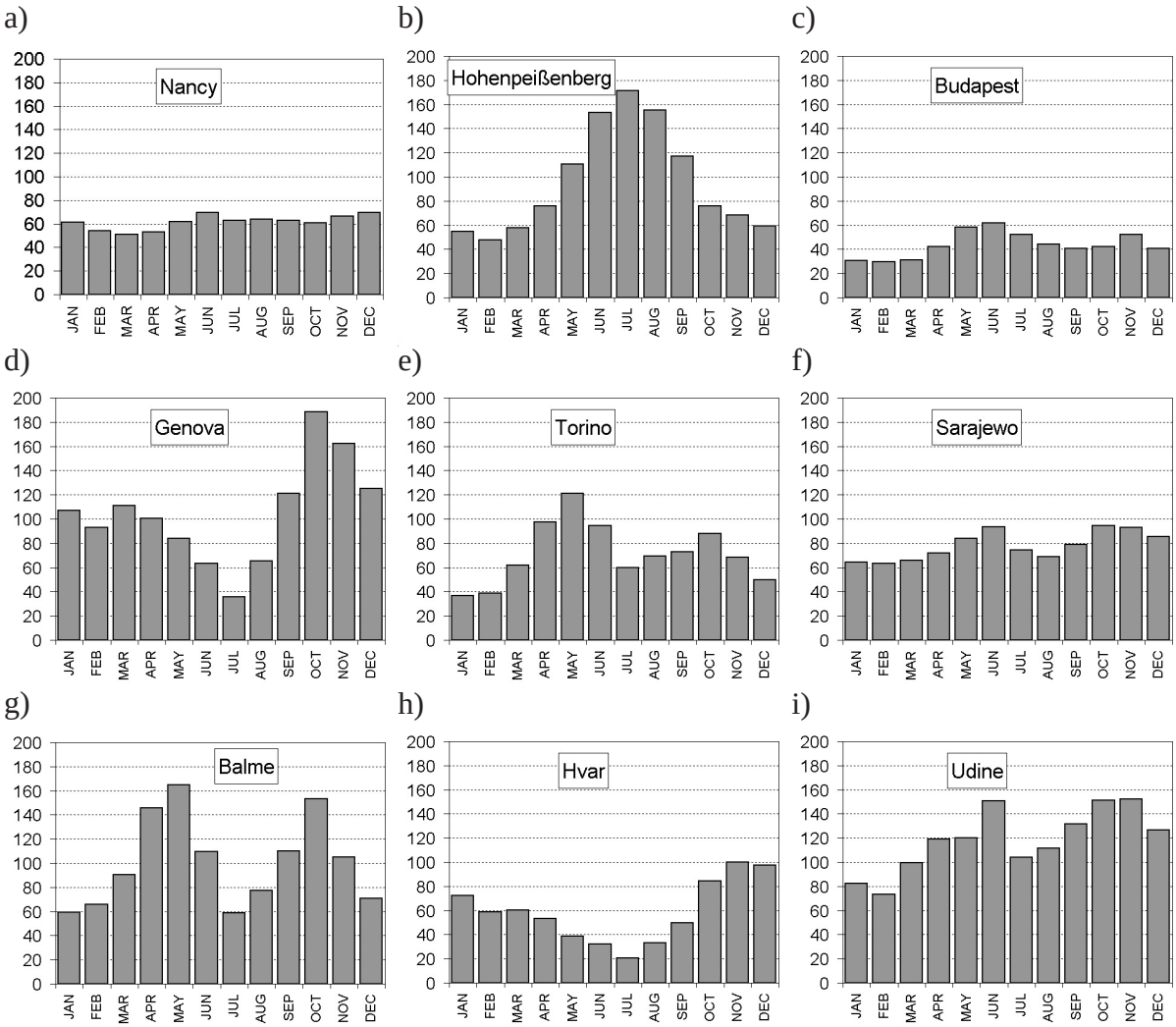

Figure 1.5: Selected examples for typical mean annual precipitation cycles in the Greater Alpine Region (monthly means 1901-2000 in mm). a) to f) referring to the subregions shown in Figure 1.4, a) to f) respectively, g), i) examples from the two ”wet spots” in the Piemonte and Friuli southerly congestion regions, h) one of the few examples with fully developed Mediterranean ”summer-minimum vs. winter-maximum annual precipitation cycle.

Considering the strong variations of absolute precipitation totals in the region described for the greater part of GAR in Schwarb et al. (2001); Baumgartner et al. (1983) or Fliri (1974); Frei and Schär (1998) and for some national regions e.g. Auer et al. (2001); Gajic-Capka et al. (2003); FOWG (2004); Mercalli et al. (2003); HZRS (1995), the relative annual courses of Figure 1.4 may mislead to a certain extent. The set of examples of annual courses shown by monthly precipitation totals in mm in Figure 1.5 shall reduce this biasing potential. The diagrams a) to f) show one typical single station representative for each of the principal types shown in the respective a) to f) diagrams of Figure 1.4. a) compared to c) visualises the general drying when proceding from the Atlantic towards the Eurasian continent. This steady decrease is sharply modified through obviously orographically enhanced (summer-) precipitation in the realm of the northern Alps (b). The Mediterranian (d, e, f) types show in general higher precip-

itation – in maritime as well as in continental surrounding. Only the 3 northern alpine summer months match the monthly totals in the south. The 3rd row of Figure 1.5 shows three additional examples not visible in the anomaly curves of Figure 1.4. Diagram h (the island Hvar in the southeast of the GAR) shows one of the two mentioned 'pure Mediterranean' examples with fully developed winter maximum. The other two (g and i) represent the two extreme 'wet spots' in two subregions (Balme in Piemont in the West, Udine in Friuli in the East) with great topographic dynamics and strong moisture sources at southerly airflow. Together with the Genova and the Rijeka regions it is here and only here where excessive monthly precipitation amounts of more than 1000mm are measured, values twice as much as the respective 'extremes of the extremes' north of the Alps. Only some (not all) small high elevation central alpine locations (e.g. Hohe Tauern) are similarly wet. Due to the yet unsolved problems of high elevation precipitation measuring, and the resulting severe quality problems also in terms of homogeneity, such series (e.g. Sonnblick, Grand St. Bernard, Zugspitze, Säntis) are not yet included in HISTALP.

Resuming the shortly described basics of the regional climate in the GAR the higher spatial coherence of the temperature field (after elimination of vertical effects through normalising the series as deviations from a common reference period) makes temperature the preferred candidate to detect and analyse 'outstanding past decadal-scale climate events'. There is evidence (shown and discussed in Chapter 2) that - especially at lower than annual frequencies - temperature variability is rather uniform within the GAR and also similar to European scale variability. Preciptation variability will be used – together with evidence from the radiation component and from glacier variability – to additionally support the detection and to round-up the analysis and description and the understanding of the outstanding periods.

1.3 Layout of the study

The structure of the study is pictured in Figure 1.6. It can be seen that the particular order of Chapter 2, 3 and 4 is arbitrary. However, all of them have to be completed when entering Chapter 5, which in turn can appear in reverse order with Chapter 6.

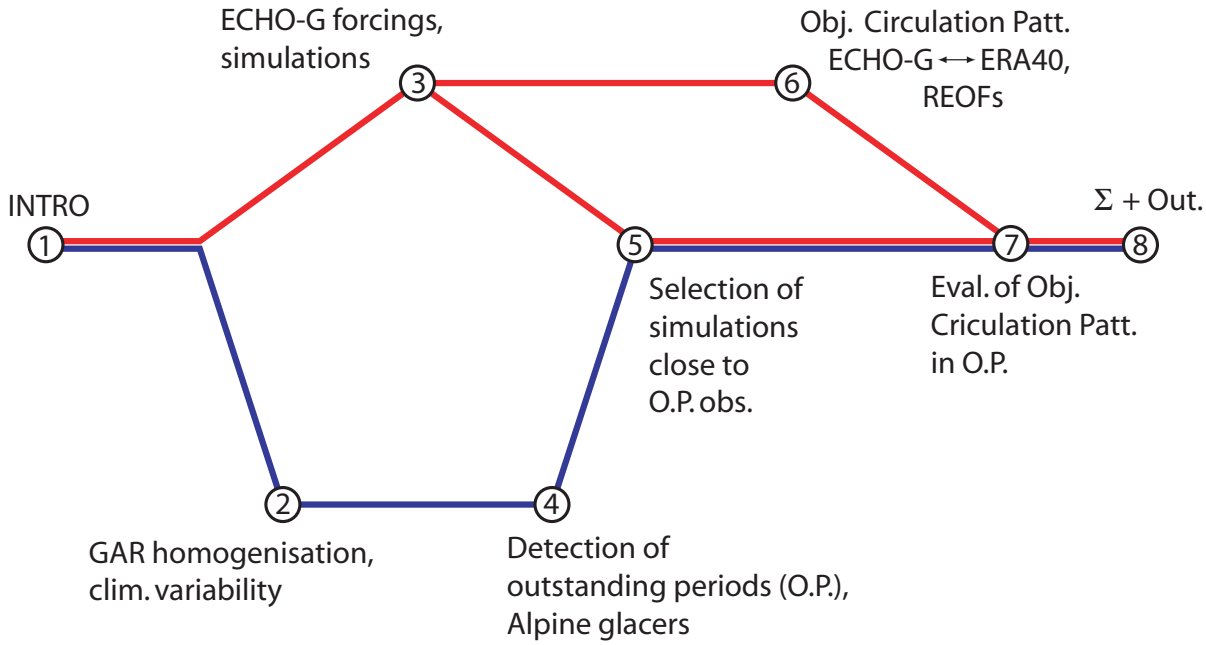

Figure 1.6: Map that displays the structure of the study; *Points and numbers* indicate chapters; The *red line*: stands for the synoptic scale (ECHO-G) and the *blue line*: for the regional scale (GAR);

2. GAR homogenisation, clim.variability This chapter is devoted to GAR's climate of the past 250 years. Its goal is to provide a thorough description of the study's regional scale dataset. The discussion is based on temperature and it comprises (i) a description of the generation of the homognised dataset called HISTALP, (ii) a regionalisation of temperature (i.e. the detection of homogeneous temperature regions within GAR), (iii) a detailed, seasonal based comparison of the temperature evolutions pertaining to different regions, which contributes to the ongoing discussion whether particular areas as, for instance, high elevations are especial sensitive to the observed changes or not, (iv) a comparison of different ways how to subdivide the observation period to allow for a meaningful detrending and (v) a trend analysis, which provides currently ongoing discussions with observations.

3. ECHO-G forcings, simulations Chapter 3 introduces ECHO-G, the Atmosphere/Ocean General Circulation Model that provides the study's large scale dataset. The reconstruction of solar variability and volcanic activity are briefly motivated and the different forcings that drive the simulations are introduced. This chapter gives an account of the model and introduces the experiments which form a central part of the present study.

4. Detection of outstanding periods (O.P.), Alpine glaciers Central part of Chapter 4 is the detection of outstanding GAR periods during the past 250 years. This is done by a long term subset that reasonably covers GAR and by an investigation of the fraction of all

stations that show significant high or low temperature values. Thereby not only the classical seasons are taken into account but also any successional sequence of three month. The core of the chapter is Table 4.1 that contains a listing of the so-called outstanding periods. These periods are supported by the behaviours (advances/retreates) of Alpine glaciers which is discussed in some detail.

5. **Selection of simulations close to O.P. obs.** Chapter 5 compares 2m temperature of all ECHO-G simulations to the observations within all outstanding periods. This process is based on quantifiable parameters but on subjective decision too. Outcome of this chapter is a list of simulations that reasonably traces observed temperature within the outstanding periods regarding winter, summer and the whole year.

6. **Objective Circulation Patterns ECHO-G↔ERA40, REOFs** Within the first part of this chapter SLP from 1958–1990, as simulated by the historical forced ECHO-G is compared to the ERA40 reanalysis. Then SLP of all simulations is entered into a REOF analysis for an objective decomposition of circulation into diverse patterns. This is done for the whole simulation period (1756–1990) as well as for winter, summer and the whole year. Output of the chapter are tables that list the contributions of the circulation patterns to the outstanding periods.

7. **Evaluation of Objective Circulation Patterns in O.P.s** This is the Conclusion chapter. It puts all findings together and derives the final results. This is done by identification of circulation patterns which appear more often in connection with warm or cool GAR conditions. For winter and the year as a whole this item as well as the influence of different forcings on the ECHO-G simulations and in turn some observed regional scale counterparts seem to issue the model some ability in tracing outstanding climate events.

Chapter 2

The homogenized instrumental record within GAR

2.1 Collection and homogenization of data

It is a matter of fact that also 'state of the art measured' instrumental climate data always contain an additional fraction of non climatic information (noice) as, for instance, changes in the surroundings of a site or changes in the instrumentation. In particular if longer timescales (decadal to centennial) are envisaged for a climate variability study, non climatic inhomogeneities have to be removed at first (see e.g. Peterson et al. 1998 or Aguilar et al. 2003, among many others).

Long-term climate data acquisition and quality control in terms of homogeneity in the study region started in Austria with some national attempts in the early 1990s (e.g. Böhm 1992; Auer 1993). Similar attempts in other countries of the study-region followed in the mid-1990s (e.g. Aschwanden et al. 1996; Begert et al. 2003; Brunetti et al. 2000; Herzog and Müller-Westermeier 1998; Katušin 1994; Moisselin et al. 2002) well accompanied and supported by the bi- to tri-annual 'Budapest Seminars on homogeneity' organized by the Hungarian Meteorological Service (e.g. Szolgála) 1996; Szalai and Szentimrey 1999; Szalai 2004; Szolgála) 1996).

Soon it was realized that, especially for a climatologically interesting but organizationally very patchy region like GAR, a supra-national cooperation had to be the next necessary step. Such a cooperation does not only provide the basis for a better understanding of climate (which does not follow national borders) but also helps to detect remaining inhomogeneities masked through nationwide simultaneous inhomogeneities. Typical examples for this kind of inhomogeneities are introductions of new technologies, new observing hours and other changes, that – particularly in well organized meteorological services – usually happen at the same time and thus cause no results in relative homogeneity testing, because all series are infected and no reference is available. In the study region such supra-national attempts started with ALOCLIM (a cooperation of Austria with a number of neighbouring countries, Auer et al. 2001) and soon developed into a full coverage of GAR under the umbrella of data work packages of the projects ALPCLIM (Wagenbach et al. 1998), CLIVALP (Ungersböck et al. 2002), and ALP-IMP (Böhm 2004).

The experience gained in our group along the described respective path of activities led to a clearly defined list of conditions we require for a dataset appropriate for climate variability research in the instrumental period. Such a dataset should fully exploit the given potential concerning:

- sufficient length (this is claimed for because of two reasons at least: (i) to include the early instrumental period, which is mainly dominated by natural forcings i.e. not much influenced by antropogenic activity and (ii) to allow for an adequate samples sizes to study extremes);
- proper spatial and temporal resolution (meeting the demands in respect to de-correlation in space and time);
- multi-dimensionality (several, at least the main climate elements);
- high data quality in terms of homogeneity (non climatic breaks removed, non climatic trends detected and at least flagged);
- high data quality in terms of outlier detection and elimination.

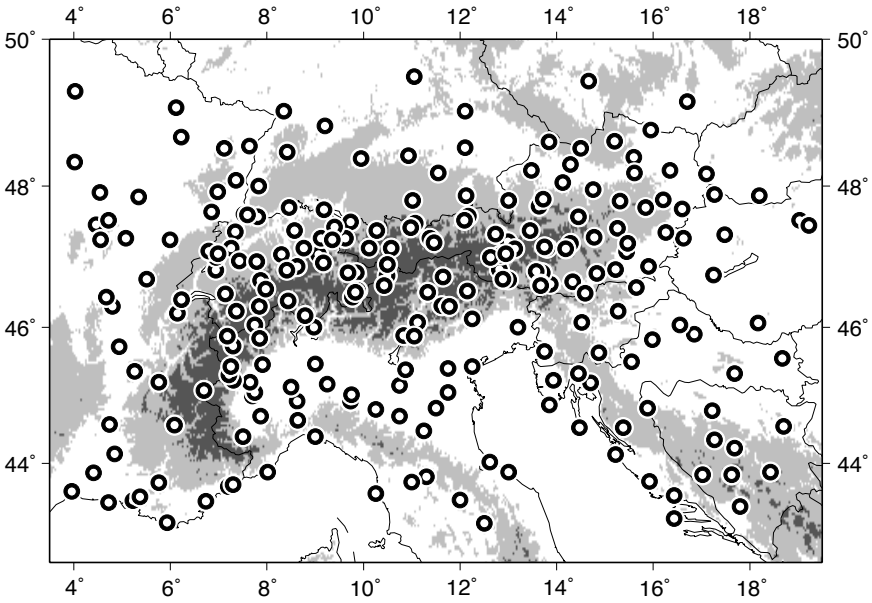

Figure 2.1: The HISTALP network of long-term climate time series in the Greater Alpine Region (GAR). Status: 2005; Sites provide at least one of the five main climate elements (air pressure, air temperature, precipitation, sunshine and cloudiness).

During the past few years we have established a database called HISTALP (Ungersböck et al. 2003) that uses the above listed principles as basic requirements. So far, HISTALP covers the entire GAR for three main climatic elements (temperature, precipitation, air pressure) at a monthly resolution and major parts of GAR for sunshine duration and cloudiness (see Figure 2.1). Data, which are available up to now in HISTALP, are near to fully exploiting also the early instrumental period in respect to homogenizable and still existing measuring sites. The longest series start as early as 1760 (Figure 2.2). On a monthly resolution (which is the scope of this study) network density meets the demands in respect to spatial de-correlation to a high degree (compare Scheifinger and Böhm 2005). Maps in Figure 2.2 show the spatial coverage of GAR by time series of 5 (temperature, precipitation, air pressure, sunshine duration and cloudiness) of the main climate elements. Activities to enter daily resolution have already

started, but arising problems and solutions in regard to network density and homogenising will be described elsewhere.

Recently, all HISTALP-series have been re-analysed and treated by the same homogeneity and outlier detection and removing procedures, which are the result of the experience gained during the past 15 years. A detailed description (at the example of precipitation) is given in Auer et al. (2005) and can be taken as an example for other climate elements too. The enormous number of detected and removed inhomogeneities and outliers (see Table 2.1) makes the HISTALP-hom series certainly one of the highest quality climate variability databases existing so far.

Table 2.1: Synopsis of statistical parameters describing the collected dataset and the homogenisation procedure.

	temperature	precipitation	pressure	cloudiness	sunshine	unit
no. of series	131	192	72	66	55	no.
available data (incl. filled gaps)	19312	26276	10215	7889	7886	year
available data (incl. filled gaps)	231746	315316	122581	94672	58627	month
mean length of series	147.4	136.9	141.9	119.5	88.8	year
dedected breaks (total)	500	1174	256	234	366	no.
mean breaks per station and year	0.026	0.045	0.025	0.030	0.075	no.
mean homogeneous subperiod	38.61	22.37	39.95	33.76	13.36	year
filled gaps	12392	14847	4217	3513	2011	month
mean gap rate	5.3	4.7	3.4	3.7	3.4	%

Together with network density and the now enhanced coverage of the early instrumental period it opens a realistic opportunity to study climate variability in an interesting region at the crossing of three continental scale climate realms and additional vertical effects. The climate time series present in HISTALP are available in station-mode (original, homogenised absolute and homogenised anomalies) and moreover in two different grid-modes. Grid-1 has a spatial resolution of 1 deg lat-long and consists of anomaly grid-point series relative to 20th century means in two vertical layers (below and above 1500m altitude). The interpolation methods for Grid-1 are described in Böhm et al. (2001). Since then the Grid-1 datasets have been recalculated (already available for temperature and precipitation) based on the (spatially denser and completely re-analysed) respective 2004-station mode versions. Grid-2 consists of monthly absolute climate fields at higher spatial resolution. A first draft version for precipitation at 10' resolution has been recently produced for precipitation (Efthimiadis et al. 2005). For temperature the work on Grid-2 mode is not finished yet. The envisaged spatial resolution is 1km.

The scope of our paper is the identification, analysis and description of multi-annual to decadal-scale climatologically special or outstanding sub-periods as well as its relation to large scale climate as simulated by the climate circulation model ECHO-G. The identification will be performed on basis of the GAR temperature dataset. As it is 'a priori' not clear whether such special periods appear homogeneously in GAR as a whole, it is necessary to first analyse the spatial pattern of temperature variability within the study region (GAR). Both already existing data modes are used – station mode (version homogenised anomalies) and Grid-1 mode; the

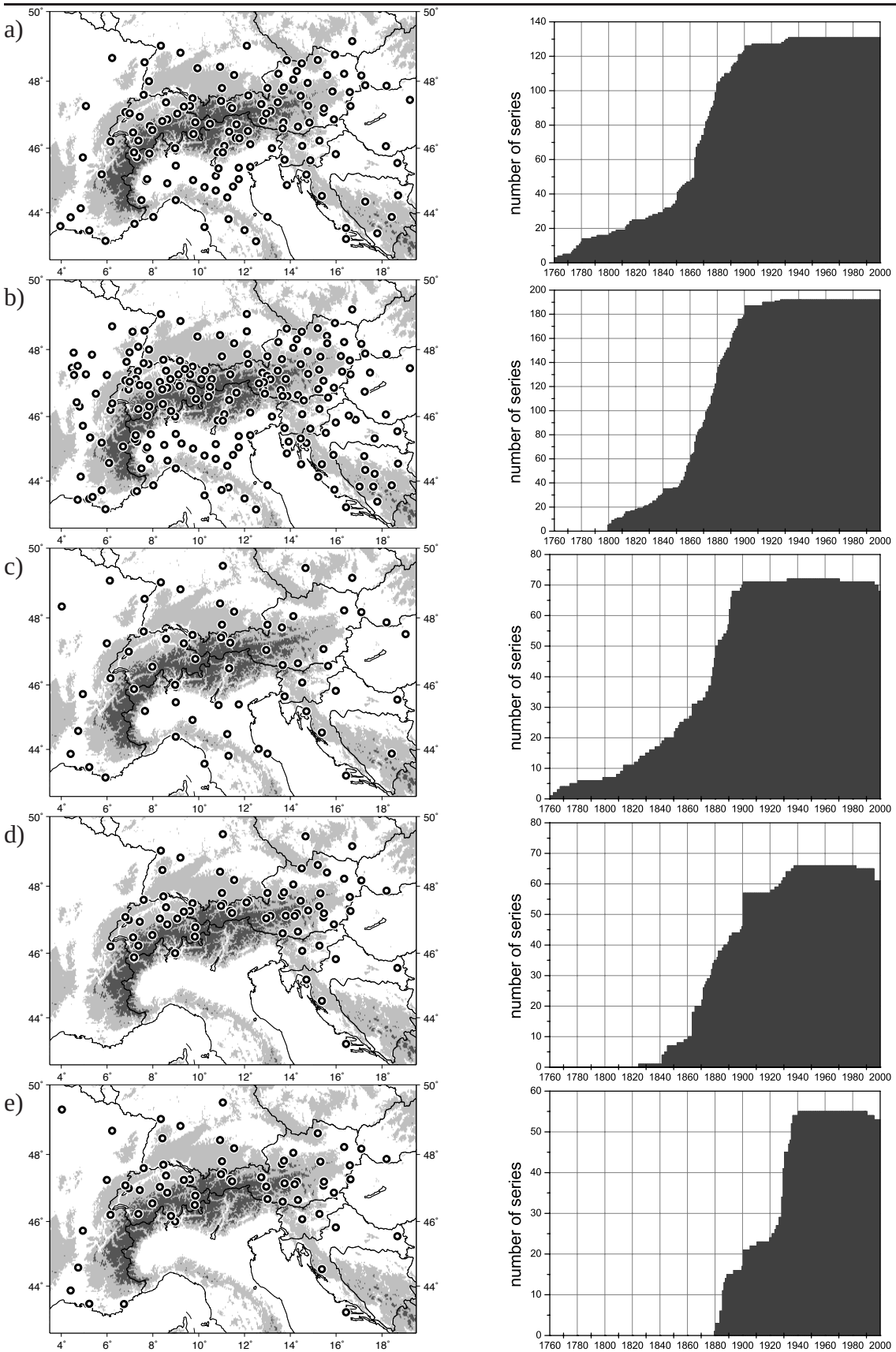

Figure 2.2: *right column*: Temporal coverage of GAR by HISTALP time series of a) air temperature means, b) precipitation totals, c) air-pressure means, d) cloudiness and e) hours of bright sunshine (number of existing non-interrupted and homogenised series per year since 1760); *left column*: HISTALP network of the corresponding stations.

former to find and spatially confine homogeneous subregions in the GAR, the latter to calculate the respective subregional mean time series. The detection of homogeneous temperature subregions within GAR via Rotated Empirical Orthogonal Functions (REOFs) is the subject of the following section.

2.2 Regionalisation of temperature

The detection of different homogeneous regions, typically regarding vegetation and somewhat less often temperature or precipitation is usually named 'regionalization' and has a long history in climatology (Köppen 1918; Blüthgen and Weischet 1980). However, there is a number of useful applications of regionalization besides e.g. climatological characterization of locations. Some of these are: (i) Application in downscaling and impact studies (Woth 2001; Penlap et al. 2004; Matulla 2005), (ii) validation of climatological and forecasting models, (iii) comparison of different statistical methods (Matulla et al. 2003) (iv) detection of climatic fluctuations (Böhm et al. 2001; Auer et al. 2001) and (v) station network design.

There are a number of techniques, which can be used for the detection of such homogeneous regions. One among them is called 'Rotation of Empirical Orthogonal Functions' (REOF) and was introduced to meteorology by Richman (1986) and its goal is the deviation of simple but meaningful structures describing the dispersion of e.g. meteorological fields. A significant description of the method can be found in von Storch and Zwiers (1999). Ehrendorfer (1987) used REOFs to identify homogeneous precipitation regions for summer and winter half-years in Austria. He utilized somewhat less than 30 stations from 1951 to 1980 and found three regions for both half-years. Widmann (1996) used REOFs to detect precipitation regions in Switzerland from 1961 to 1990. Recently, Matulla et al. (2003) compared homogeneous precipitation regions in Austria throughout the 20th century as found by REOF to those found by Cluster-analysis and Artificial Neuronal Networks. For GAR, a regionalization of a network of 98 monthly temperature series (1927–1998) was performed by Böhm et al. (2001). They used REOF and found 5 low-elevation and one high-elevation subgroups. Since that time the GAR network of homogenized long term climate series was greatly enhanced and covers now the study region with a much higher density and with a more homogeneous distribution of stations. The number of temperature stations increased from 98 to 131 single series and several additional early parts of series were discovered and included. Hence, a new regionalization is certainly necessary.

Before a rotation of Empirical Orthogonal Functions (EOFs) can take place a Principal Component Analysis (PCA, von Storch and Zwiers 1999), that derives the EOFs, has to be conducted. PCA is used to identify a low dimensional subspace of the original data-space that contains most of its variability. This subspace is spanned by the leading EOFs. At times, the EOFs themselves are not easy to explain in terms of physical processes. In such cases it is beneficial to further transform the EOFs into 'simpler' patterns. The desired 'simple' patterns, are obtained by application of an orthonormal transformation onto the EOFs. This transformation solves a variational problem, which minimizes a cost function. The cost function characterizes the shape of the REOFs. Within this study the so-called 'varimax' method is used. Simplicity can be achieved for the REOFs or their time coefficients but not for both at the same time. As the case may be the REOFs are either orthogonal or the coefficients are uncorrelated. In the present study we investigate both options. Figure 2.3 shows the flow

chart of the applied approach.

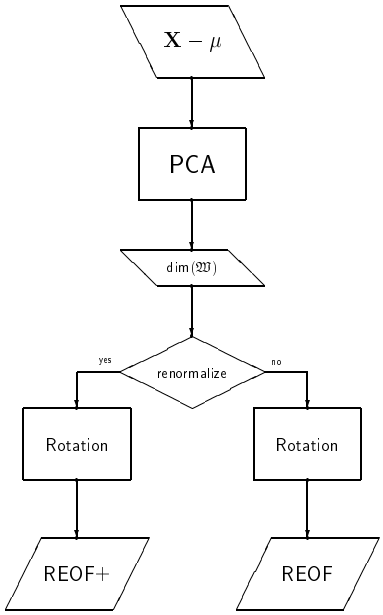

Figure 2.3: Flow chart of the REOF technique. The rigth branch is based on normalized EOFs while the left one on re-normalized EOFs.

$\mathbf{X}$ in Figure 2.3 is the random variable and μ is its long-term mean. In the present study calculations are done on the basis of monthly values and on the basis of seasonal values. Hence, depending on the case under investigation $\mathbf{X}$ resembles monthly values or seasonal values. In those cases where series of monthly values are to be used an elimination of the dominating annual course is necessary as step 1 (discussed later). The second step in Figure 2.3 is to perform a PCA on the random variable, i.e. to diagonalize the covariance matrix. The corresponding eigenvectors (EOFs) form an orthogonal basis and their time coefficients are uncorrelated. The EOFs are unique except for a constant. Hence, their length and orientation is not fixed but usually they are normalized to length one. The resulting eigenvalues are utilized, via the so called 'logarithm of eigenvalue plots' (LEV, Preisendorfer 1988), to determine the dimension of the subspace containing the main fraction of variance. This step is symbolized by '$\dim(\mathfrak{W})$' in Figure 2.3. In the present study, the dimension of the linear space, spanned by the EOFs, was successively chosen as 4, 5 or 6. The IF-condition in Figure 2.3 indicates the above described choice. If the EOFs and the corresponding time coefficients are re-normalized the REOFs are no longer orthogonal but the time coefficients remain uncorrelated. This case is symbolized by REOF$^+$. If, on the other hand, the EOFs remain at length one, the patterns are orthogonal but the time coefficients are not independent anymore.

Here, winter (DJF), summer (JJA) and the year as a whole (YAR) are investigated in both ways (via REOF$^+$s and via REOFs, i.e. the left and right subpart in Figure 2.3). The evaluation is based on seasons (i.e. one value per year) and on monthly values (i.e. 3 values per year in the case of DJF or JJA and 12 values in the case of YAR). In the latter case the long term monthly means are removed and thereby the dominant annual cycle is eliminated. For each of the two

Table 2.2: Dimension of eigenspaces and the fraction of explained variance depending on (*left*) seasonal based anomalies and (*right*) monthly based anomalies.

mode	sea	EOFs	%	mode	sea	EOFs	%
	DJF	4	93.4		DJF	4	92.7
	DJF	5	94.6		DJF	5	94.1
sea.	JJA	4	90.8	mon.	JJA	4	91.8
	JJA	5	91.7		JJA	5	92.5
	YAR	4	91.5		YAR	4	91.1
	YAR	5	92.5		YAR	5	92.8

approached rotation is conducted using 4, 5 or 6 EOFs, respectively. Below, we will mostly refer to the results achieved for 4 and 5 EOFs, as the main information is covered by these cases. Figure 2.4 shows the LEV-plots (Logarithm of EigenValue) for DJF based on monthly (right) and seasonal (left) values and Table 2.2 contains the percentage of explained variance achieved by the first 4 or 5 leading EOFs for DJF, JJA and YAR.

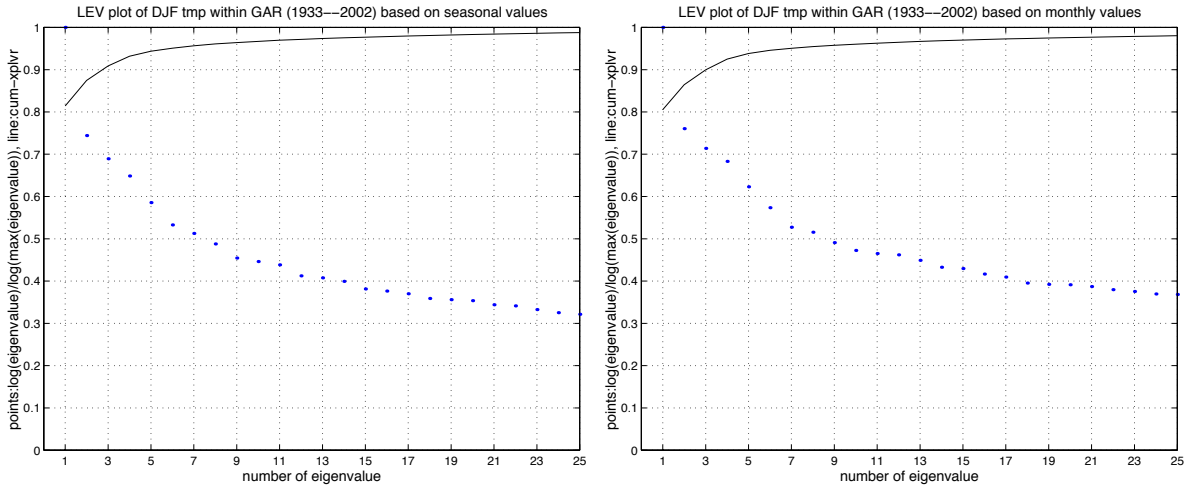

Figure 2.4: *Points* Logarithm of eigenvalue as fraction of Logarithm of largest eigenvalue; *x-axis*: number of eigenvalue in order of magnitude; the curve shows the summed explained variances; *left*: saisonal and *right*: monthly based analysis.

In all seasons, the subspaces spanned by the first four (or more) EOFs contain more than 90% of the intra-annual variance. However, the quality of the EOFs declines with increasing number and hence, regarding more and more EOFs will not contribute to a better solution. von Storch and Hannoschöck (1985) showed that the variance of the eigenvalue estimates is large and biased. In general large eigenvalues are overestimated and small ones are underestimated. These errors become considerably large if the degree of freedom exceeds the sample size.

During winter and for four EOFs there is not much of a difference between the two approaches (REOF$^+$ and REOF). In both branches of Figure 2.3 there are almost the same regions (not graphically shown here). These are roughly: One region in the North of the main Alpine chain that stretches from Germany to Hungary; the second in the south of the Alps covering former Yugoslavia and the South-Eastern part of Italy; the third captures Switzerland and France and the fourth contains parts of Austria, the Po valley and reaches to the Mediterranean east of the Alpine crest. When rotation takes place in five or six dimensions the two approaches do

no longer produce very similar results. The most striking feature is, that in case of REOF$^+$s the fifth region consists of only four stations, while in the REOF mode Northern Italy forms a region on its own, at the expense of region two and four above (Yugoslavia and the South-Eastern part of Italy) and parts of Austria plus the Po valley. In case of 6 EOFs only five regions are found, that is the loadings of the sixth REOF$^+$ are nowhere higher than any of the other REOF$^+$'s loadings. The regions signified by the five other REOF$^+$s are almost identical to the case, where only 5 EOFs are entered into rotation. For the REOFs the fourabove introduced regions still exist, but the area around the Austrian main alpine peaks and Italy forms now a North-South dipole structure.

Taking into account the results of the here described analysis and the highly similar results of two independently executed REOF-based regionalisation attempts of D. Efthimiadis and M. Brunetti (personal comm. 2005) a final division into 5 subregions was conducted. The result is shown in Figure 2.5. There were no problems in defining the borders along the greatest part of the main chain of the Alps. However, some problems arose in separating the northwestern and the northeastern subregions. First, there is no sharp topological border there and second, seasonal fluctuations are visible. These fluctuations express themseves by the ' Atlantic' region NW protruding to the east during the warm season and the ' Continental' region NE doing so in winter. In order to allow for intercomparisons of seasonal subregional time series the decision was drawn to use the 12-months (YAR) analysis to define this border.

Another subjective decision was to disregard an 'Inner Alpine low-elevation' group, which was present in the regionalisation shown in (Böhm et al. 2001). In spite of the enhancement of network density since then, there is still a very small number of station series belonging to such a subgroup and all of them have a 'second choice', which is just as well arguable, to belong to one of the four 'Extra Alpine low elevation' groups. That is, the difference between inner homogeneousness of the 'Inner Alpine low-elevation' group and the outer separation to other 'low elevation' regions next to it, is indistinct. Thus the question of the existence of such a specific inner alpine group must be left unanswered. It affords a much denser dataset in the respective region than HISTALP provides.

Most interesting was the decision drawn in the case of Hohenpeissenberg (Germany), which is a hilltop station of less than 1000m altitude. It was assigned to the HIGH-group. All three REOF-analyses, the one shown above plus those done by D. Efthimiadis and M. Brunetti, had it in one group together with the classic high elevation sites between 1500 and 3500m in the cold season and in the NW-SW-group in summer. So, the decision to assign it to the low elevation group as done in the 2001-regionalisation was rather subjective and is not repeated here.

A second similar 'interesting if not questionable' border postulated by all three REOF-analyses is the one separating SC from SE (see Figure 2.6 for the abbreviations) and assigning Firenze, Arezzo and Perugia to the 'Adriatic' subgroup SE, although the main chain of the Appennino separates these three sites from the main part of the subregion. Again, only further analyses based on a much denser network may bring more trust in the analysis results which were quite clear so far.

Compared to the 2001-regionalisation important progress was achieved as now it is possible to clearly define the border between NE-E and SE. The considerably enhanced network density due to the inclusion of Bosnian and also some other new time series solved the remaining uncertainty there. Assuming the described regionalisation results and including the additional comparability demands (and therefore no different subregions for different seasons desired) the 5 subregions shown in Figure 2.5 can be regarded as robust and well usable for further analysis of possible subregional variability patterns.

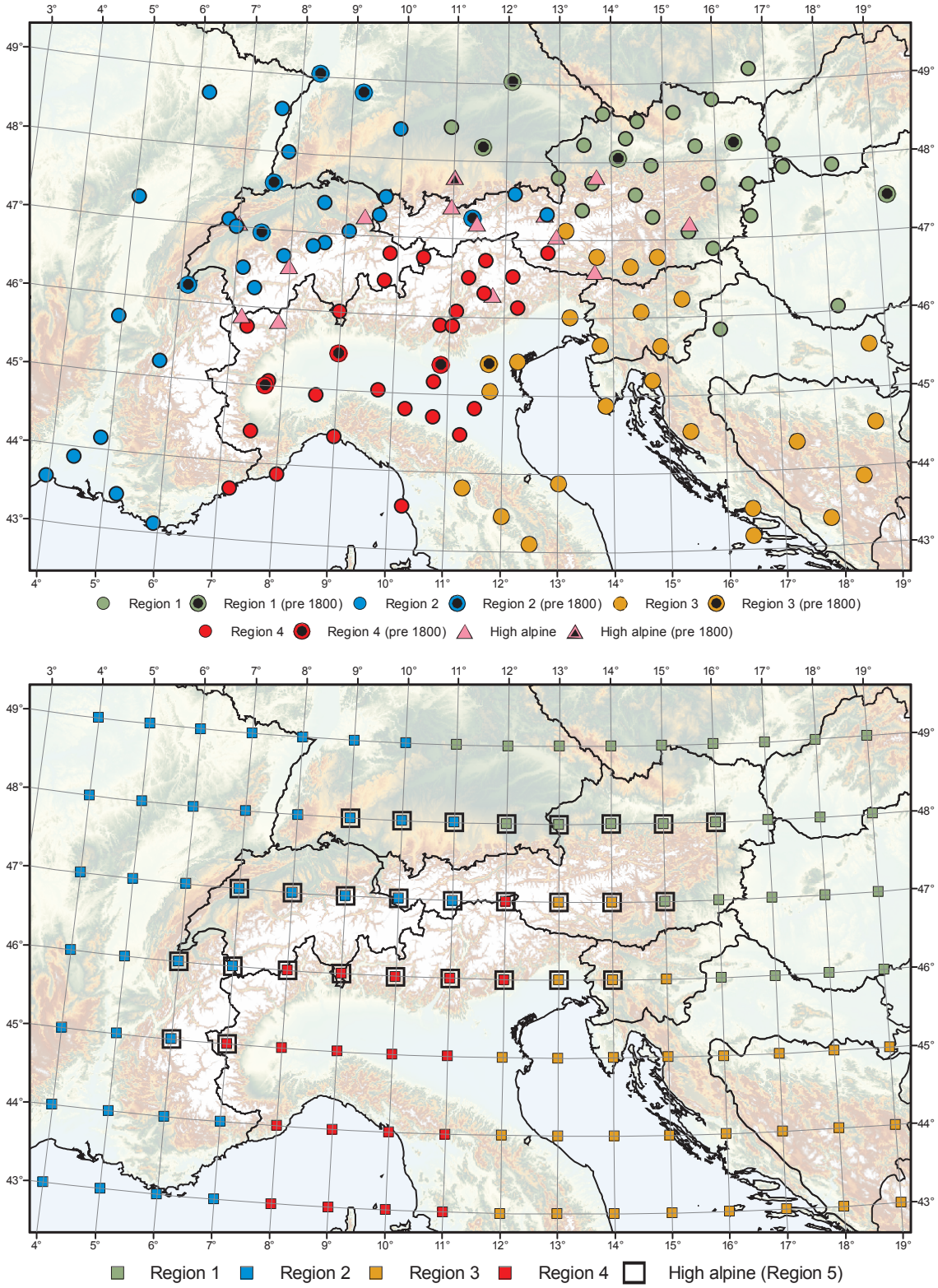

Figure 2.5: GAR temperature regions as detected by REOFs; *upper panel*: Station mode and *lower panel*: Grid-1 mode (facts about the different modes can be found in the text).

2.3 Temporal and spatial temperature variability and trends

Below we will argue in favour of the use of one single 'all-GAR' regional mean temperature time series instead of a splitting into subregions, for the detection of outstanding sub-periods. To be correct – 'single' refers to spatial subregions not to seasonal differences. We will show that the former differences can in fact be neglected, the latter not. The most pronounced spatially different evolutions should be visible for the 5 subregions isolated via REOFs (see Figures 2.5 and 2.6a). Therefore we will use the mean temperature series averaged seperately over these subregions and compare them with the all-GAR mean series (low-pass-difference-series, linear trends in different subperiods). This will also be done among differently recombined 'super-subregions' shown in Figure 2.6b, c and d.

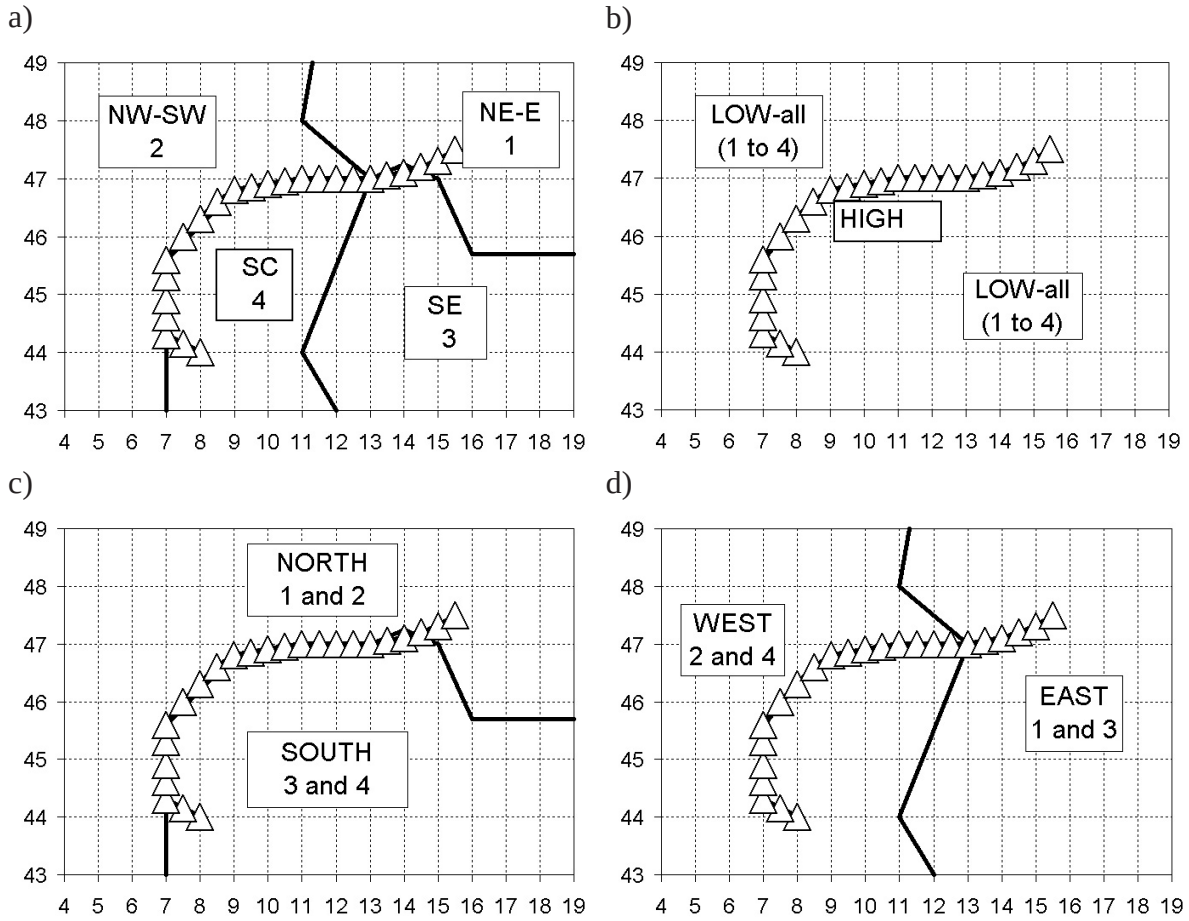

Figure 2.6: Schematic diagrams of the 4 different ways how GAR is sub-divided: a) the 4 low-elevation sub-regions; b) LOW (alpine valleys and basins included) vs. HIGH (mountain and saddle positions); c) NORTH vs. SOUTH (combined 1-2 vs. 3-4); d) WEST vs. EAST (combined 1-4 vs 1-3); x: deg E, y: deg N, line of triangles: main chain of the Alps, bold lines: subregional borders.

Figure 2.6 comprises schematical diagrams of the homogeneous temperature regions and of some combinations. These diagrams will be used below when describing results to indicate the region that forms the basis for the findings. A first example for the quite distinct seasonal differences is shown in Figure 2.7.

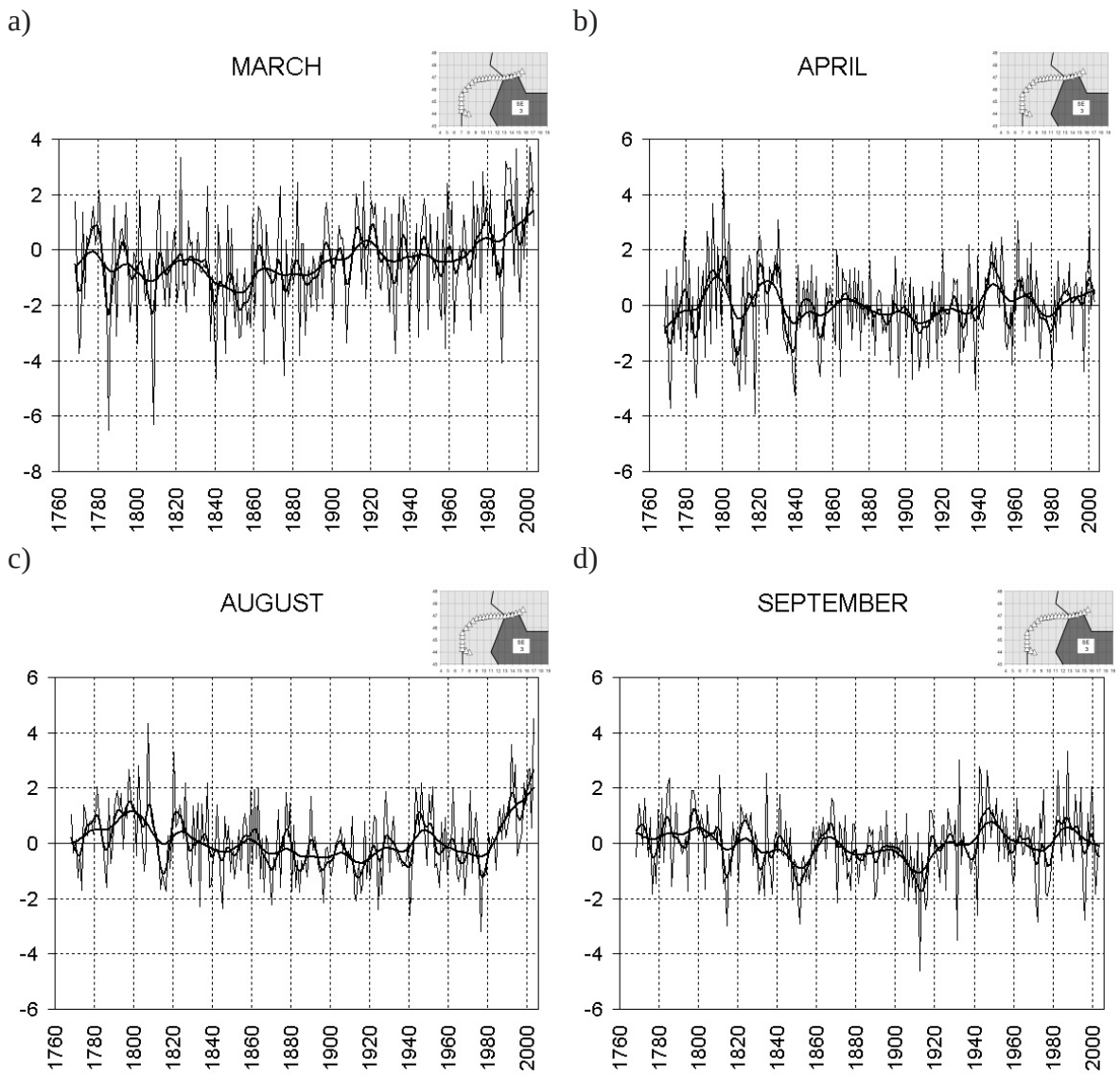

Figure 2.7: Examples of mean monthly time series in subregion SE (see sketch in the upper right-hand corner of the panels) for 1768–2003; a) March, b) April, c) August and d) September; Shown are single years and the respective 11-year low-pass filtered curves; all values are anomalies to the 1901–2000 mean in centigrades.

The region SE time series for March, April, August and September provide a first impression about the existing range of different decadal to centennial trends, different variances, changes of variance, outstanding sub-intervals, at any time of the past 240 years of the instrumental period in GAR. March supports best the recent public opinion about 'a unique climate warming that was never experienced before'. We see a cold 18th and 19th century and a remarkable warming trend of about 2.5 deg since then. The large inter-annual variability however, puts also this trend in perspective in terms of significance. The April-curve shows no long-term trend, neither when the early (slightly less reliable) instrumental period is included nor when it is let out. August shows a pronounced positive trend since about 1980 together with the exceptional August of 2003, which is the warmest on record. Again, the recent hot years are relativised if compared to the years around the turn from the 18th to the 19th century. Furthermore, Figure 2.7 sharply

depicts the exceptionally cold 1810s.

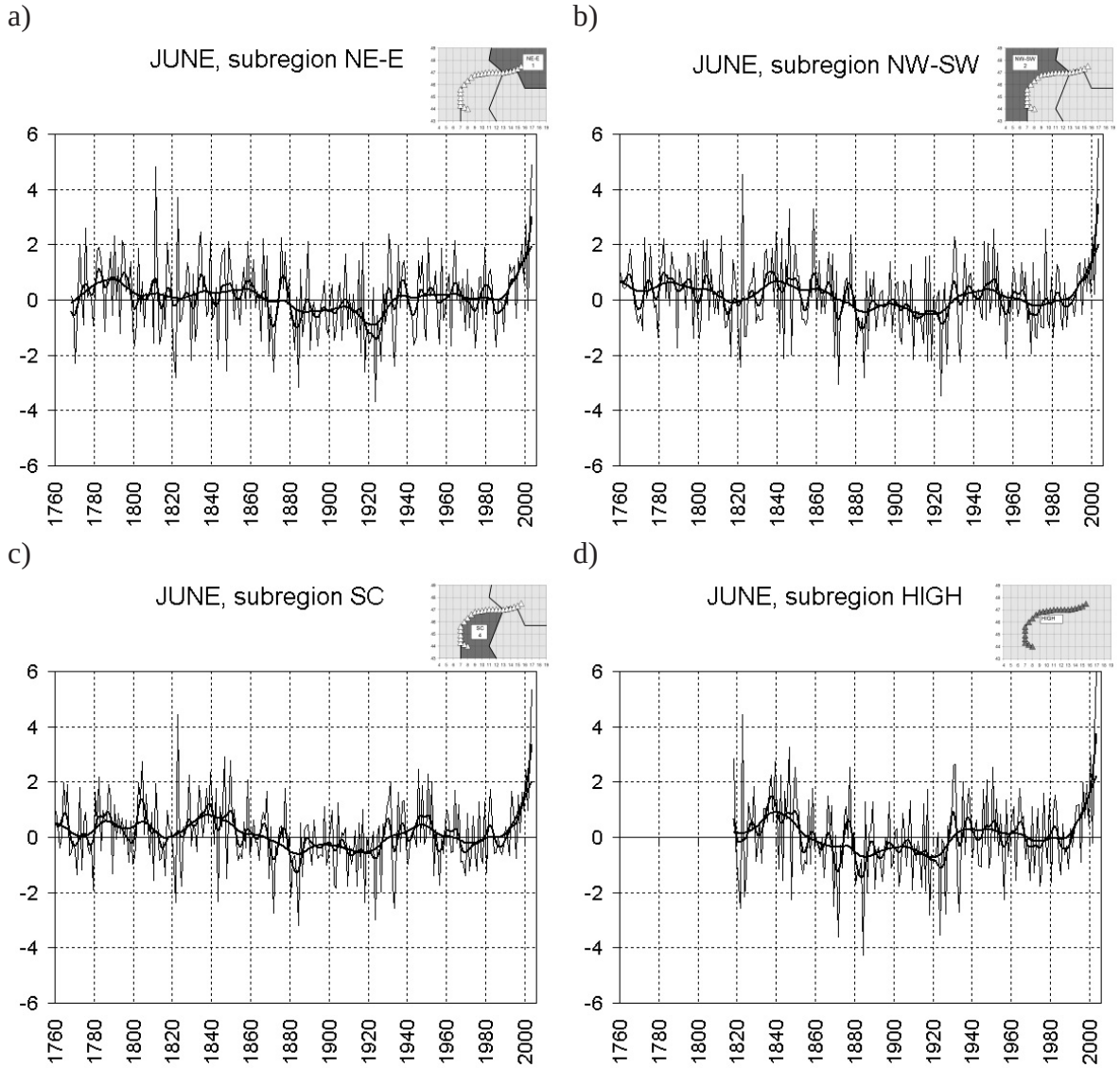

Figure 2.8: Examples for mean June-time series in the remaining 4 subregions (which were not shown in Fig. 2.7 see sketch in the upper right-hand corner of the panels); Shown are single years and the respective 11-year low-pass filtered curves; all values are anomalies to the 1901–2000 mean in centigrades a) NE-E (1768–2003), b) NW-SW (1760–2003), c) SC (1760–2003) and d) HIGH (1818–2003).

This period is one of the 'outstanding periods' (see Chapter 4 for definition and detection) that will be studied later on in some detail. Proceeding from August to September there is a change back to a zero trend. No pronounced warm early period, no warming during recent decades and a relatively flat long term course. Figure 2.8 serves, at the example of June-curves, to point up the above mentioned similarity of temperature in space. In regard to the long term evolution (the smoothed curves) temperature within different sub-regions are in fact highly similar. June has seen the strongest recent short-term temperature increase of all months, cumulating in the often described and discussed extraordinary 2003-event (e.g. Beniston 2004; Schär et al. 2004; Schönwiese et al. 2004).

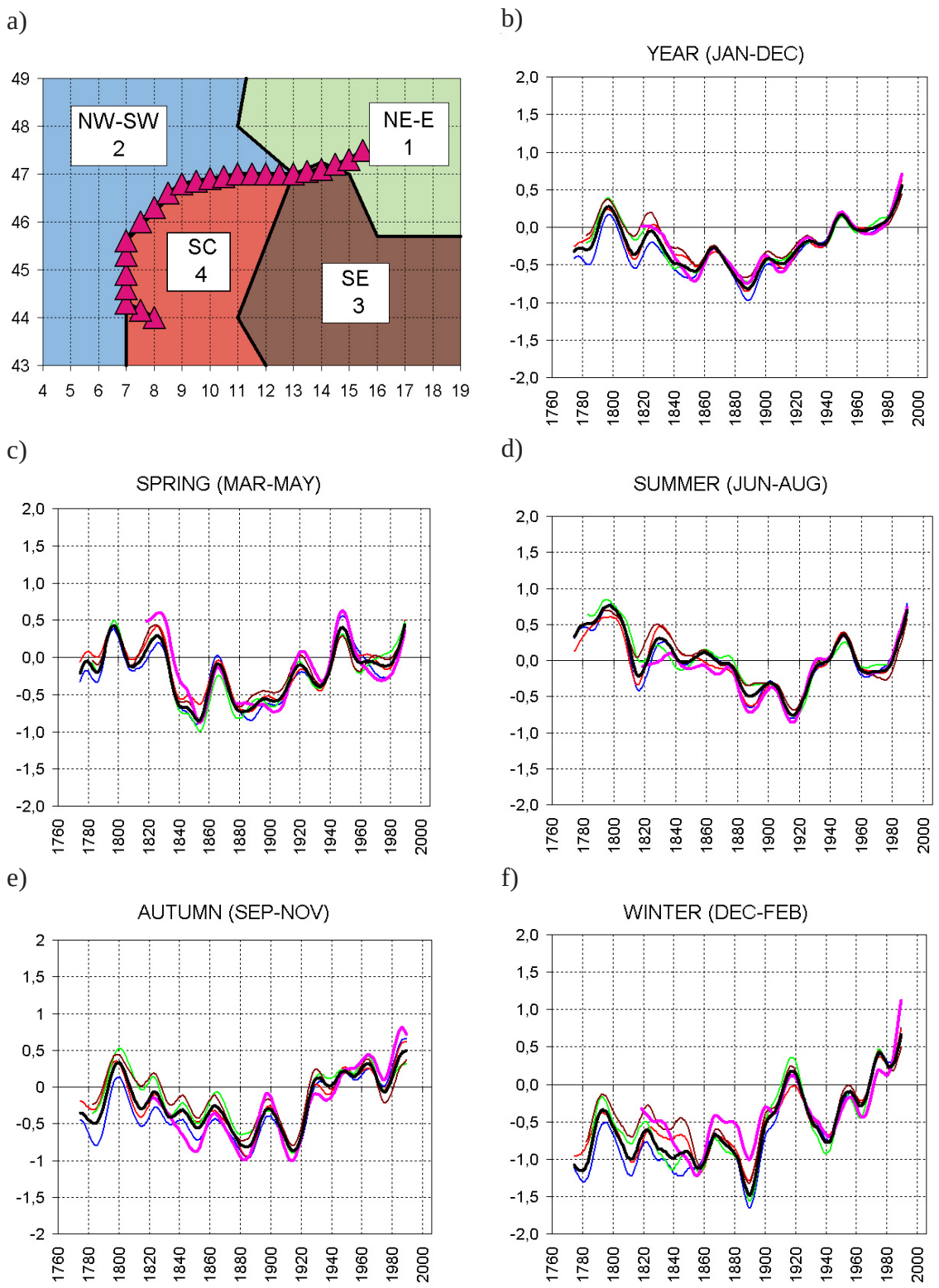

Figure 2.9: 31-year low-pass filtered subregional and all-GAR mean (black) temperature 1760–2003 a) sketch of subregions, b) year, c) spring, d) summer, e) autumn f) winter; all values are anomalies to the 1901–2000 mean in centigrades; Colour code in b to f is according to sketch in a).

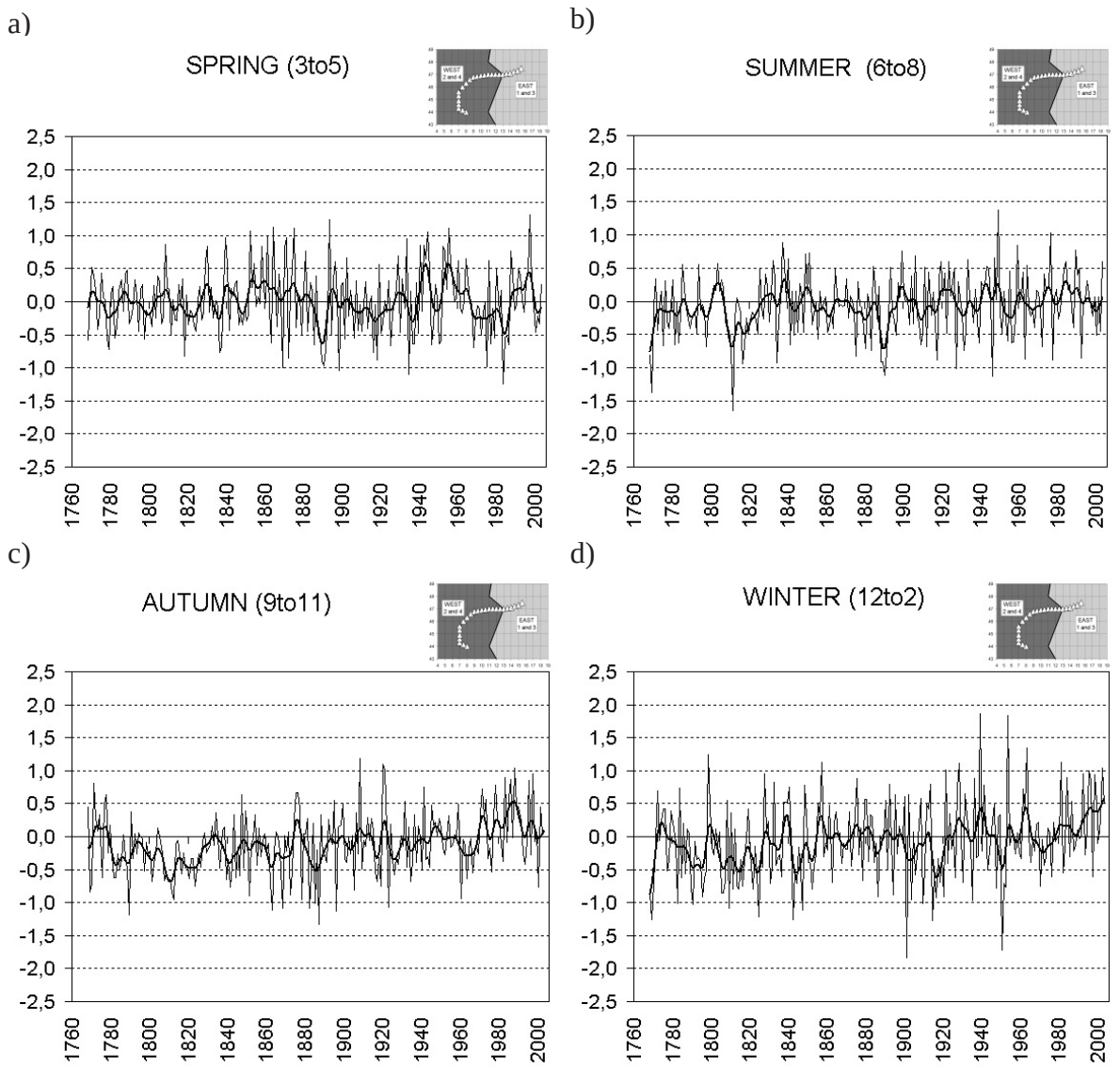

Figure 2.10: Seasonal 'super-subgroup difference' series WEST minus EAST (Atlantic versus continental; sketch of the regions is displayed in the upper right corner of the panels) 1768 to 2003; a) to d) seasons throughout the year; shown are single years and the respective 11-year low-pass filtered curves; all values are anomalies to 1901–2000 mean in centigrades.

June 2003 is in fact the warmest month on record in all subregions although another (intensively tested and proved) outstanding June in 1822 puts the often heard classification of a 'millennium event' for June 2003 in perspective. The example of June 1822 gives an idea of the dangers accompanying excessive extrapolations from relatively short data samples (even if sophisticated statistical methods are used) and it also underlines the advantage of having a longer (and therefore more convenient) database for such estimates. See von Storch et al. (2004) for further insights into errors gained by the use of insufficient datasets when deriving conclusions about long term climatic behaviour.

Figure 2.9 illustrates more systematically than Figure 2.8 the relatively weak subregional deviations from the all-GAR mean. More precisely, it is the low-elevation mean. The subgroup HIGH was not included to allow for HIGH-LOW comparisons. However, there are two more

reasons that militate in favour of excluding the high elevation stations from the all-GAR mean. First, they represent a significantly smaller area than the other groups and second, HIGH covers an area that overlaps with that of the other groups. In general, the band width of the long-term smoothed subregional curves is of the order of 0.2 to 0.3 degrees with a tendency to higher diversification in the early period and in winter.

Figures 2.10, 2.11 and 2.12 provide a closer look at subregional differences. They, respectively, compare two of the so called 'super-subregions' shown in Figure 2.6 and in the upper right corner of the panels. Figure 2.10 compares the western (more Atlantic) with the eastern (more continental) part of GAR. Figure 2.11 shows the difference series between the northern (temperate westerlies) and the southern (Mediterranean) parts and Figure 2.12 compares the 4 combined low-elevation subgroups with the sample 'HIGH'.

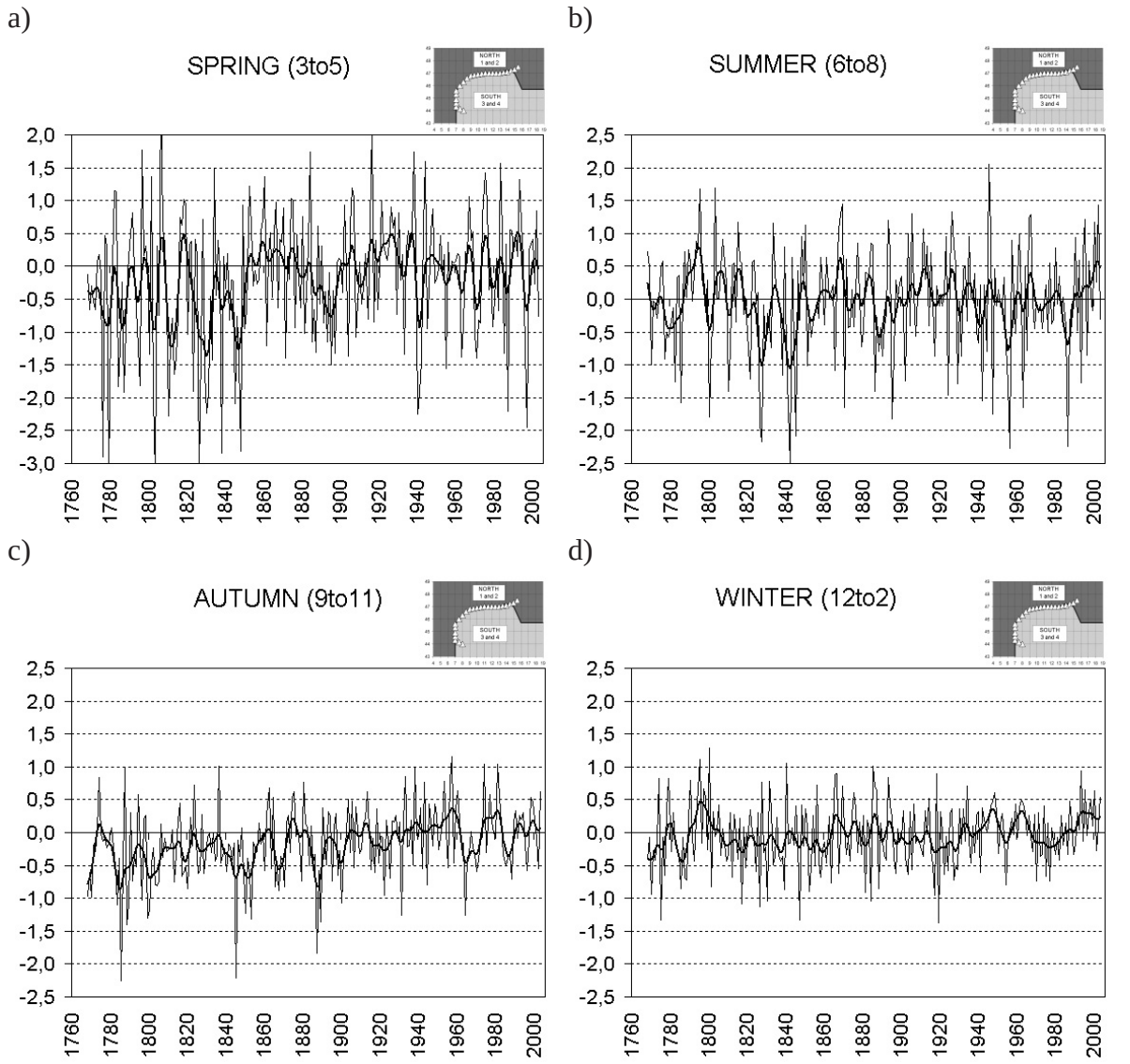

Figure 2.11: Seasonal 'super-subgroup difference series' NORTH minus SOUTH (Temperate versus Mediterranean; sketch of the regions is displayed in the upper right corner of the panels) 1768 to 2003; a) to e) seasons throughout the year; shown are single years and 11-year low-pass filtered curves.

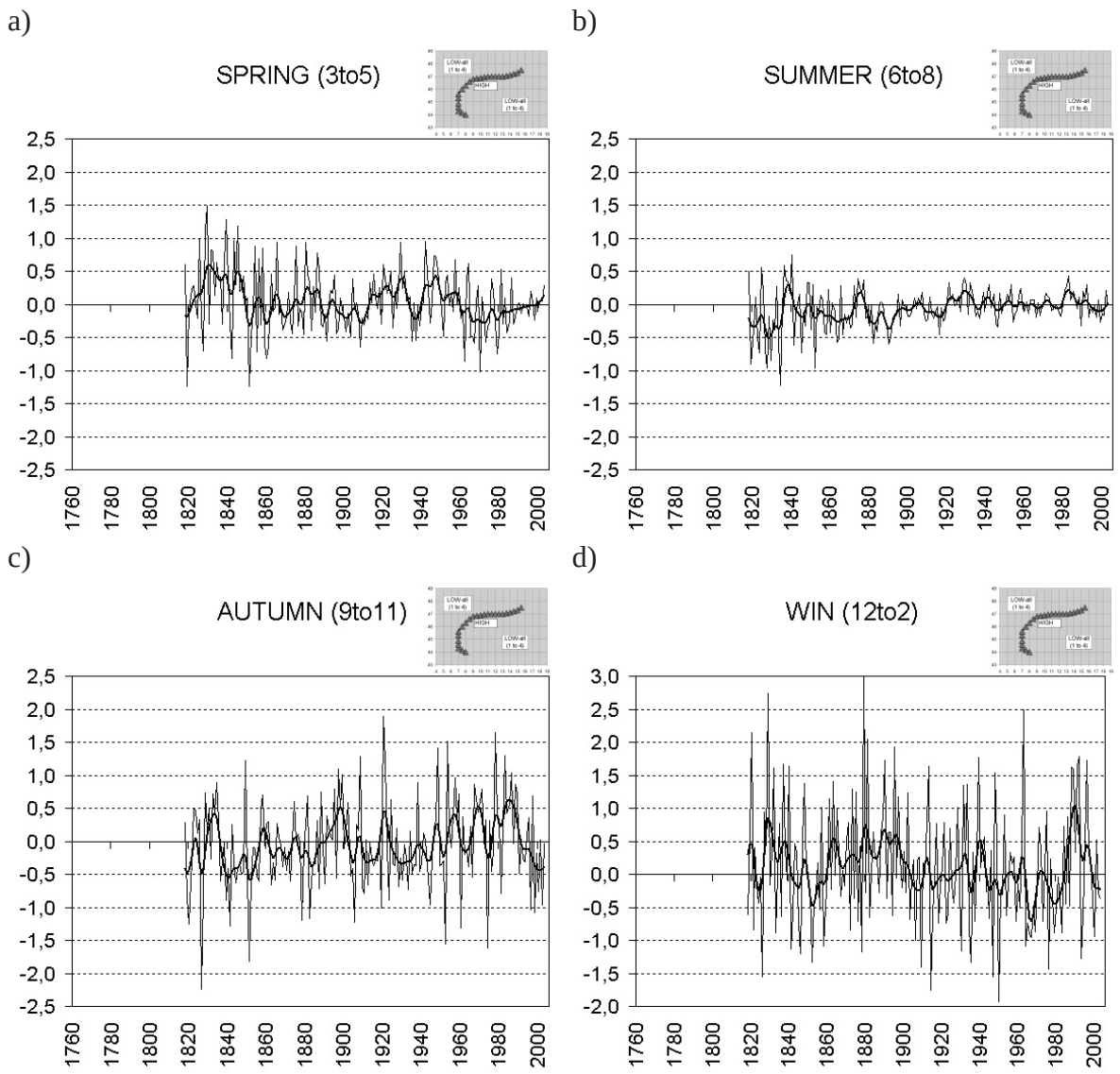

Figure 2.12: Seasonal 'super-subgroup difference series' HIGH minus LOW (Alpine summits and saddles versus low elevation sites; sketch of the regions is displayed in the upper right corner of the panels) 1818 to 2003 a) to e) seasons throughout the year; shown are single years and 11-year low-pass filtered curves.

With a few exceptions at time scales shorter than several decades the general result of the analysis of the low-elevation difference series (Figures 2.10 and 2.11) is the non-existence of long-term trends. Neither the visible shorter deviations from zero, nor the apparently lower N-S-autumn level of the 19th versus the 20th century (Figure 2.11c) are significant. Due to the relatively high interannual variability, they remain insignificant at even lower trend to noise ratios (TNR) below 1 in most, below 2 in all cases (also those not shown here).

West-East differences are in general less distinct in GAR than those of North-South. This is obviously a result of the existence of the predominantly zonal barrier of the Alps that tends to intensify meridional climatic gradients and exerts less influence on zonal ones. The W-E difference series are similar for all seasons whereas the N-S comparisons show a pronounced annual cycle with the strongest meridional gradients in spring and summer and significantly

weaker ones in autumn and winter. The latter are comparable to the zonal gradients whereas the former are approximately twice as large and range from -3 to +2 deg. An even more pronounced annual cycle is present in the HIGH-LOW difference series (Figure 2.12). Here, the annual cycle is reverse to that of the North-South gradients. The strongest HIGH-LOW differences occur in winter closely followed by autumn. In the Alps these seasons exhibit a frequently occurring decoupling of a low atmospheric layer (<800m asl. in most cases) from the high elevations sites above 1500m caused by inversion layers in between.

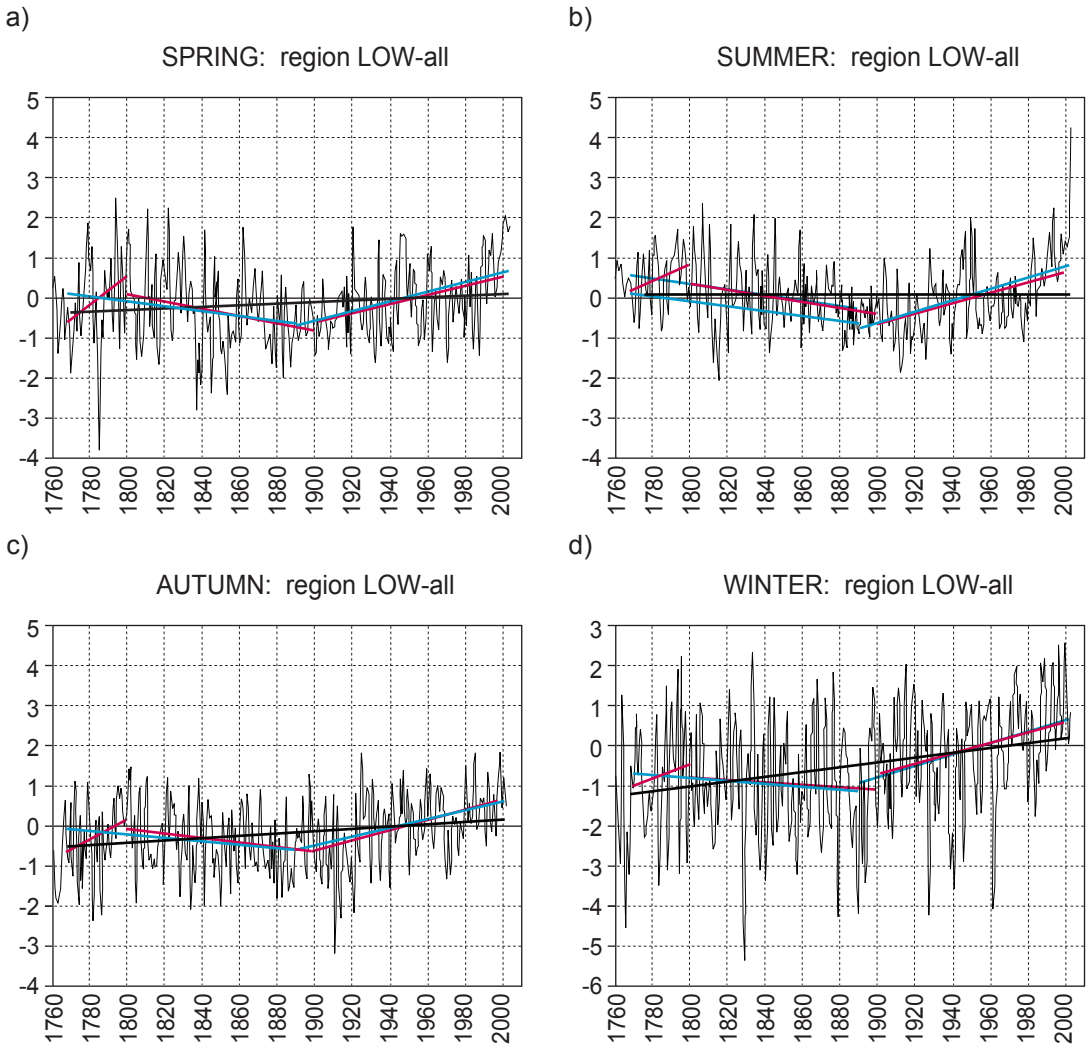

Figure 2.13: GAR-low-mean seasonal temperature evolution 1760–2003 and subregional linear regressions; blue: 2 sections (1768–1890, 1890–2003); pink: 3 sections 1768–1800, 1800–1900, 1900–2000); black: 1 section (1768-2003).

This causes a total range of (seasonal mean!) temperature differences HIGH minus LOW of 5 degrees in winter compared to one of less than 2 degrees in summer and less than 3 degrees in spring, which are the two seasons with much stronger vertical mixing and higher similarity of the low- and high elevation temperatures. Again, the already mentioned large interannual variability is also in this case the reason why e.g. two apparent long term trends in autumn and

winter (Figure 2.12c and d) are not significant. In autumn we see a slight long-term relative warming of the mountains versus low elevation and an opposite cooling in winter, but both at TNRs below 0.5 (for the 1840-1980 period). Only the following (1980-2003) relative cooling in Autumn of 1.0 deg in 23 years is slightly significant at a TNR-level of 1.5. If this trend keeps on in the future it is worth for further analysis.

So far our argumentation was mainly based on the qualitative discussion of time series of temperature and temperature differences and visual comparison of curves. To support the described findings some final quantitative trend analyses shall allow a final brief overview. Trend analysis always needs an a priori postulated definition of the time-intervals in question which should be adjusted to the actual course of long-term variability. The often used linear trends over the longest available time-span make sense in rare cases only.

Considering the long-term structure of the typical GAR-smoothed temperature curves shown and discussed in Figure 2.9 two different fragmentations were done. The first fragmentation breaks the whole timespan into two and the second one in three subintervals. In fact the courses in the different seasons would have afforded different segmentations for different seasons (and months). However, for the purpose of inter-seasonal comparisons the final decision was based on the annual means as the largest common intersection. The '2-section' partition uses the year 1890 as break point, the '3-section' case uses the years 1800 and 1900 as breaks. The latter is partly based on climate itself (which shows a trend-change before 1800 near to the parting year considered in the 2-section case) but also on pragmatic reasons to allow for comparisons with the often elsewhere used '20th century warming' trends.

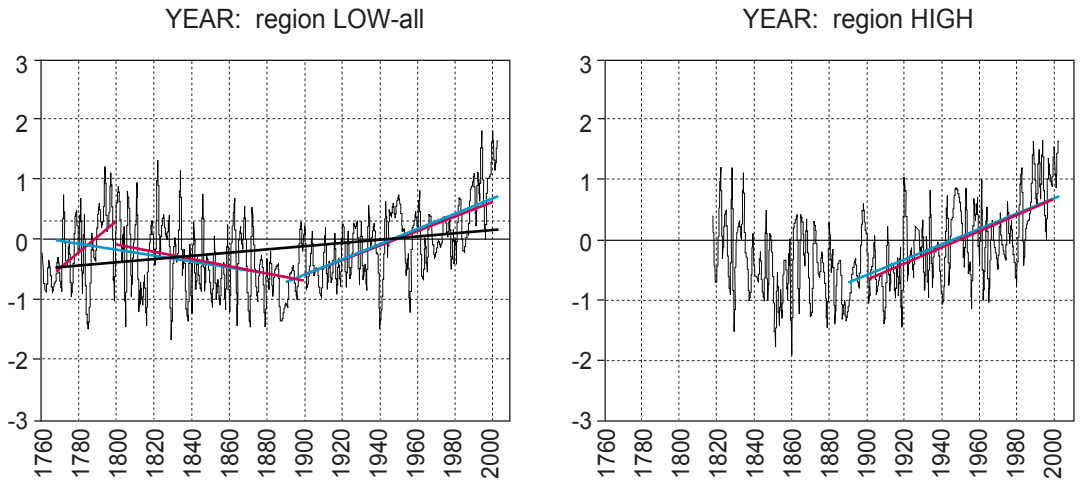

Figure 2.14: GAR-low (left) and HIGH (right) -mean annual temperature evolution 1760-2003 and subregional linear regressions (same sections as in Figure 2.13).

Figure 2.13 and Figure 2.14 illustrate and compare the respective 5 subinterval- and the overall temperature trend over the entire 1768-2003 period (which is the longest common period for all 4 low-elevation subregions). Figure 2.13 shows the GAR-all mean-curve and the linear regressions corresponding to the different temporal sections for all seasons, while Figure 2.14 depicts the curves of the HIGH and LOW means for the year as a whole (the latter only for the post 1890 subintervals).
Figure 2.15 shows the appendant monthly variations of the linear trends calculated for the 5 temporal sections and the total period calculated for all sub-regions throughout the annual cycle.

Tables 2.3 and 2.4 comprise the full range of calculated linear trends together with simple TNR-based (trend to noise) significance estimates.

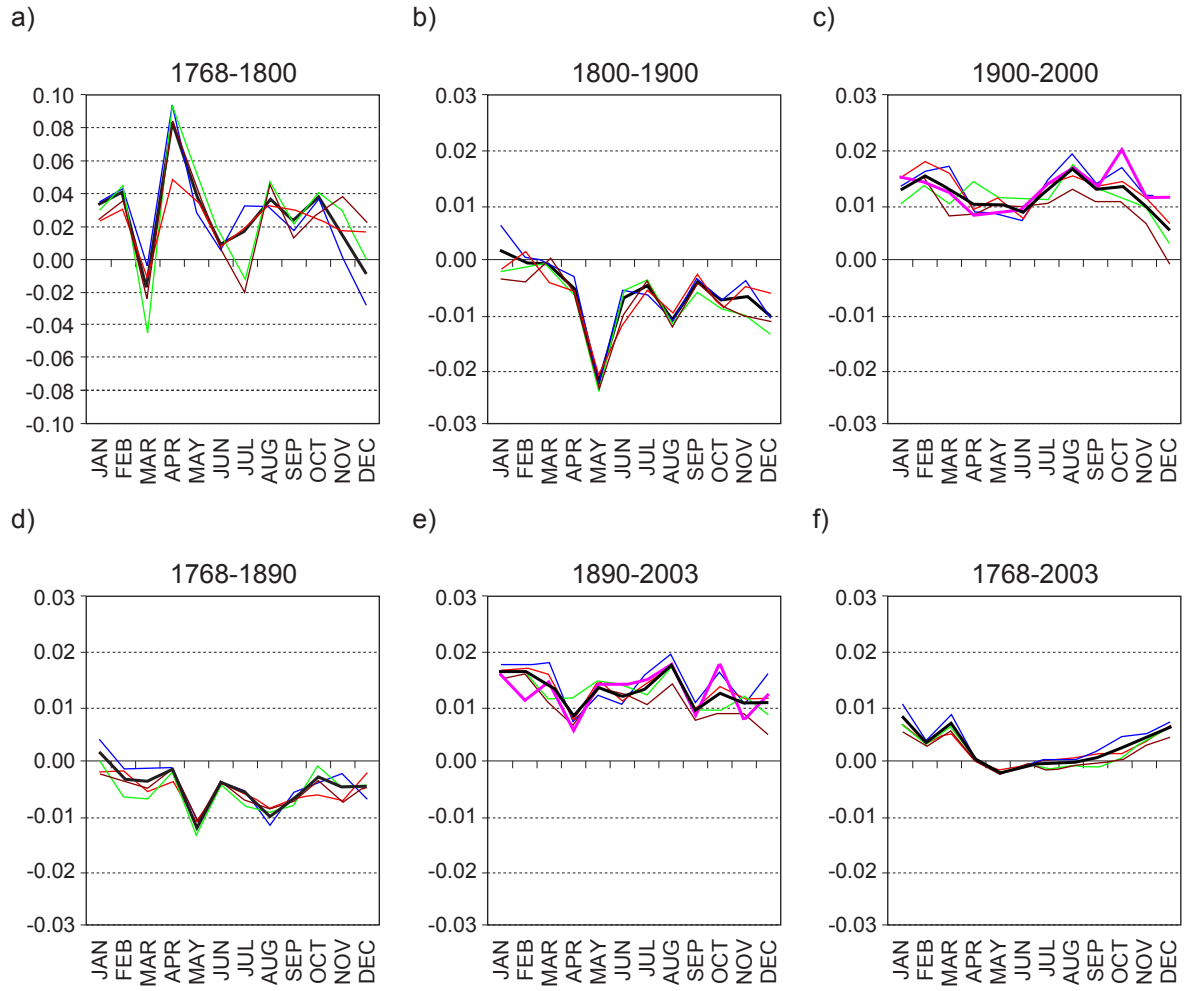

Figure 2.15: Monthly linear temperature trends in all sub-regions of GAR: a) 1768–1800, b) 1800–1900, c) 1900–2000, d) 1768–1890, e) 1890–2003, f) 1768–2003; Trends in centigrades/year; Note that 2.15a has a stretched ordinate; bold black: all GAR-low; bold pink: HIGH; blue: NW-SW; green: NE-E; brown: SE; red: SC.

The graphs make clear, that in spring and summer a subdivision into at least two intervals is absolutely necessary, as the overall trend, for instance, completely maskes the opposite subinterval trends (cooling in the first part, warming in the second). But also for autumn, winter and the annual course the two subsection composite is much nearer to the real variability features than the overall linear regression. The two versions of the break at 1890 or at 1900 do not make much of a difference although the 1890-version fits better. The two break-point version, with an additional subdivision at the year 1800, fits considerably better in all four seasons and for the year. On the other hand the shortness of the first pre-1800 subinterval complicates comparisons with the much longer other two sections (19th and 20th century) and also lets any detected trends vanish against the background of the strong inter-annual variability.

Table 2.3: Monthly based linear trends during different temporal segments and their significance.

	2 NW-SW	4 SC	1 NE-E	3 SE	5 HIGH	1 to 4 LOW-all
					deg / 32 years	
1768-1800						
JAN	1.12	0.75	0.97	0.77		1.07
FEB	1.37	1.00	1.45	1.16		1.32
MAR	-0.12	-0.35	-1.42	-0.74		-0.55
APR	2.99	1.55	2.95	2.64		2.69
MAY	0.93	1.15	1.67	1.41		1.23
JUN	0.18	0.24	0.46	0.22		0.29
JUL	1.06	0.63	-0.38	-0.63		0.54
AUG	1.03	1.05	1.52	1.48		1.18
SEP	0.56	0.97	0.72	0.43		0.74
OCT	1.21	0.79	1.32	0.91		1.20
NOV	0.06	0.57	0.94	1.25		0.45
DEC	-0.90	0.53	-0.02	0.72		-0.27
1768-1890					deg / 123 years	
JAN	0.48	-0.27	0.01	-0.31		0.17
FEB	-0.18	-0.24	-0.82	-0.48		-0.42
MAR	-0.20	-0.71	-0.87	-0.65		-0.47
APR	-0.15	-0.48	-0.29	-0.17		-0.25
MAY	-1.54	-1.38	-1.69	-1.36		-1.54
JUN	-0.49	-0.54	-0.56	-0.47		-0.54
JUL	-0.72	-0.76	-1.02	-0.91		-0.76
AUG	-1.46	-1.08	-1.19	-1.11		-1.28
SEP	-0.75	-0.86	-1.02	-0.92		-0.86
OCT	-0.51	-0.78	-0.12	-0.45		-0.37
NOV	-0.29	-0.90	-0.62	-0.94		-0.61
DEC	-0.86	-0.29	-0.55	-0.56		-0.59
1768-2003					deg / 234 years	
JAN	2.45	1.68	1.65	1.27		1.95
FEB	0.98	0.97	0.77	0.66		0.87
MAR	2.05	1.25	1.56	1.33		1.67
APR	0.24	0.03	0.28	0.10		0.18
MAY	-0.50	-0.29	-0.45	-0.41		-0.44
JUN	-0.12	-0.07	-0.07	-0.13		-0.10
JUL	0.15	0.03	-0.25	-0.33		-0.03
AUG	0.09	0.18	-0.11	-0.13		-0.01
SEP	0.50	0.39	-0.24	-0.02		0.18
OCT	1.11	0.42	0.24	0.10		0.60
NOV	1.26	0.93	1.14	0.75		1.09
DEC	1.73	1.58	1.46	1.10		1.52

	2 NW-SW	4 SC	1 NE-E	3 SE	5 HIGH	1 to 4 LOW-all
					deg / 100 years	
1801-1900						
JAN	0.66	-0.16	-0.17	-0.30		0.20
FEB	0.09	0.18	-0.10	-0.38		0.00
MAR	-0.03	-0.38	-0.07	0.07		-0.05
APR	-0.27	-0.55	-0.62	-0.58		-0.47
MAY	-2.27	-2.07	-2.36	-2.24		-2.23
JUN	-0.50	-1.09	-0.55	-0.97		-0.68
JUL	-0.60	-0.51	-0.32	-0.36		-0.44
AUG	-1.08	-0.94	-1.10	-1.19		-1.08
SEP	-0.31	-0.22	-0.54	-0.36		-0.37
OCT	-0.67	-0.85	-0.84	-0.80		-0.71
NOV	-0.34	-0.45	-0.97	-0.99		-0.63
DEC	-1.05	-0.57	-1.32	-1.10		-1.00
1890-2003					deg / 114 years	
JAN	1.99	1.86	1.70	1.70	1.77	1.82
FEB	1.98	1.91	1.78	1.78	1.26	1.87
MAR	2.03	1.79	1.28	1.17	1.63	1.59
APR	0.81	0.85	1.32	0.76	0.63	0.92
MAY	1.35	1.66	1.65	1.48	1.58	1.51
JUN	1.17	1.25	1.57	1.39	1.55	1.33
JUL	1.80	1.61	1.35	1.15	1.68	1.49
AUG	2.21	1.97	1.92	1.62	2.00	1.95
SEP	1.20	1.10	1.06	0.84	0.96	1.06
OCT	1.84	1.53	1.04	1.01	1.99	1.39
NOV	1.19	1.31	1.35	0.97	0.86	1.19
DEC	1.80	1.27	0.97	0.53	1.39	1.19
1901-2000					deg / 100 years	
JAN	1.36	1.52	1.03	1.32	1.53	1.30
FEB	1.63	1.83	1.39	1.50	1.42	1.57
MAR	1.73	1.60	1.04	0.82	1.25	1.31
APR	0.90	0.94	1.45	0.85	0.82	1.02
MAY	0.85	1.16	1.17	1.05	0.86	1.03
JUN	0.73	0.77	1.12	0.97	0.94	0.89
JUL	1.51	1.44	1.13	1.05	1.40	1.29
AUG	1.95	1.57	1.79	1.32	1.71	1.68
SEP	1.40	1.36	1.32	1.07	1.35	1.29
OCT	1.72	1.46	1.13	1.06	2.04	1.37
NOV	1.20	1.14	0.98	0.69	1.16	1.01
DEC	1.16	0.69	0.31	-0.10	1.16	0.56

Table 2.4: Seasonal based linear trends during different temporal segments and their significance (HY abbreviates 'half-year').

		2 NW-SW	4 SC	1 NE-E	3 SE	5 HIGH	1 to 4 LOW-all	
1768-1800	SPRING	1.25	0.77	1.08	1.11		1.12	deg / 32 years
	SUMMER	0.78	0.65	0.53	0.36		0.69	
	AUTUMN	0.57	0.80	1.05	0.91		0.80	
	WINTER	0.56	0.57	0.45	0.51		0.56	
	SUM-HY	1.09	0.94	1.15	0.91		1.10	
	WIN-HY	0.47	0.53	0.59	0.67		0.55	
	YEAR	0.81	0.74	0.80	0.75		0.82	
1768-1890	SPRING	-0.64	-0.86	-0.93	-0.71		-0.75	deg / 123 years
	SUMMER	-0.87	-0.79	-0.95	-0.83		-0.86	
	AUTUMN	-0.54	-0.82	-0.54	-0.72		-0.60	
	WINTER	-0.33	-0.41	-0.68	-0.67		-0.45	
	SUM-HY	-0.89	-0.86	-0.99	-0.85		-0.90	
	WIN-HY	-0.35	-0.61	-0.57	-0.63		-0.46	
	YEAR	-0.52	-0.69	-0.75	-0.73		-0.62	
1768-2003	SPRING	0.60	0.32	0.48	0.37		0.48	deg / 234 years
	SUMMER	0.06	0.04	-0.17	-0.22		-0.05	
	AUTUMN	0.94	0.60	0.42	0.30		0.63	
	WINTER	1.72	1.38	1.26	0.96		1.42	
	SUM-HY	0.03	0.04	-0.16	-0.17		-0.06	
	WIN-HY	1.59	1.11	1.14	0.85		1.27	
	YEAR	0.85	0.59	0.49	0.34		0.63	
1800-1900	SPRING	-0.86	-0.99	-1.00	-0.89		-0.91	deg / 100 years
	SUMMER	-0.71	-0.86	-0.68	-0.85		-0.73	
	AUTUMN	-0.43	-0.49	-0.76	-0.71		-0.55	
	WINTER	-0.16	-0.20	-0.64	-0.63		-0.34	
	SUM-HY	-0.86	-0.89	-0.94	-0.95		-0.89	
	WIN-HY	-0.28	-0.42	-0.68	-0.64		-0.44	
	YEAR	-0.51	-0.63	-0.74	-0.76		-0.61	
1890-2003	SPRING	1.40	1.43	1.42	1.14	1.28	1.34	deg / 114 years
	SUMMER	1.73	1.61	1.61	1.38	1.72	1.59	
	AUTUMN	1.41	1.31	1.15	0.94	1.27	1.21	
	WINTER	1.94	1.70	1.50	1.35	1.51	1.64	
	SUM-HY	1.42	1.40	1.48	1.20	1.38	1.38	
	WIN-HY	1.80	1.61	1.37	1.19	1.49	1.51	
	YEAR	**1.61**	**1.51**	1.41	1.20	1.44	**1.44**	
1900-2000	SPRING	1.16	1.23	1.22	0.90	0.97	1.12	deg / 100 years
	SUMMER	1.40	1.26	1.35	1.11	1.34	1.29	
	AUTUMN	1.44	1.32	1.15	0.94	1.52	1.22	
	WINTER	1.54	1.48	1.09	1.10	1.47	1.31	
	SUM-HY	1.22	1.20	1.33	1.05	1.16	1.20	
	WIN-HY	1.54	1.44	1.06	1.00	1.47	1.27	
	YEAR	**1.34**	**1.30**	1.15	0.96	1.31	1.19	

The main message of Table 2.3 and 2.4 is the absolute sparseness of significant trends. No single monthly trend surpasses the TNR-ratio of 2 (standing for a linear change within the subinterval greater than 2 sample standard deviations which is a 95.45% range). Only the 1890–2003 and the 1900–2000 warming in the two western subregions and the respective all GAR-low warming for 1890–2003 is significant versus the TNR-2 threshold. In the case of cooling just one linear negative monthly trend (May, 1890–1900) is significantly negative ($1<TNR<2$). Weak significant coolings are also present in some subregional spring and summer series of the 19th century. Some weak significant warmings can be found in spring- and summer months during the 20th century and for most of the seasonal, half-annual- and annual 20th century series. The visually strong warming in the short 18th century section (as mentioned before) is only weak significant during the summer half year and the year as a whole (due to the reduced interannual variability in the warm season and for the annual average).

Therefrom, the following conclusions can be drawn from the findings of the regionalisation attempts of temperature variability and trends:

- temperature variability is spatially highly similar in the entire study region. Hence, it is very likely that GAR temperature represents an even larger region as for example Central Europe;
- temperature variability shows considerable differences on the monthly and seasonal scale;
- most of the visible long term trends are statistically not or only weakly significant due to the still existing strong interannual variability. Although a great number of single series have been used for the subregional and regional samples, averaging has not considerably reduced the variance compared to single series;
- the subdivision into 2 sections before and after the year 1890 is a good fit for linear detrending (which is the basis for the following study).

Chapter 3

Large scale climate data generated with ECHO-G

The main purpose of this Section is to give a brief description of the generation of the model data and the climate model itself. The model dataset is the large scale counterpart to the regional scale GAR dataset and hence, is an essential part of the study. To allow the present study for rudimentary being self-contained we decided to mention some short parts of Wagner (2004) here, which form a basis necessary to understand further matters.

A sketch of the solar and volcanic forcing is followed by a brief description of the model and the conducted experiments.

3.1 Reconstructions of solar and volcanic forcings

The solar irradiance and the effect of volcanic eruptions have been derived from the reconstructions of past net solar forcing (Crowley 2000). The forcing was reconstructed from concentrations of ^{10}Be in ice cores spliced to historical observations of sun spots (Lean and Rind 1999). The difference in the total solar irradiance between present values and the Late Mounder Minimum (LMM) is 0.3%. This is well within the range of other different solar reconstructions (cf. Bard et al. 2000).

The volcanic effects on the optical density of the stratosphere was estimated by an empirical model. This model links observations of radiative forcing changes in recent volcanic eruptions with acidity changes in ice cores (Robock and Free 1996). The uncertainty in this reconstruction has been estimated to be about 50% (Hegerl et al. 2003). A more detailed description of the reconstruction of the solar and volcanic forcings can be found in Wagner (2004).

As we will pay attention to periods affected by volcanic activity it appears worthwhile to briefly touch the involved mechanism. Figure 3.1 schematically displays the coaction of incoming solar radiation, outgoing infrared emissions and sulfur aerosols caused by volcanic sulfur ejected into the stratosphere.

To illustrate the effects of explosive volcanism on climate Figure 3.1 shows a schematic diagram. The most important effect is on solar radiation. Since the sulfate aerosols are about the same size as visible light they strongly interact with solar radiation by scattering. Part of the sunlight is backscattered increasing the net planetary albedo and reducing the amount of solar energy that reaches the Earth's surface. This backscattering is the dominant radiative effect at the surface and results in a net cooling. A large portion of the solar radiation is forward scattered, resulting in enhanced downward diffusive radiation compensating for the large reduction

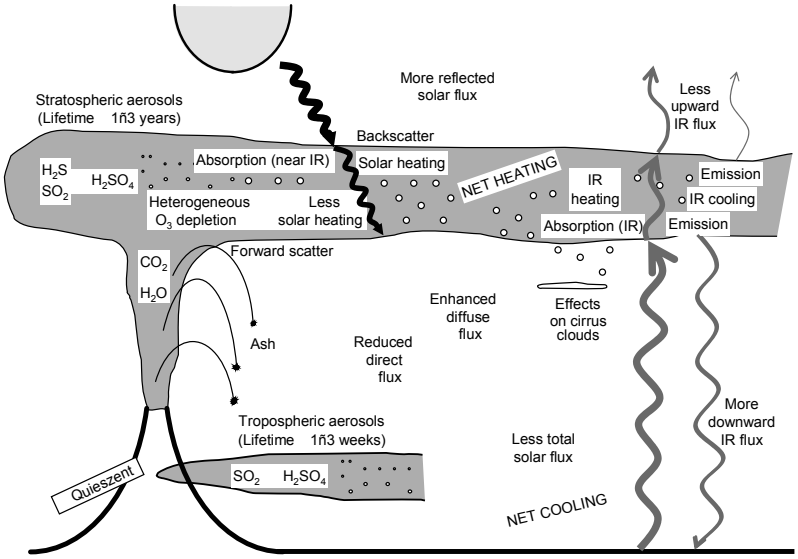

Figure 3.1: Schematic diagram of volcanic inputs into the atmosphere and their effects on the balance of radiation. (*Source*: Robock 2000)

in the direct solar beam. However, in the stratosphere the sulfate aerosols also absorb some of the near infrared sunlight. This leads to a net heating of the stratosphere (Robock 2000). The net effect of explosive volcanism is thought to be a cooling of global near surface temperatures (Robock and Mao 1995), but regional deviations might occur, particularly in winter. Graf et al. (1993) analyzed the Pinatubo eruption in 1991 in terms of winter climate effects by means of the global climate model ECHAM2 forced with stratospheric aerosols. Within their perpetual January simulations they find a dynamical atmospheric response with a stronger polar night jet in the Northern Hemisphere extending into the lower troposphere. This results in higher near surface temperatures in Eurasia and North America, which is consistent with observations. Dynamically this mechanism can possibly be related to the differential heating caused by the stratospheric sulfate aerosols leading to an increased speaks of the mild-winter cool-summer phenomena in the aftermath of volcanic events. This implies an influence of the atmospheric dynamics on temperatures in winter and an influence of the direct radiative forcing in summer (Robock and Free 1996).

3.2 Model description

The climate model ECHO-G (Legutke and Voss 1999) is a coupled Atmosphere-Ocean General Circulation Model (AOGCM) consisting of the atmospheric model ECHAM4 (Roeckner et al. 1996) and the ocean model HOPE (Hamburg Ocean Primitive Equation model; Wolff et al. 1997). ECHO-G also includes a dynamic-thermodynamic sea-ice model with snow cover Hibler (1979) (Marsland et al. 2003).

The 4th generation atmospheric general circulation model (ECHAM4) was developed at the Max Planck Institute for Meteorology (MPI) in Hamburg. It is one in a series of models originally evolving from the spectral weather prediction model of the European Center for Medium Weather Forecasts (ECWMF). This version has still many features in common with the current ECWMF model. However, to apply the model to climatic issues some of the physical parameterizations have either been replaced or modified.

The ECHAM4-model is based on primitive equations. The prognostic variables are vorticity, divergence, logarithm of surface pressure, temperature, specific humidity, mixing ratio of total cloud water and optionally a number of trace gases and aerosols. The vertical extension is up to a pressure level of 10 hPa, which corresponds to a height of approximately 30 km. A hybrid sigma-pressure coordinate system is used with 19 irregularly ordered levels and with highest resolution in the atmospheric boundary layer. The bottom level is placed at a height of about 30 m above the surface corresponding approximately to the surface layer. In this study the ECHAM4 model has a horizontal resolution of about 3.75° lat x 3.75° lon.

The ocean model HOPE (Hamburg Ocean Primitive Equation) is an ocean general circulation model (OGCM) based on primitive equations with the representation of thermodynamic processes. It is a non-eddy resolving circulation model. HOPE-G has a horizontal resolution of approximately 2.8° lat x 2.8° lon with a grid refinement in the tropical regions from 10° N to 10° S. This meridional grid refinement reaches a value of 0.5° at the equator allowing for a more realistic representation of ENSO (El Niño Southern Oscillation) variability in the tropical Pacific Ocean (Marsland et al. 2003). The ocean model has 20 vertical, irregularly ordered layers. To get an impression of the model resolution, Figure 3.2 shows the land-sea mask of ECHAM4 (a) and the interpolated HOPE-G (b) model. Time stepping is 24 minutes for dynamics and physics, except for radiation which is calculated at 2-hour intervals. The state of the ocean is retrieved once per day.

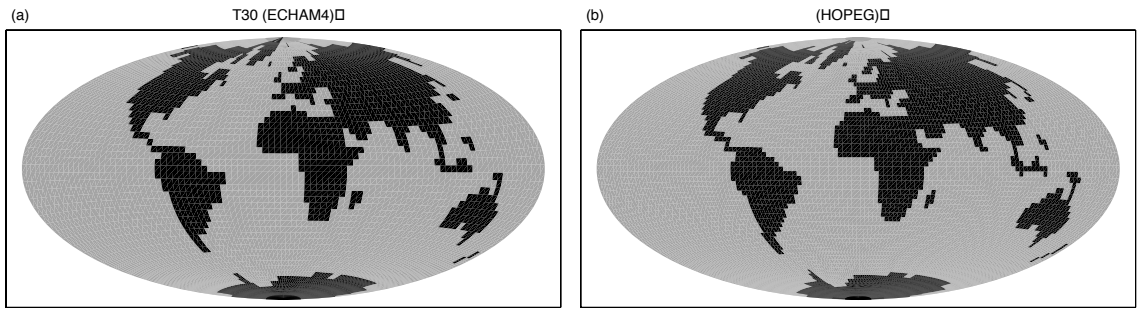

Figure 3.2: Land-sea mask of the atmosphere model ECHAM4 (a) and the ocean model HOPE-G (b). Note the coarse resolution e.g. for the European continent.

The coupling as well as the interpolation between the atmosphere and the ocean model is controlled by the coupling software OASIS (Terray et al. 1998). Concerning the coupling dynamics, at a distinct frequency the atmospheric component of the model passes heat, fresh water and momentum to the ocean and gets information about surface conditions of the ocean. This frequency is equal for all exchange fields and describes a 'coupled time step'. The fields that are exchanged are averaged over the last coupled time step.

Further aspects of the exchange processes are flux corrections due to the interactive coupling between ocean and atmosphere in order to prevent climate drift. These heat- and freshwater fluxes were diagnosed in a coupled spin-up integration. Accordingly, the sea-surface-temperature and sea-surface salinity were restored to their climatological observed values. This flux adjustment is constant in time and its global average is zero (Zorita et al. 2004).

A critical issue concerning climate drift is the amount of flux corrections applied in climate models, often taking values of the same order than the fluxes themelves. Flux corrections are especially high at the sea-ice water boundary as well as in regions of vertical convection. and they are introducing new uncertainties (Cubasch et al. 1995).

An important point related to climate model experiments is the sensitivity of the climate

model. That is, for instance, the climatic reaction to a particular rate of change in external forcings. The sensitivity of the ECHO-G model is located in the middle of the range given by the IPCC simulations with a 1% annual increase of atmospheric greenhouse gases. Within these climate change experiments the sensitivity of the ECHO-G model is 1.70 K at the doubling of the present CO_2 concentrations. Accordingly, the sensitivity of the ECHO-G model to changes in the radiative forcing is consistent with that of other models (Zorita et al. 2004).

The above mentioned sensitivity is not related to the equilibrium temperature. The estimation of the equilibrium temperature based on Tahvonen et al. (1994) for doubled CO_2 (equivalent, relative to 1990 levels) concentrations yields plus 2.88 K for the global averaged temperature with upper and lower 95% confidence intervals of 1.14 K and 4.61 K, respectively. This result compares even better to the sensitivity range suggested by the IPCC which is located between 1.5 K and 4.5 K with a 'best guess' sensitivity of 2.5 K (Houghton et al. 2001).

3.3 Experimental setup

In order to investigate the influence of different external forcings on climate, three different experiments with the climate model ECHO-G were undertaken. The basis of all experiments is a historical simulation with the same climate model, starting in the year 1000 (González-Rouco et al. 2003), hereafter being called 'HIST' or 'a01'. This simulation is forced with variable solar and volcanic output as well as with changes of greenhouse gas concentrations concerning CO_2 and CH_4. The CO_2 and CH_4 concentrations were derived from trapped air in Antarctic ice cores (Etheridge et al. 1996).

In this study the volcanic forcing is not directly introduced into the climate model. The major reason for this is the poorly represented stratosphere within this version of the climate model. However, in order to account for the volcanic activity, the optical depth of the sulfuric aerosols is translated into a so called 'effective solar constant'. The rationale behind this approach is the already mentioned net-cooling effect of volcanic aerosols illustrated within Figure 3.1. Accordingly, the peaks within the curve in the upper right panel of Figure 3.3 represent the effect of the volcanic eruptions, while the slow variations signify the changes in the solar output. A close inspection of the solar curve also resolves the 11-year solar Schwabe cycle.

One of the fundamental shortcomings of this approach is the disregard of the latitude-specific impact and influence of the volcanic aerosols. Thus, the whole globe receives a reduced amount of solar insolation independent of the latitude of eruption. Another shortcoming is the unresolved temporal eruption date within the annual cycle.

The further shortcoming may be overcome in the future by the use of a newer dataset Robertson et al. (2001) including a latitude-specific resolution. In spite of the different reconstruction approaches the globally averaged aerosol optical depths coincide quite well. However, different results can be obtained through the conversion into a short-wave radiation forcing, depending on the treatment of large eruptions.

The first experiment, denoted 'NV' (no volcanoes), is forced without any volcanic impact, only with the solar forcing and a variable CO_2 and CH_4 forcing (cf. Figure 3.3, left column). This experiment is most similar to that of Cubasch et al. (1997) and Cubasch and Voss (2000) but uses a different version of the atmospheric and oceanic climate model.

In the second experiment, denoted 'SC' (sun constant), the model was driven by volcanic forcing and atmospheric trace gases. The solar irradiance was held constant at the level of 1364.56 W/m^2. This corresponds to our mean value of the period 1790–1830 (Figure 3.3,

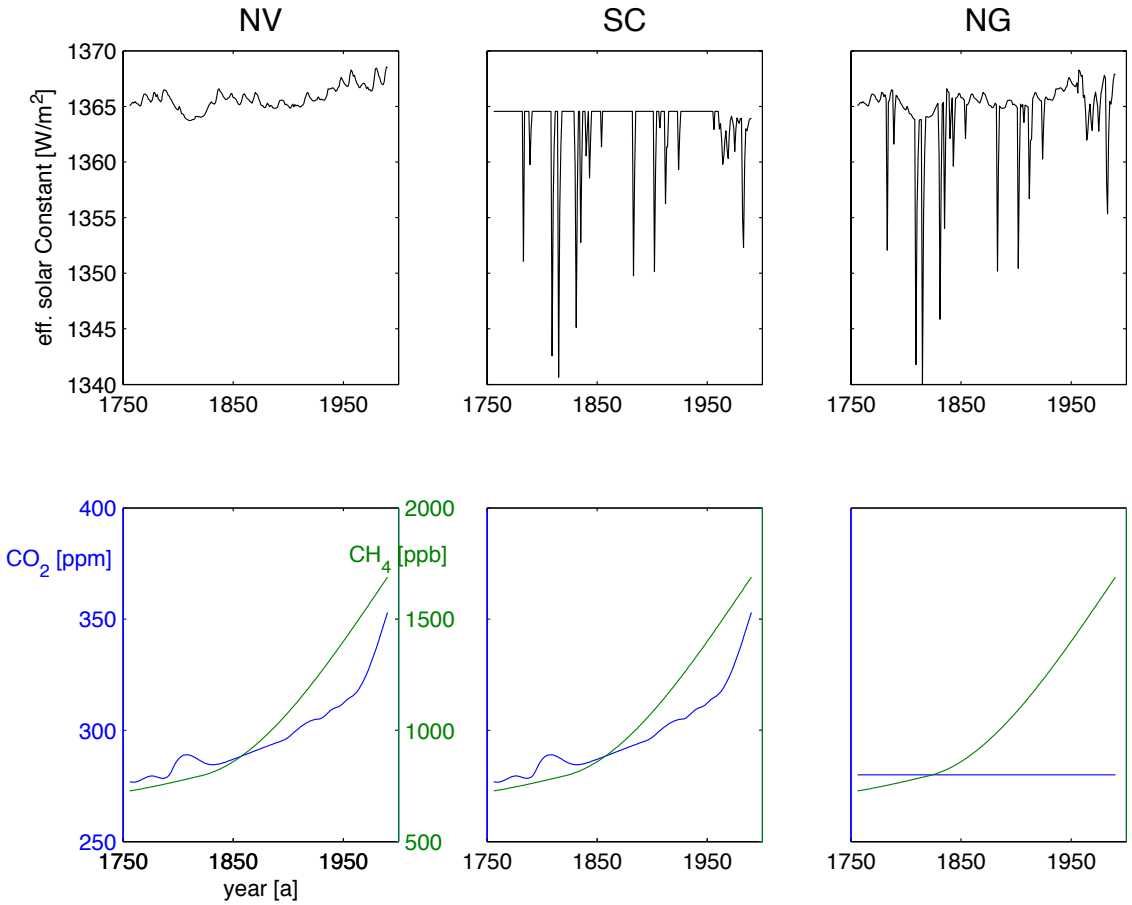

Figure 3.3: Different forcings applied on ECHO-G. The NV experiment is only forced with solar variability (left column). The SC experiment is forced with volcanic influence and the mean solar constant of the Dalton Minimum (middle column). The NG experiment is forced with both solar and volcanic variability but with constant CO_2 concentrations at 280 ppm (right panel).

middle column).

The third experiment, denoted 'NG' (no greenhouse gas CO_2 increase), addresses on the rising CO_2concentrations at the beginning of the 19th century. The CO_2concentrations are kept at a constant pre-industrial level of 280 ppm throughout the whole integration. Furthermore, the CH_4 concentrations were not kept constant, as the emphasis was on the effect of CO_2. This experiment is externally forced with the variable output of solar and volcanic activity (cf. Figure 3.3, right column).

For each of these setups (SC, NG, ..) three simulations have been carried out. For the first set of simulations the initial conditions were exactly the same as those simulated in HIST in year 1755 (indicated by a blue star and numbered by 1 in Figure 3.4). Accordingly, these simulations are a continuation of HIST with different forcings from year 1755 onwards. Besides these simulations Wagner (2004) has carried out two further sets of simulations, which have been initialized with different conditions for the atmosphere and the ocean taking care that the mean global temperature of the years, corresponding to these conditions, is similar to the HIST temperature simulated in 1755. The chosen years are located in the second half of the 16th century and are indicated by red and green stars and numbered by 2 and 3 in Figure 3.4. The

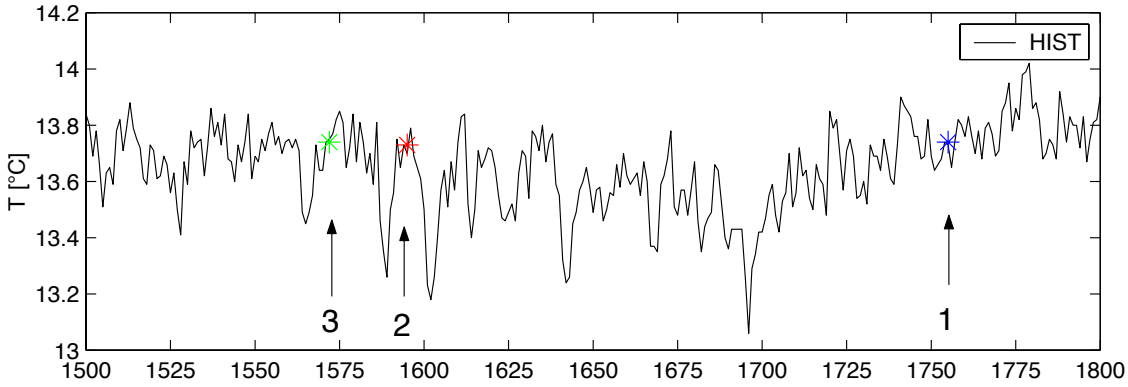

Figure 3.4: Mean global near surface air-temperatures for the a0 experiment and initial conditions taken to initialize different sets of simulations.

atmosphere-ocean conditions pertaining to these years were used to initialise ECHO-G which was started a few decades before 1756, the beginning of the simulations.

Within the present study we concentrate on the first set of simulations, which is in continuitation to HIST (González-Rouco et al. 2003). Hence, these simulations develop from a climate experiment that is already several centuries 'on the way'. This choice is motivated by the intended purpose of the present study – the investigation of special periods in GAR during the past 250 years. And because some of these periods are located in the 18th and 19th century, relatively close to the beginning year 1756, we have chosen those simulations where ECHO-G had plenty of time for the adjustment of the different components of the climatic system.

Chapter 4

Detection of 'outstanding periods' within GAR

This chapter is devoted to the detection of outstanding periods within GAR during the last 250 years. The investigation is based on temperature since temperature is, compared to precipitation, even in space and hence temperature measured within GAR is likely to be representative for an even larger region. As shown in Chapter 2, regional differences, which can be large on a seasonal or annual scale, gradually disappear on a multi-annual scale. So it is reasonable to expect GAR temperature on a multi-annual scale to be a good estimator for Europe's temperature. Thus, outstanding periods detected from GAR temperature are likely to stand for Europe too.

The detection and definition of outstanding periods within the first part of this chapter is based on two approaches: on the mean evolution of a long term subset of stations being representative for GAR and on the fraction of stations that show significantly different values as a function of time. The second approach is based on all reporting stations. The second part of the chapter is devoted to the temporal behaviour of Alpine glaciers since 1760, which is known from the literature. The reason for the involvement of Alpine glaciers is that they constitute an independent record of past climatical conditions for GAR. It turns out that periods of glacier advances and retreats are in good agreement with outstanding temperature periods, although the mass balance of glaciers is triggered by many more parameters than temperature alone.

4.1 Objective detection of outstanding periods

To find outstanding periods we have investigated the *classical* seasons as well as *moving* seasons, which are periods of any three successional months, not fixed to the usual winter (DJF), spring (MAM), summer (JJA) and fall (SON) scheme. For brevity, figures and tables often refer to winter, summer and the whole year (YAR). However, detection of outstanding periods rely on findings derived from all seasons – classical and moving seasons.

As already elaborated in Chapter 2 the density of reporting stations is increasing in time towards the end of the 20th century. Hence, there are stations whose observation period refers to the whole period, while other stations refer to significantly shorter periods. Therefore, anomalies derived from station averages are not comparable for stations that report since the beginning of the whole period and others that start many decades later. One way to achieve comparability between stations is to take into account only those stations that cover a period of time not much shorter than whole period. Such a subset of long-term stations has to allow for a reasonable coverage of GAR. Figure 4.1 (first row, left panel) shows the distribution of stations that start to

report before 1800. Further enlargement of this subset of stations would imply to wait about a decade for the next station to enter but, this station and the ones that would follow, do not allow for a significantly better coverage of GAR. Hence, it was decided to restrict ourselves to 16 stations. As elaborated in detail in Chapter 2, temperature variability within different sub-regions (see Figure 2.5) of GAR becomes increasingly the same on an extending timescale. Using this finding together with the reasonable coverage of GAR by the long term stations it is very likely that the long term subset accurately describes GAR temperature variability on a multi-annual to decadal timescale.

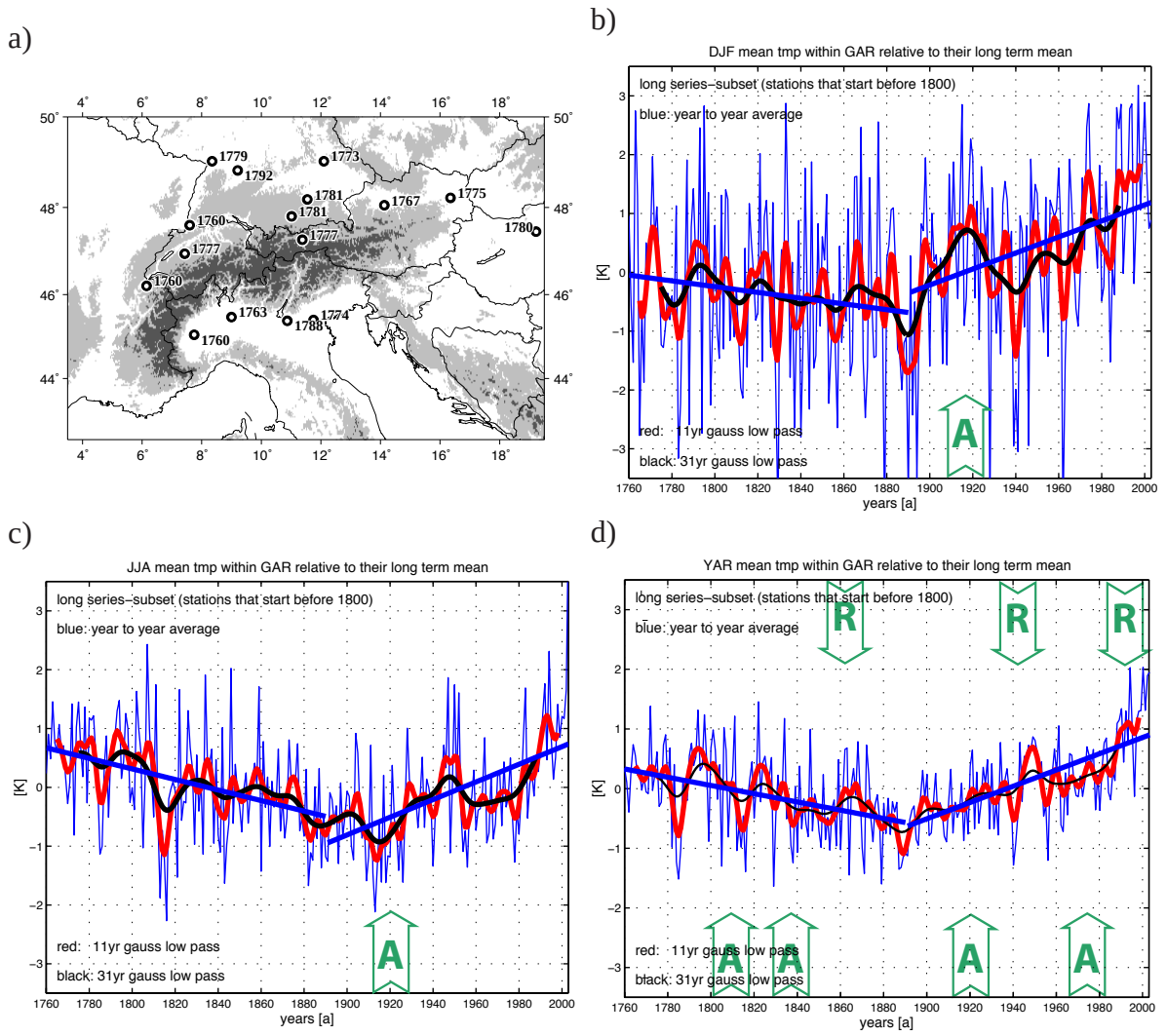

Figure 4.1: *first row, left panel*: Location of stations that start to report before 1800 together with starting years. Note that the distribution of the stations constitutes a reasonable coverage for GAR. *first row, right panel*: Evolution of mean winter (DJF) temperature; *2nd row, right and left panel*: the same for summer (JJA) and year (YAR), respectively; Up- or downward directed arrows indicate phases of advancing or retreating Alpine glaciers.

Panels b) to d) in Figure 4.1 comprise temperature curves relative to the temporal mean of the total observation period and spatially averaged over the long-term subset during winter, summer and the year as a whole. The removal of the temporal mean assures that there are no artificial effects introduced into further analysis caused by stational altitudes. It can be seen

from the panels that there is a negative trend during the 19th century and a positive one during the past century. This is very clear for winter and the whole year and somewhat staggered to later times (the 1930s) in the case of summer. This segmentation into two periods is explicitely discussed and compared to segmentations into three parts and no segmentation in Chapter 2 (see e.g. Figure 2.13). There it was found that the subdivision as shown in Figure 4.1 is appropriate.

Expectedly, temperature variability is largest for winter and there is a constant alternation of warm and cool periods on a multi-annual to decadal timescale (called special periods within this study). Up- and downward directed arrows indicate periods of advancing and retreating Alpine glaciers, respectively. These glacial periods are in accordance with special temperature periods, although this is not necessarily the case. The 1920s, for instance, constitute such an exception. Relatively cool summers and mild but wet winters have led to advancing Alpine glaciers (indicated in panels b and c), however no counterpart can be found in the annual temperature curve c). Glacier behaviour during the 19th and 20th century will be discussed in Section 4.2.

Regarding the temperature leap at the outgoing 20th century (the so-called 'second leap'), the period from 1885 to 1920, that comprises minimum temperature values of DJF, JJA and YAR, is sometimes called the 'first temperature leap'. As shown in the panels this 'first leap' is most prominent in winter. This is different from the 'second leap', which is prominent in all classical seasons, although there are also months showing almost no increase of temperature (see the analysis in Chapter 2, in particular Figure 2.7).

These ups and downs indicate special periods, but as there are so many of them another constraint, is claimed for. This constraint deals with the fraction of stations that show significant different values than on average and will be described in detail below. Curves shown in Figure 4.1 are spatial averages and hence, they do not tell much about the fraction of stations that is actually warmer or cooler than on average. To retrieve information about the spatial extent a further approach is applied. This approach is based on the whole dataset after the trends based on the long term subset have been removed. As already elaborated above, Figure 4.1 shows that there are two periods within the total observation period which contain contrary linear trends. The exact length of these two periods vary from season to season and because there are many seasons (moving and classical) it was decided to define the edges of the two periods for all seasons in the same way. A detailed discussion and comparison of different ways how to remove trends from this dataset is given in Chapter 2. The first intercept was defined from the very beginning to 1890 and the second from 1891 to the end of the observations. Then, for each season the trends in these periods are calculated and subtracted from the observations. For all seasons the fraction of reporting stations that show significant temperature deviations from the long-term averages of the detrended curves is calculated as a function of time (see Figure 4.2). In doing so, eleven year sub-samples are drawn from the detrended dataset and are moved at 1-year steps throughout the whole period. For each of these sub-samples averages and variances are derived station-wise and compared to those of the whole period.

A multi-annual period, in which a large fraction of stations show significant positive or negative deviations relative to their long-term mean values, is called an 'outstanding period'. This claim for a multi-annual sequence exhibiting a large faction of stations that show significant deviations from their long-term detrended means, is the added constraint.

The results shown below in Figure 4.2 refer to the 0.9 level of confidence. So, sub-sample averages are counted only, if they are located outside of the 0.9 confidence level, within the critical region, where the hypothesis that the averages of the sub-sample are indistinguishable from the averages of the total, detrended observation period, has to be rejected. Once more, compared to Figure 4.1 Figure 4.2 provides additional information as it tells about the fraction

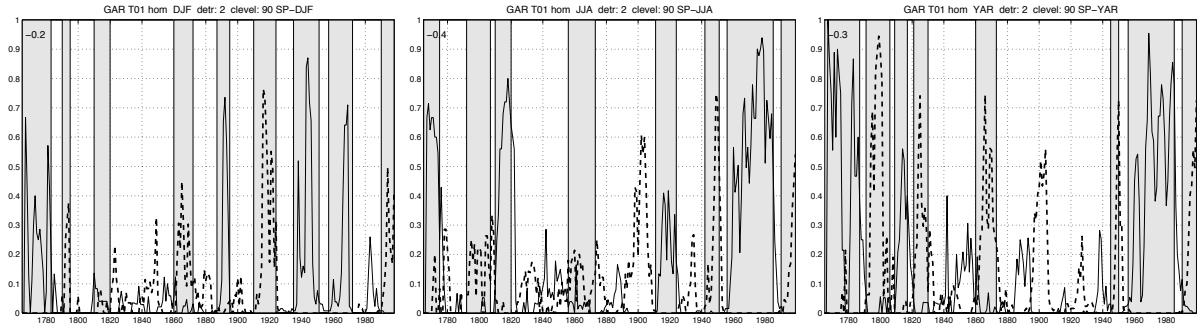

Figure 4.2: Fraction of stations that show a significantly lower/higher average values than their long-term mean (trends are removed). *x-axis*: years [a], *y-axis*: fraction of stations; *solid/dashed* lines indicate significantly *lower/higher* values; significance level 0.9; *from left to right*: winter, summer and year. Shading indicates outstanding periods.

of stations actually reaching significant high or low values. Thereby it adds to results of Figure 4.1. During winter, for instance, Figure 4.1 (first row, right panel) shows low temperatures from 1810 to 1820. Figure 4.2 on the other hand, points out that this feature is not shared by a large fraction of stations. So, from the definitions given above this DJF-period is 'special' but not 'outstanding'. Shaded intervals of time in Figure 4.2 indicate 'outstanding' periods. There are different periods for winter, summer and the whole year and their choice is not only based on classical seasons shown in the panels but also on surrounding, moving seasons. To elucidate this approach we state an example. During the 1860s, for example, in JJA (Figure 4.2, middle panel) the fraction of stations that show high temperatures is not very large. However, this period is selected as an 'outstanding' period because it shows a substantially larger fraction during other moving seasons that contain summer-months (so-called summer-near season). These are AMJ (April-May-June) to ASO (August-September-October). Figur A.1 presents results for all (classical and moving) periods can be found in the Appendix A. However, most of the winter, summer and yearly 'outstanding periods' are sufficiently motivated by Figure 4.2. Based on these findings the following periods of time, which will be discussed below, are identified as 'outstanding' periods.

Table 4.1 contains ten 'outstanding' periods. Some of them are to be found in all seasons all year round, showing the same feature while others show opposite behaviour during summer and winter. Few of them occur only during a few of the seasons. There is a period at the beginning of the 20th century, most prominent in summer (Figure 4.2), which is not listed in the Table, as it is caused by the way we have detrended the observations (see Figure 4.1). In summer the minimum of the total observation period is reached later than 1890 (the border between the two sub-periods in which the total observation period was split). Hence, the deviations in summer at the beginning of the 20th century are overestimated. The last period, that starts in the early 1990s will not be further investigated here as it lies outside the temporal range of the ECHO-G model simulations which end in 1990 (see Chapter 3).

The first four periods in Table 4.1 are part of the so-called Little Ice Age (LIA), which extends from the middle of the 15th to the middle of the 19th century (Mann et al. 1998; Jones et al. 1998). Seen from a hemispherical point of view, LIA has to be considered as a period of modest cooling of the Northern Hemisphere (NH) of less than 1°C relative to the 20th century levels. However, in more detail the 400 year period of LIA was characterized by a high temporal variability for air temperature and precipitation which is also reflected in a sequence of periods

Table 4.1: List of outstanding periods considering temperature and seasons within these periods are to be found. Emphasis is put on winter (DJF), summer (JJA) and year (YAR). Additional information referring to Alpine glacier behaviour is included and taken from the following section, where explanations can be found.

	no.	periods		seasons that exhibit the feature
	1	1760–1783	cool	all year round but in general somewhat shorter
	2	1790–1795	warm	weak; all year round and more pronounced in summer several evidences that Alpine glaciers retreated;
	5	1860–1872	warm	all year round but weak during some seasons; pronounced glacier retreats from LIA maximum extents;
DJF	6	1887–1895	cool	to be found from OND till JFM (minimum in DJF); many Alpine glaciers advanced;
	7	1910–1924	warm	warm from NDJ to JFM but cool from JJA to SON; advancing glaciers (mechanism explained in the text)
	8	1935–1951	cool	to be found from OND till JFM (JJA–ASO: warm); embedded into a period (≈1930–1960) characterized by strongly retreating glaciers;
	9	1957–1972	cool	from NDJ till MAM; during most of the other seasons this period lasts even longer; advancing glaciers;
	*	1990–now	warm	almost all year round; strongly retreating glaciers;
	1	1760–1775	cool	all year round;
	2	1792–1807	warm	all year round; more pronounced during the warm season; several evidences that Alpine glaciers retreated;
	3	1810–1820	cool	from MJJ till ASO; Alpine glaciers strongly advanced towards their LIA maximum extent;
	5	1856–1873	warm	almost all year round; pronounced retreat from LIA maximum glacier extents;
JJA	7	1911–1924	cool	from JJA to SON and warm in winter; advancing glaciers;
	8	1942–1951	warm	from MAM to ASO but cool during winter (NDJ, DJF); embedded into a period of strong glacier retreates;
	9	1956–1985	cool	the full period is to be found from about MAM to JAS and shorter ones all year round; up to 70% of the Alpine glaciers advanced;
	*	1990–now	warm	almost all year round; strongly retreating glaciers;
	1	1760–1787	cool	all year round; partly for a shorter period;
	2	1791–1806	warm	all year round; sometimes weakly pronounced; several evidences that Alpine glaciers retreated;
	3	1809–1817	cool	during the summer-seasons; advancing glaciers;
YEAR	4	1821–1830	warm	all year round but very weak in some seasons (DJF, JFM, MJJ); several glaciers still advancing towards their LIA maximum;
	5	1860–1873	warm	all year round but weakest for JFM and JJA; retreating Alpine glaciers;
	8	1945–1950	warm	mainly during the summer-seasons; glaciers were retreating during this period;
	9	1956–1985	cool	all year round, most pronounced in summer glaciers were advancing;
	*	1991–now	warm	all year round; strongly retreating glaciers;

of glacier advances and glacier retreats. Moreover, LIA was characterized by considerable geographical variations rather than by even temperature conditions around NH (IPCC 2001). Glaciers located within GAR show an increased glaciation up to middle of the 19th century (to the end of LIA). After that period glaciers generally retreated up to now with some interuptions of glacier advances around 1890, 1920 and 1980. The degradation and builtup of LIA maximum extent reached from 1820 to 1850 within a century of generally decreasing air temperature (up to about 1890, see linear trends in Figure 4.1) reflects the complex glacier-climate relation and can be understood only when also taking precipitaion into account (see the section below for details).

The first period in Table 4.1 is characterized by cool temperatures. It starts somewhere before the onset of measurements in 1760 and persists for about thirty years. Recently, the middle of the 1780s were discussed in popular science (Vasold 2004) and in the public (Breuer 2005). There, it is argued that the eruption of Laki in Island caused climate to change for the worse in Europe. Anyway, Figure 4.1 actually shows particularly cool temperatures within GAR.

The second special period, is located around 1800 and is accompanied by retreating glaciers. These retreates are not as pronounced as the others explicitely indicated as green arrows in Figure 4.1 but there are several evidences that Alpine glaciers retreated during this period Slupetzky and Slupetykz (1995). It is a short intervening period of relative warm temperatures in GAR, which can be found in all seasons but is most pronounced in spring (see Figure A.1 contained in the Appendix). Lauscher (1980) named this period 'Josephinische Wärmeinsel' and claimed it to be a regional phenomenon of the Central European Danube region. However, based on recently homogenized historical series, investigations suggest it as a larger scale phenomenon that was felt in whole Europe.

The third period covers the 1810s and is pronounced in summer. During this period of generally enhanced volcaniv activity, the strongest volcanic eruption, that of the Tambora in 1815, took place. The Tambora eruption is the largest of the past 250 years (Robock 2000) and there are widespread evidences of cool conditions in Europe and America (Harington 1992). Within GAR summer temperatures are significantly cool (see Figure 4.2). During winter mean temperatures shows low values too (see Figure 4.1) but there are not many stations whose temperatures are significantly cool (see Figure 4.2). So, during winter this period is not an outstanding period. However, it is a special period and because we are further investigating the 1810s we will account for winters in the 1810s later on, too. The specific behaviour during summer and winter may be related to the ejection of vast amounts of aerosols and sulphur emissions up into the lower stratosphere (see also the discussion on volcanic forcing in Chapter 3). Volcanic inputs to the atmosphere cause a reduced direct flux of incoming solar radiation and an enhanced downward flux of reflected infrared radiation that is received by the earth (Robock 2000). Hence, volcanic eruptions may serve as a mechanism that causes relative low temperatures during summer and does not significantly alter winter temperatures, because temperature in summer is mainly dominated by solar radiation whereas winter-temperature is to a large part influenced by infrared emissions. In the 1810s some Alpine glaciers already reached their LIA maximum extent, while others continued to grow until the middle of the 19th century.

The latter two of the above described periods and the fourth in the Table are part of the so called Dalton Minimum (DM; 1790–1830 see Eddy 1976 for the exact extend), which is a pronounced minimum in solar radiation (Lean and Rind 1999). However, within GAR the reduced solar forcing during DM does not cause a continuous period of low temperatures. Instead, observations indicate a short warm period, which arises in all seasons around 1800, followed by the cool summers of the 1810th and then by relative warm yearly averages (see Figure 4.2).

The fifth special period is already outside DM and LIA. This relative warm period spans the 1860s and can be found almost all year round (see Figure 4.2 and the Figures in the Appendix A). and Alpine glaciers begin to retreate from their LIA maximum extent. Lamb (1989) tells that 1868 summer temperatures in England reached frequently reached values of more than 30°. At the 22th of July temperatures in Tonbridge reached 38.1°, a record so far. The winter 1868/1869 was the warmest ever measured in England. In Austria the Neusidler See dried up during this period (see e.g. Auer (1993) and litertature cited in there).

The sixth period, centered around 1890, should be seen in conjunction with the seventh period that contains the 1910th. As already elaborated above these two periods acting together mark the first temperature leap (based on the total observation period), which is especially pronounced during winter. The sixth period itself is characterized by low winter temperatures and advancing Alpine glaciers. These cold winters exert influence on the yearly averages, even through the summers are not significantly cool. The seventh period is cool in summer but warm in winter. This points to an enhanced maritime influence. The cool summers even out the warm winters and hence, the yearly averages are not significantly different from the long-term, detrended mean. That helps to understand why we have plotted the glacier advances, which are caused by the cool summers and mild but wet winters, in Figure 4.1b), and c) but not in d). Figure 4.1b) and c), comprising winter and summer, the glacier advances coincide with special temperature periods while there is no special period to be found for the whole year as can be seen in Figure 4.1a).

The eighth period may reflect continental conditions because cool winters occur together with warm summers. However, in this case the seasons do not balance and there are yearly averages significantly higher than the long-term, detrended mean. This period exerts the opposite effect on Alpine glaciers than the maritime 1910s and early 1920s and retreates are the consquence.

The second-last period reflects cool conditions during summer and winters at the same time. It starts in the middle of the 1950th and spans to the middle of the 1980th and is accompanied by advancing glaciers (up to 70% of the Alpine glaciers advanced). The last period starts at the beginning of the 1990th and is still going on. This period is characterized by strongly retreating glaciers, significant warm conditions for all seasons and it contains the hottest years on record.

4.2 Comparison to Alpine glacier records

In the above section objective methods for the detection of outstanding periods based on seasonal air temperature have been applied. However, identification and characterisation are often done on the basis of glacier advances and glacier retreats, too. The little ice age period (LIA), for instance, is a well known example of such an outstanding climate period also identified by glacier proxy information (well developed frontal moraines observed worldwide). One drawback is that glacier behaviour is not a simple proxy of climate change but a complex system that comprises the interplay of climate, local topographic effects and ice flow dynamics. Actually, only the mass balance of a glacier is directly (without any delay) linked to climate variation (Kuhn 1980). Time series of mass balance measurements cover only the last 60 years (Haeberli 2004) and even those only for selected glaciers (about 30 in the Alps).

For Alpine glaciers mass balance is determined by the sequence of mass gain during winter and mass loss during summer. In winter (from about October to May) the mass gain (accumulation) is caused basically by snowfall events, snow relocation processes by wind and by snow

avalanches. In summer (from about June to September) mass loss (ablation) is determined by melt processes due to enegy transfer from shortwave radiation and sensible heat. Consequently, the high correlation between incoming shortwave radiation and air temperature explains the sensitivity of glacier mass balance to air temperature. From this (accumulation and ablation) sensitivity of glacier mass balance to winter precipitation and summer temperature can be expected.

Because of glacier flow dynamics, front position changes are in contrast to the glacier mass balance not directly linked to climate variations but are delayed. In glaciology this delay is called the response time of a glacier and is stated in the literature in the range from 10 years or even somewhat below for small Alpine glaciers up to about 100 years for big Alpine glaciers (e.g. Aletschgletscher; see Haeberli and Holzhauser 2003). So, long term series of front position measurements, which date back to the end of the 19th century, cannot be directly related to climate variations for time scales below or in the same order of magnitude of the glacier response time. In contrary to mass balance measurements front position measurements are available for a much larger sample of Alpine glaciers. However, this sample is biased towards large valley glaciers.

However, for time scales larger than the response time of a glacier (Oerlemans 2000) showed that front position changes (periods of glacier advance/retreat) can be correlated to climate evolution. Another fact that complicates the glacier-climate relation is that the mass balance of a glacier is linked to winter precipitation and to summer temperature. Schöner et al. (2000) showed that the relation between glacier mass balance, summer temperature and winter precipitation is not constant in time and that the climate sensitivity of glacier mass balances depends on continentality of climate, too.

Major periods of glacier advances/retreats within the Alps (green arrows in Figure 4.1) are also well known from a lot of investigations (Patzelt 1970a; Patzelt 1970b; Kasser 1993; Haeberli and Holzhauser 2003).

Figure 4.3 shows the number as well as the percentage of advancing/retreating/stationary glaciers of the Alps. The total glaciated area of the Alps was about 2909 km^2 in 1988 (Haeberli et al. 1989). Thereof 19% is located in Austria, 14% in France, 21% in Italy and 46% in Switzerland (Haeberli et al. 1989). Germany holds about 1 km^2. It can be seen in Figure 4.3 that front positions of most glaciers (about 70 to 80% – orange or blue areas) show a fast response (almost undelayed) to climate variations. Whereas these glaciers have to be close to the equilibrium state the remaining 20-30% are away from equilibrium and can therefore not reflect climate signals at high frequencies. The outstanding periods of the present study are such high frequent signals. This finding makes clear that Alpine glacier behaviour (advancing/retreating) is not so much sensitive to shifts in the absolute level of air temperature (and/or precipitation) but to deviations from the long term trend of air temperature (and/or precipitation). The mechanism behind this is that glaciers adapt to absolute temperature by moving to higher (colder) or lower (warmer) altitudes. To put things in perspective, the total mass of glaciers of course does depend on absolute levels but advancing and retreating is triggered by deviations from the long term course. Consequently, this supports the general idea of our study in two ways. First, it is reasonable to determine outstanding periods as deviations from long term temporal trends and second, it approves the detrending procedure that splits the HISTALP temperature period into subsamples. We have also drawn similar Figures for the Austrian glaciers alone. The runs are rather similar but there is somewhat more information further back in time. On that account, and because we refer to this information in the list below they are shown in Appendix A (Figure A.2).

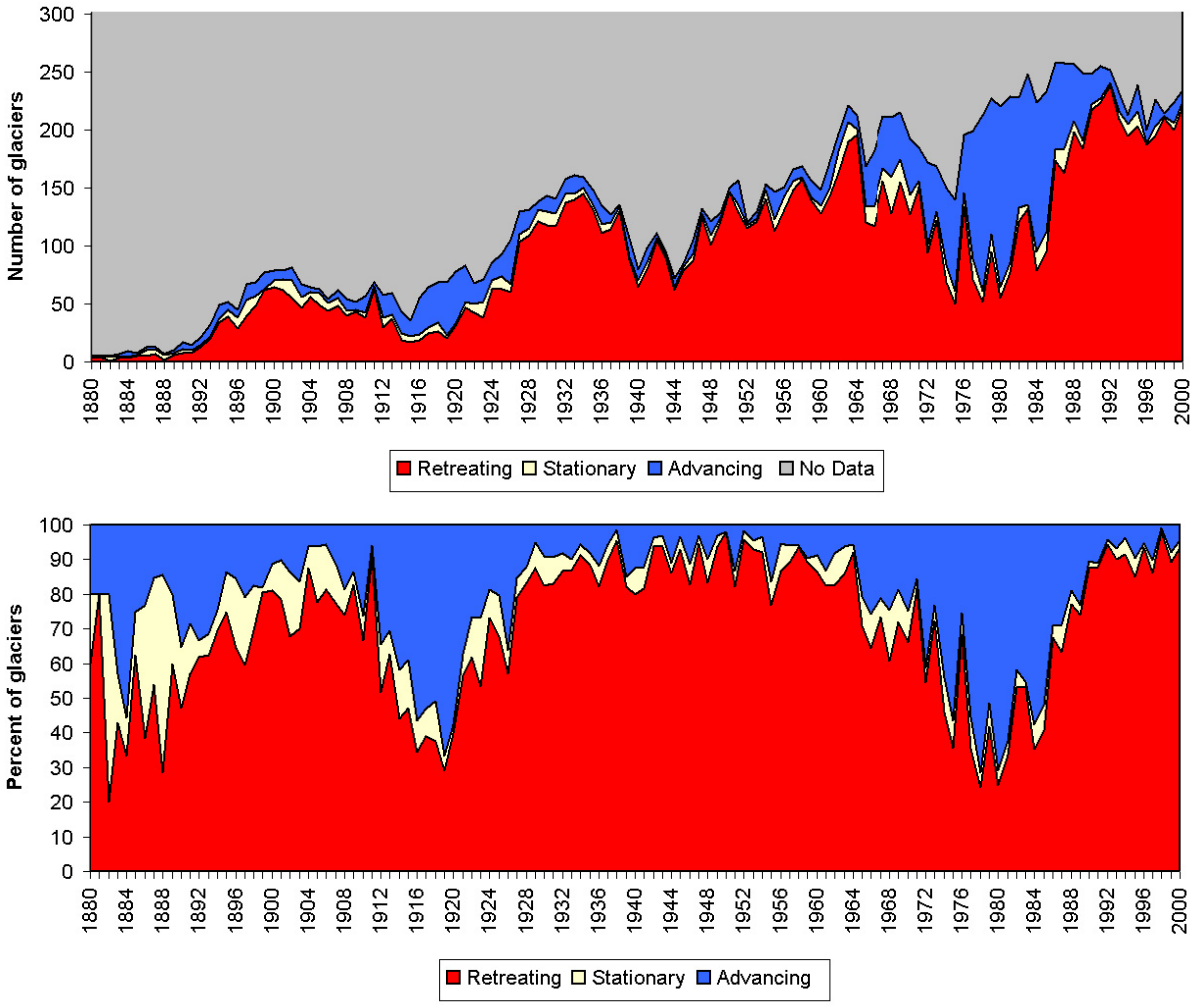

Figure 4.3: Advances and retreats of Alpine glaciers; *orange* indicates glacier retreats, *blue* advances and *yellow* no change; *upper panel*: actual number of glaciers contributing to the analysis against time; lower *panel*: percentage of the total number of contributing glaciers against time. *Source*: World Glacier Monitoring Service.

Several general features of Alpine glacier behaviour can be derived from Figures 4.3, A.2 as well as from the literature (e.g. Patzelt 1970b; Slupetzky and Slupetykz 1995; Haeberli and Holzhauser 2003) and a comparison of temporal behaviour of Alpine glaciers with outstanding periods as detected above shows a rather good agreement:

- the cool summers of the 1810s. Many Alpine glaciers strongly advanced toward their LIA-maximum during that time. This is known from the above cited literature and indicated in Figure A.2;

- the all year round warm period 1856–1873. This is known as a period whithin most Alpine glaciers strongly retreated from their LIA maximum extend and in accordance with Figure A.2;

- the period 1887–1895, which shows cool winters and summers. This period contained a comparable large fraction of stationary and advancing glaciers (see Figure 4.3);

- the maritime period 1910–1924 (mild winters cool summers) coincides with the 1920ies glaciers moraines; The combination of cool summers and warm winters caused up to 70% of the Alpine glaciers to advance;
- the continental 1940s coincide with a period of glacier retreat. High summer temperatures cause negative mass balances during this period;
- the all year cool period 1956–1985 most significant in summer. Even somewhat more than 70% of the Alpine glaciers advanced;
- the all year round warm period that started 1990, with a very pronounced glacial retreat.

4.2.1 Precipitation and Alpine glaciers

Besides the similarities between glacier behaviour and special periods of air temperature there are some open questions left:

- Why did Alpine glaciers advance to their LIA maximum state of 1850 in spite of some rather warm periods near 1800 and in the 1820s (see Figure 4.1)?
- How can the following strong retreat from the LIA maximum extent be explained by only two warm decades during a period of a general cooling trend which lasts until 1890 as shown in Figure 4.1)?
- Why didn't the cold Period 6 (1887–1895) help Alpine glaciers to gain mass?
- How can the 1920s–advances be explained in spite of remarkably warm winters?

These questions can better be answered if precipitation is taken into account. However, interpretation of precipitation behaviour is not as simple as that of air temperature. This is because, within GAR, precipitation trends show a strong regional dependence. Figure 4.4a) shows these regions, which result from a REOF based regionalization using normalized monthly HISTALP precipitation series (Brunetti 2005). The rest of the panels (b to f) depict the temporal (30 year Gaussian low pass filtered) run of precipitaion within these regions, according to the seasons. This gives information about regional and seasonal variability of precipitation from 1800 onwards within the GAR precipitation-subregions and identifies substantial regional as well as seasonal differences. On the long run (200 years) spring and the year as a whole show approximately zero trends, summer and autumn negative trend values and winter a positive trend. However, these bi-centennial treds are quite variable in different subregions and show even stronger variability on multi-annual to decadal-scale.

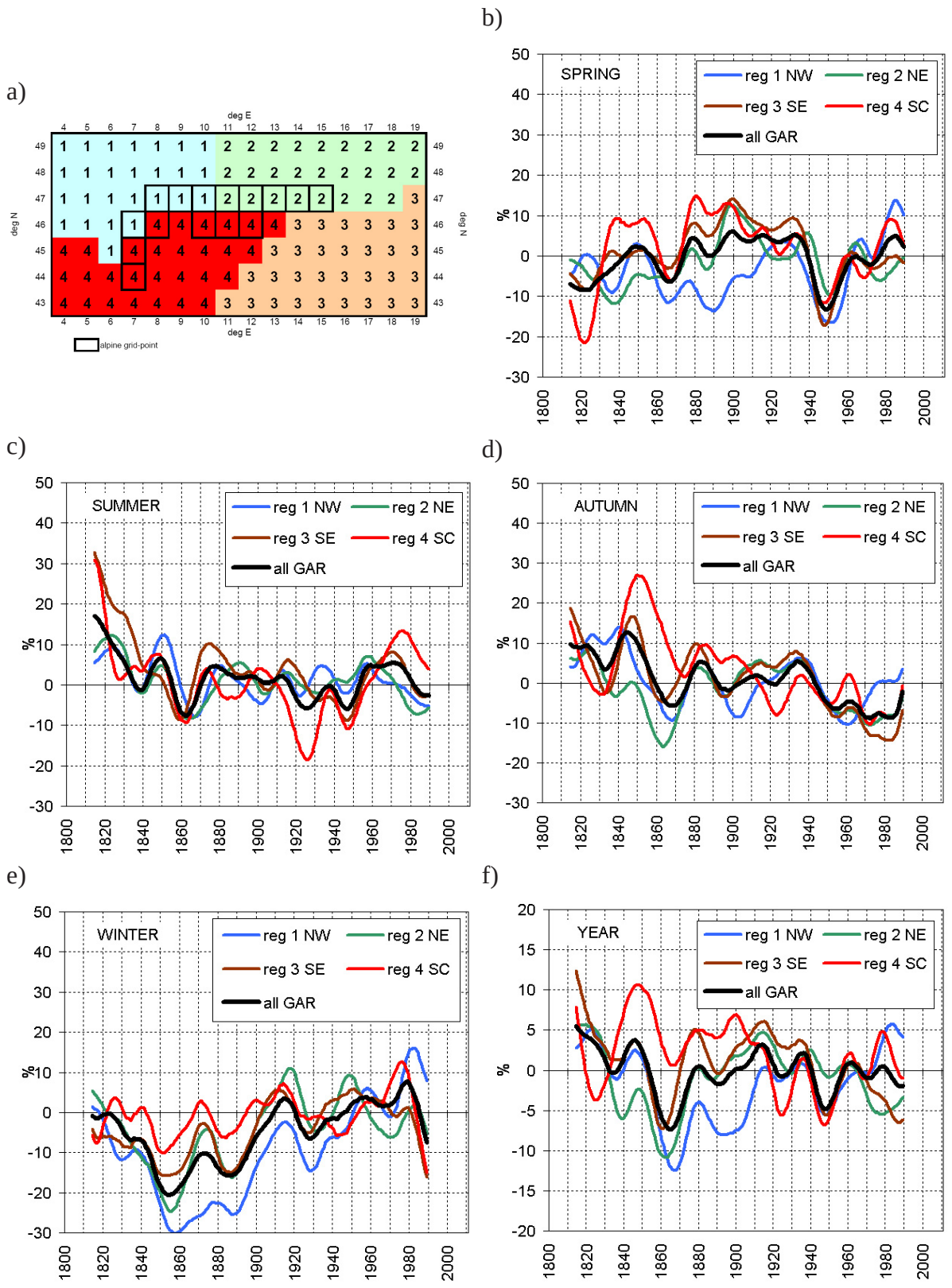

Figure 4.4: Seasonal precipitation course relative to the 20th century mean within different GAR sub-regions (31 year Gaussian low pass filtered). a) indicates the regions as derived from (Brunetti 2005); b) to f) depicts the regional behaviour during spring, summer, autumn and winter, respectively. Note the particular dry decades 1851–1860 and 1881–1890 and the comparable wet 1910s.

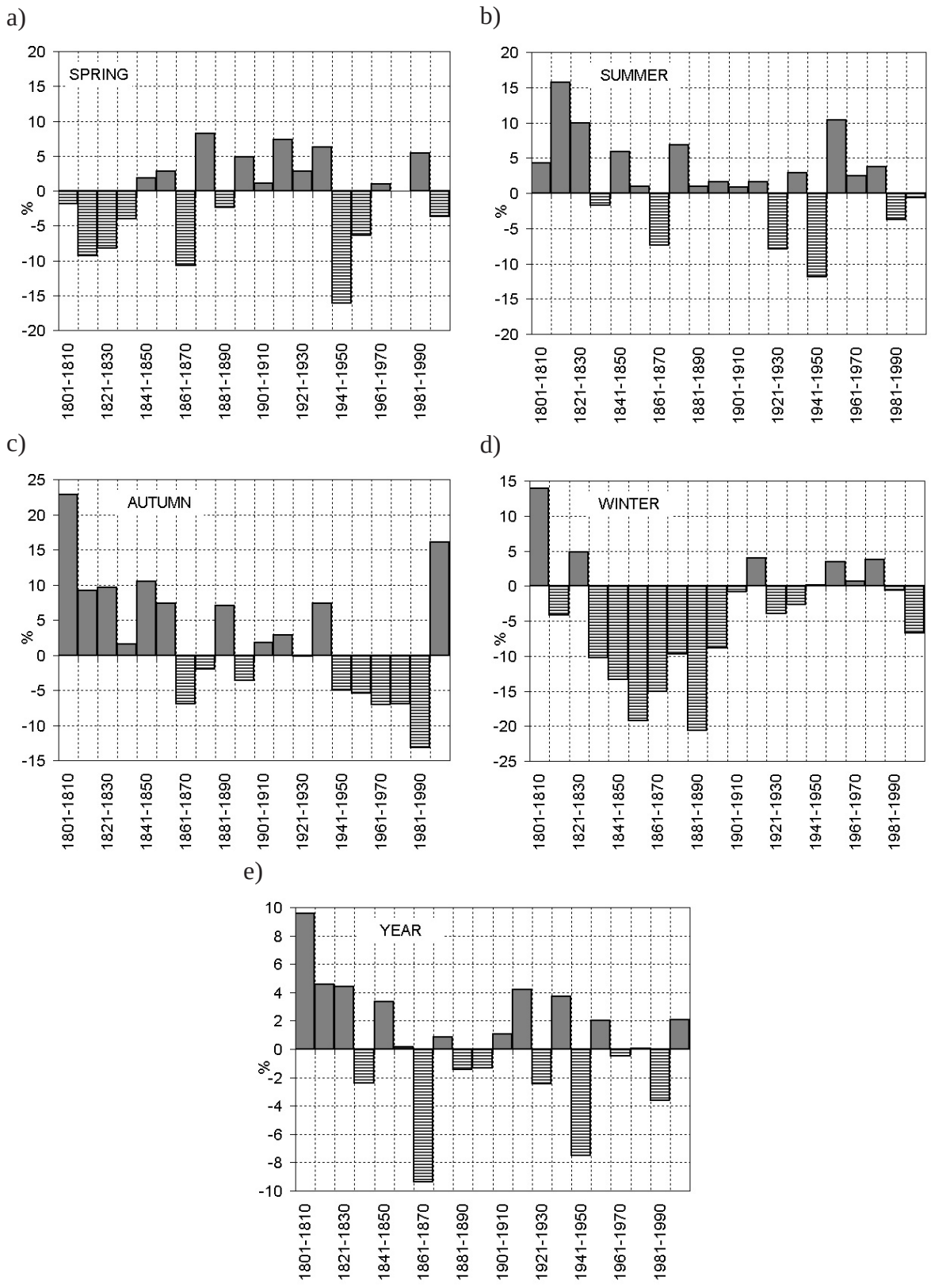

Figure 4.5: Seasonal precipitation in fixed decades course within GAR as a whole; a) to e) stand spring, summer, autumn and winter, respectively. Again, as in Figure 4.4, values are relative to the 20th century mean and analysis is based on the Grid-1 dataset.

Figure 4.5 shows the seasonal variability on a fixed decadal timescale for GAR as a whole. Following, general features can be read from the Figures 4.4 and 4.5:

- 1801–1850 was remarkably wet; This is particularly true for summer and autum but not for spring;
- During 1831–1900 extraordinary dry winters occurred (most pronounced in region 1); This is in accordance with the overall GAR behaviour;
- The decade 1861–1870 was very dry all year round;
- The decade 1881–1890 was the dryest winter decade;
- The period 1910–1924 was wet in winter and all year round;
- Period 1941–1950 was exceptionally dry in spring (in all regions);
- Autumn of 1991–2000 was remarkably wet (general trend within GAR).

Precipitation evolution contributes a lot to a better understanding of several special periods of glacier behaviour. For example, the period of glacier advance to the LIA maximum located around 1820 and 1850, depending on the actual glacier, is accompanied by high summer and autumn precipitation amounts. And hence, although quite warm temperatures predominated especially the time around 1800 in Central Europe, Alpine glaciers were advancing.

It has to be stressed that up to now the onset of these major glacier advances culminating near 1820 and 1850 is not really well known. It may well be that glaciers were rather small before the 1810s (compare e.g. documentary evidence for the Austrian Hohe Tauern in Slupetzky and Slupetykz 1995) and very suddenly started to advance not earlier than after 1811. Thus the warm summer condition around 1800 would not be a contradiction if only temperature is taken into account. Documentary evidence from the well documented Unterer Grindelwaldgletscher (Zumbühl 1980) on the other hand describes one (rather large) Swiss glacier with not much retreat around 1800. So, the early 19th century glacier case must be left as not completely understood yet, but anyway the new early precipitation data brings some more light into the discussion.

Similarly, the glacial retreat after 1850 is supported by the dry decade 1861-70. Conditions during 1887–1895 appear related. There are no widespread advances although winters were cold, which may be linked to dry winters that even turn the balance of the yearly sums.

The period of glacier advance with its maximum around 1920 is in good agreement with high winter temperatures associated with high precipitation amounts. Even more, this event as being a maritime period is especially interesting in contrary to the more continental period from about 1940 to 1950. As already stated above within periods of less continentality glacier mass balance is more sensitive to winter precipitation, whereas within periods of higher continentality it is more sensitive to summer temperature. This mechanism helps to understand the advances during the 1910s as a positive feedback to increased winter precipitation and the retreates from about 1940 to 1950 as a positive feedback to the high summer temperatures.

The striking 1990s precipitation feature with especially high precipitation in autumn (also considering the temporally parallel decreasing temperature trend) and hence increased accumulation in autumn, without any positive effect on the annual mass balance cannot be understood without any more detailed modeling. However, the above discussion suffers from the fact that precipitation within GAR is so far necessarily obtained from low level sites (less than

1500masl mainlz) and hence may not properly reflect conditins at high elevations. Moreover, interpretation is based on qualitative arguments and not on thorough analysis. A detailed quantitative analyses based on a climate-glacier model will be done within the ALP-IMP project (www.zamg.ac.at/ALP-IMP). ALP-IMP is just on the way to deliver the necessary input data of high resolution Alpine air temperature and precipitation data (precipitation at a 10' resolution grid is shortly before being finished by Efthimiadis et al. 2005).

Chapter 5

Temperature observed in GAR and modeled over Europe

The main purpose of this chapter is the comparison of temperature as observed within GAR and as modeled with ECHO-G and the extraction of those simulations that comply with the homogenized observations. Therefore, two large scale geographical areas are selected. The first one covers most of the weather phenomena that give Europe its climate (NAEU in Figure 5.1). The western edge of NAEU covers parts of the North Atlantic, in the East it reaches into Russia. In the South it contains the Mediterranean and the Atlas, in the North Iceland. Thus, NAEU area covers a large part of weather phenomena having a strong influence on Europe's climate (see Chapter 1) . Areas similar to NAEU are generally used for short-term forecasting purposes by European weather services. The North Atlantic storm track, for instance, whose path affects the spatial distribution of precipitation is captured in NAEU as well as the North Atlantic Oscillation (NAO, Hurrell 1995), which affects the curvature of the North Atlantic storm track and has significant influence on GAR temperature and precipitation in DJFM mainly. The second geographical sector (EU) is embedded into NAEU and somewhat closer to GAR. However, it is not smaller than ECHO-G's *skillful* scale (von Storch et al. 1993; von Storch 1995). It stretches from the Iberian Peninsula to the Gulf of Finland. When comparing the observed temperature within GAR to the modeled temperature (this chapter) the smaller sector is used while when synoptic patterns are investigated in Chapter 6 the larger sector is applied.

5.1 Temperature evolutions in differently driven simulations

To receive a first impression of the simulations' behaviour during outstanding periods ECHO-G temperature within such periods is compared to the temperature within the surrounding periods. The following example illustrates the procedure. Summers from 1810 to 1820 (see Table 4.1) were found to be significantly cool for a large fraction of stations within GAR (see Figure 4.2 and the Appendix A). Now, for every gridpoint within NAEU the temporal means of two periods are calculated. First, for 1810–1820 and second, for the period, located around 1810–1820, having the same length (i.e. 1805–1810+1820–1825). This is done for all different forced simulations. Figure 5.2 contains the above example (first line), period 5 (the 1860s), which is an outstanding warm period that marks the end of LIA (second line), and period 7, located at the beginning of the 20th century. Period 7 exhibits warm winters but cool summers in GAR and is accompanied by an advance of Alpine glaciers, although observed yearly temperature does not give a hint.

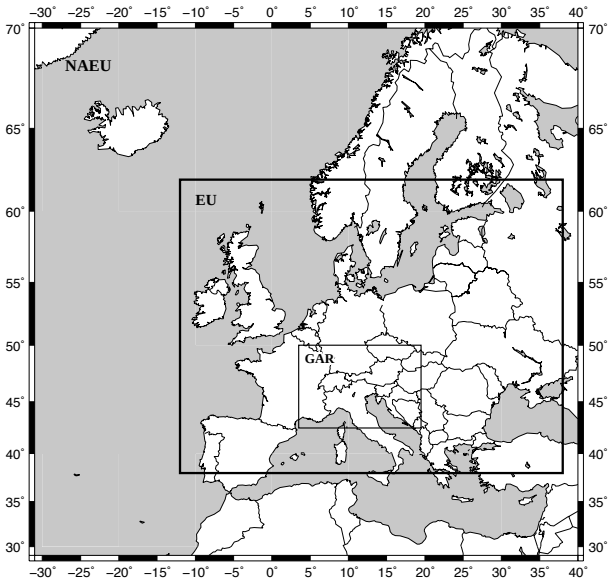

Figure 5.1: Geographic sectors used for comparison of temperature as observed and modeled. Reporting stations are to be found within GAR, while the larger regions (NAEU and EU) contain model-results.

Figure 5.2 contains ECHO-G simulations during JJA, YAR and DJF in the first, second and third line, respectively. The first line compares the 1810s to the surrounding period of the same length. Three simulations (a0, sc, ng) exhibit lower temperatures during the 1810s whereas the fourth (nv) shows higher temperatures. This resembles the observations quite well. It was also in the 1810s that remarkable glacier advances began, which produced the two last (and among the strongest) LIA glacier maxima near 1820 and 1850. As elaborated in Chapter 4 the 1810s are characterized by cool summers, which are likely to be caused by volcanic eruptions (Robock 2000). This appears to be stated by the different simulations. Cooling in any case, exept for the simulation that does not account for volcanoes.

The second line shows the 1860s which are warm, and can be found all year round in GAR. Climatic conditions in the 1860s initiated the first retreat from the LIA glacier peak level near 1850.

The panels pertain to the year as a whole (YAR) and indicate that this period is modeled somewhat warmer than the surrounding period. Differences between the simulations are small, which may indicate small variations among the different forcings prior this period.

The last row shows winters of the 1910s, a maritime period in GAR. All simulations add up to warm conditions, in accordance with the observations. Although warm winters occured in both, the latter two periods had quite different impacts on Alpine glaciers. A retreat, that marks the end of LIA in the first case and an advance in the 1910s shown in Figure 4.3. This can partly be adressed to the warm summers of the 1860s and the very cool ones in the 1910s. The other reason lies in the fact that the 1860s were extraordinary dry while the 1910s wet (see Figure 4.4). This caused glaciers to decrease in the former and increase in the latter case (Details in Chapter 4.2).

The first impression, received by this coarse approach, may indicate some skill of ECHO-G to reproduce climate conditions during outstanding periods. Figure A.3 in the Appendix A

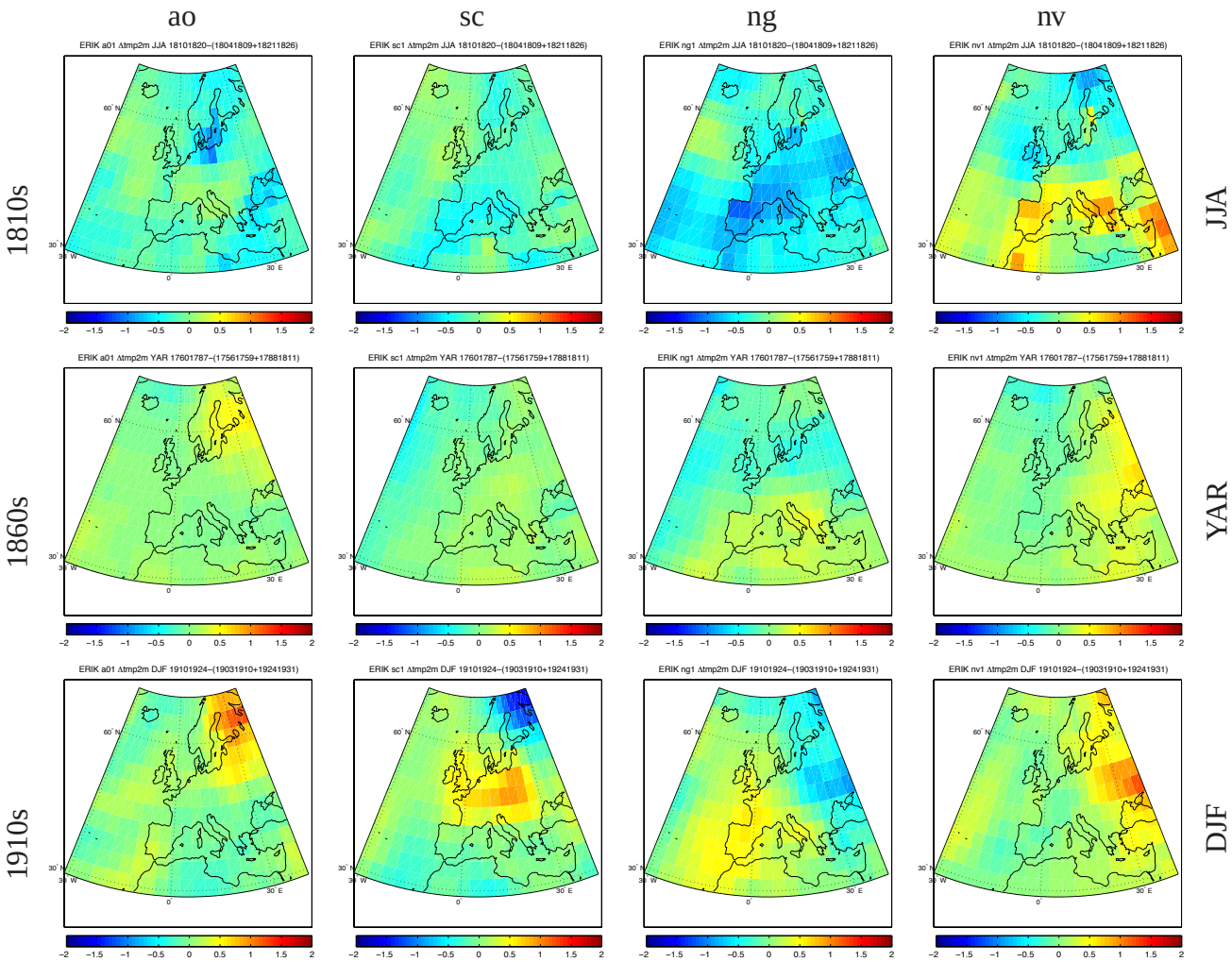

Figure 5.2: ECHO-G temperature within outstanding periods minus temperature of periods surrounding them. Columns contain different simulations (*from left to right*: a0, sc, ng, nv). Rows contain outstanding periods (*from top to bottom*: JJA of 1810s (e.g. 'Tambora'), YAR of 1860s ('end of LIA', strong glacier retreat) and DJF of 1910s ('Alpine glacier advance').

shows similar panels of all simulations for any otustanding period listed in Table 4.1.

5.2 Comparison of observed and modeled temperature

In the following, spatially averaged simulations are compared to averaged observations. As elaborated at the beginning of this chapter simulations are spatially averaged over EU, while observations are averaged over stations. Figure 5.3 shows spatial temperature averages, pertaining to differently forced ECHO-G simulations and the observations, relative to their long-term averages as functions of time. The curves are passed through a 11/31-year Gaussian low pass filter. Observations are described by a solid, magenta line whereas the ECHO-G simulations by a thin green, blue and red line and a solid, black line. In this succession the lines refer to the 'ng', 'nv', 'sc' and the historical forced simulations, respectively (see Chapter 3 for abbreviatons). Outstanding periods are indicated by yellow bars. It can be seen that the observations show a higher variance than the modeled curves.

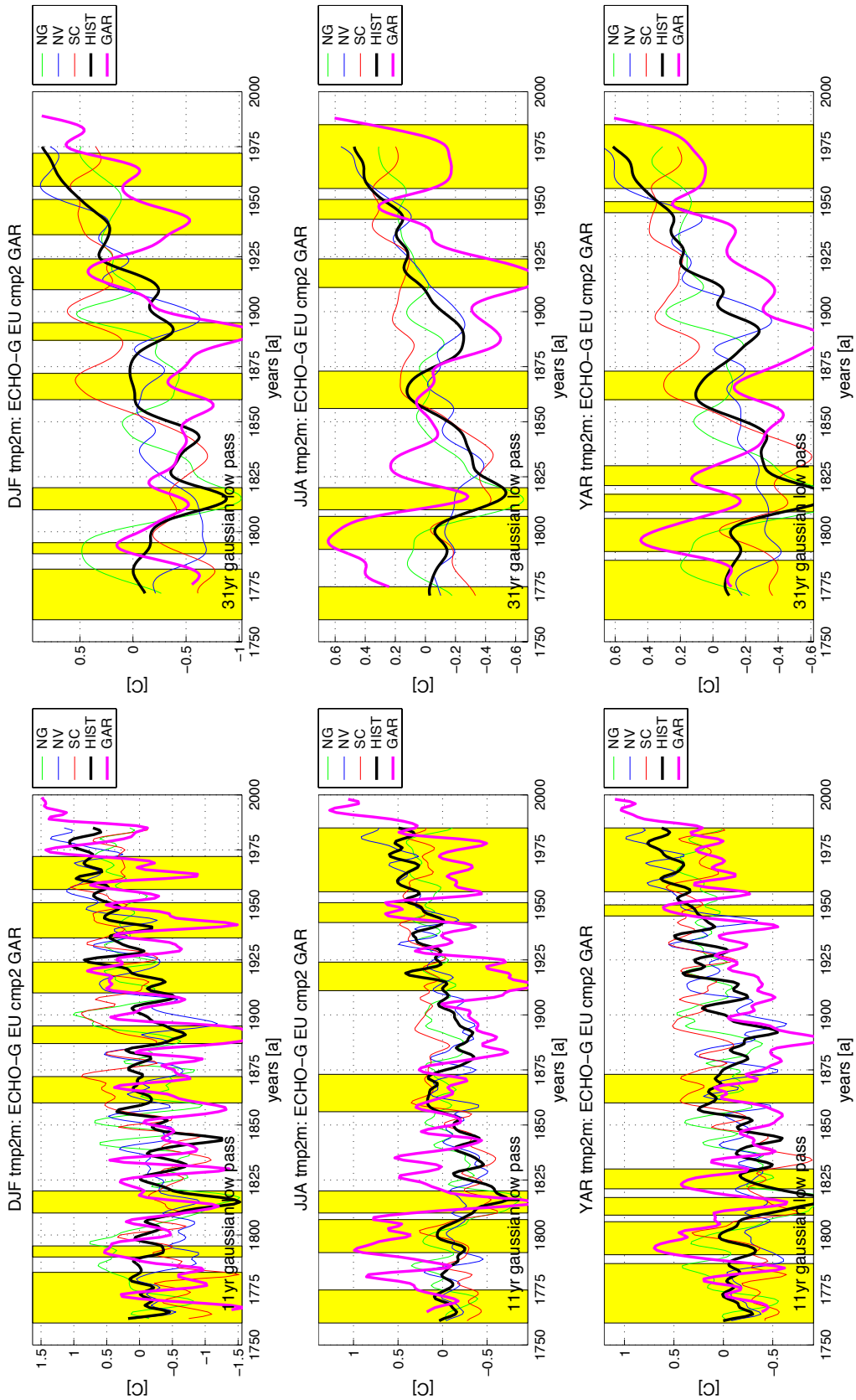

Figure 5.3: Temporal behaviour of spatially averaged observed temperature anomalies within GAR (magenta) and all ECHO-G model simulations averaged over EU (see Figure 5.1). Panels on the left hand side show 11 year Gaussian low pass filtered anomalies while the right column shows 31 year Gaussian low pass filtered data. Observations show a higher variability, which can be addressed to the smoothing effect of spatially averaging the simulations over the relatively large area of EU.

This can be related to the smoothing effect of averaging over large areas. Hence, when NAEU is chosen instead of EU the difference between the observed (GAR) and modeled variances becomes even larger (because temperature's variance within NAEU is still smaller than within EU). However, temperature averaged over NAEU and EU as a functions of time are very much alike. Depending on season and forcing the correlation coefficient r ranges from 0.90 to 0.95. The main difference is that mean temperature in NAEU exhibits a smaller variance because it is averaged over a much larger area. The next step is the detection of ECHO-G simulations, whose 2-meter-temperature simulations are in accordance with the observations during outstanding periods. Whenever the curvature of a simulation is in accordance with the observed one, the ECHO-G simulation will be retained for further statistical treatment. To form an opinion on the behaviour of the temperature simulations during outstanding periods some parameters are evaluated. First, the mean of a simulation within an outstanding period is compared to its mean derived in the period that surrounds the outstanding period. Second, the temperature range covered by the simulation is compared to the observed one and third, the number of extremes is counted. When counting the extremes we have distinguished two adjacent extremes only if they can be separated by the sixth part of the temperature range within the period under consideration. This is to take into account only compareable pronounced variations, not those having small amplitudes. According parameters are collected in Table 5.1. Moreover, we have also plotted the simulations together with the observations in a more detailed way than in Figure 5.3, which covers the total observation period. Figure 5.4 shows three examples. Again, one panel for winter, summer and the year as a hole. All the above listed criteria assist in selecing simulations that properly describe the observations within outstanding periods.

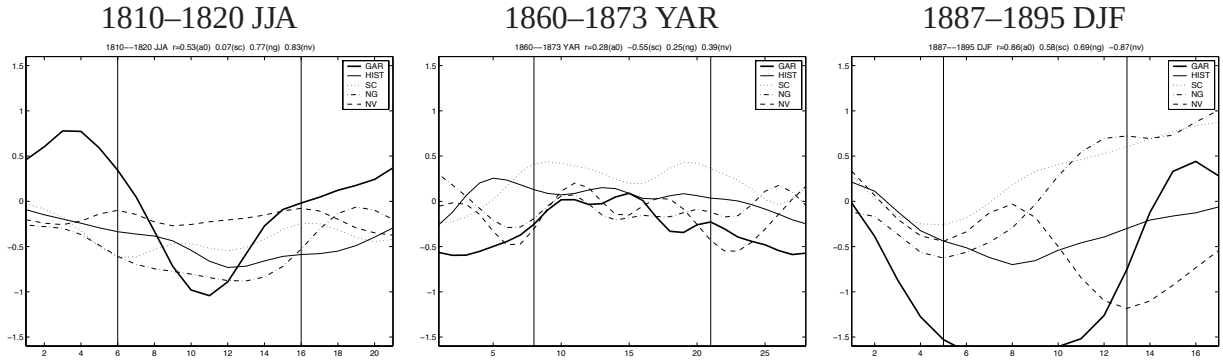

Figure 5.4: Temporal evolution of 11-yr Gaussian filtered simulations and observations within outstanding periods. From *left to right*: summers of 1810s, the whole year during 1860–1873 and winters of 1887–1895. Vertical lines mark the borders of the outstanding period and the intervals on its left and right constitute the surrounding period.

The left panel depicts the summers of 1810s and it can be seen that none of the simulations does exhibit such a clear signal as the observations. This may be related to the much larger region over which is averaged. However, the fully forced simulation (a0) and the one that does not account for the increasing greenhouse gas emissions (ng) perform better than the other simulations. The simulation which does not account for volcanic forcings (nv) depict temperatures even above those within the surrounding period. During 1860–1873 all simulations are comparably close to the observed curve. However, the simulation that relies on all forcings but does not account for variations in the solar constant (sc) exhibits temperatures that are clearly higher inside the outstanding period than in the surrounding period. This is in accordance with the

observations. The right panel shows the minimum temperatures observed in the winters of the outgoing 19th century. All simulations are somewhat too warm but the fully forced simulation reproduces the observations to some extend. Although the simulation that does not take into account volcanic effects (nv) has a local maximum within this period its temperature is, in accordance with the observations, below the temperature of the surrounding period. Other figures, pertaining to all the other outstanding periods can be found in Figures A.4 and A.5 in Appendix A.

Decisions about the simulations that describe, throughout a particular outstanding period, the observations best are based on the parameters listed in Table 5.1, the detailed plots (see Figure 5.4 or the figures in the Appendix A) and on Figure 5.3. Figure 5.3 permits for the assessment of simulations from the point of the whole period. To illustrate the coaction of figures and parameter values in decision making, DJF of period 5 (1860–1872) is taken as an example. Table 5.1 tells that three simulations take on higher values within period 5 than in the surrounding period. In this sense sc, ng and nv agree with the observations. The temperature range is best approximated by nv (0.7) and all simulations have the same number of 'extremes' as the observation (i.e. 2).

Table 5.1: Parameters that describe the behaviour of different simulations within outstanding periods (T-range, $f' = 0$) and that compare outstanding periods to their surrounding periods (ΔT). Decisions about the simulations that fit the observations are partly based on the table. Simulations actually selected for further statistical treatment are indicated with bold letters.

DJF			ΔT per-sur.per				T-range sim/ob				$f'=0$ sim and obs				
periods			a0	sc	ng	nv	a0	sc	ng	nv	a0	sc	ng	nv	ob
1	1760	1783	0.0	**-0.4**	-0.6	0.5	0.3	**0.7**	0.7	0.3	4	**4**	2	5	4
3	1810	1820	**-0.8**	0.2	**-0.6**	-0.1	**0.9**	0.4	**0.9**	0.5	**1**	1	**1**	2	2
5	1860	1872	-0.1	**0.3**	0.1	0.2	0.2	**0.4**	0.5	0.7	2	**2**	2	2	2
6	1887	1895	**-0.4**	-0.2	-0.2	-0.1	**0.4**	0.9	1.4	1.2	**1**	0	0	1	1
7	1910	1924	**0.1**	-0.1	0.0	**0.2**	**2.3**	1.9	1.5	**1.7**	**2**	2	3	**1**	4
8	1935	1951	-0.1	-0.1	-0.1	**-0.4**	0.4	0.3	0.1	**0.5**	3	3	3	**3**	2
9	1957	1972	-0.0	**-0.1**	0.2	-0.2	0.3	**0.4**	0.2	0.4	3	**1**	4	2	2
JJA			ΔT per-sur.per				T-range sim/ob				$f'=0$ sim and obs				
period			a0	sc	ng	nv	a0	sc	ng	nv	a0	sc	ng	nv	ob
1	1760	1775	0.0	-0.2	**-0.3**	-0.1	0.6	0.3	**0.9**	0.6	1	2	**1**	1	1
2	1792	1807	**0.2**	**0.3**	0.3	0.1	**0.5**	**0.9**	0.8	0.3	**2**	**1**	1	2	4
3	1810	1820	**-0.2**	**-0.2**	**-0.5**	0.1	**0.3**	**0.3**	**0.3**	0.1	**1**	**2**	**1**	1	1
5	1856	1873	**0.3**	**0.2**	-0.1	**0.0**	**0.2**	**1.0**	0.4	**0.9**	**3**	**2**	3	**2**	3
7	1911	1924	0.1	0.0	-0.0	0.1	0.8	0.3	0.6	0.5	2	3	2	1	3
8	1942	1951	-0.1	-0.1	**0.1**	-0.1	0.5	0.4	**0.3**	0.7	1	1	**2**	2	2
9	1956	1985	0.2	**-0.1**	0.1	0.4	0.3	**0.3**	0.5	0.7	6	**6**	4	4	4
YAR			ΔT per-sur.per				T-range sim/ob				$f'=0$ sim and obs				
period			a0	sc	ng	nv	a0	sc	ng	nv	a0	sc	ng	nv	ob
1	1760	1787	0.1	**-0.2**	0.0	0.2	0.4	**0.6**	1.2	0.6	4	**5**	3	3	4
2	1791	1806	**0.2**	**0.4**	0.3	0.0	**0.6**	**1.0**	1.1	0.5	**2**	**1**	1	2	3
3	1809	1817	**-0.3**	**-0.3**	**-0.4**	-0.0	**1.0**	**0.5**	**0.6**	0.3	**1**	**1**	**1**	2	2
4	1821	1830	**0.3**	0.2	0.3	-0.0	**0.5**	0.3	0.4	0.4	**1**	2	3	1	1
5	1860	1873	**0.1**	0.3	-0.1	0.2	**0.3**	0.6	0.6	1.5	**4**	3	4	2	2
9	1956	1985	0.3	**-0.1**	0.1	0.5	0.8	**1.1**	0.9	1.1	4	**5**	4	6	6

However, Figure 5.3 (first line) reveals that two simulations, namely nv and ng are not warm compared to temperature oscillations somewhat farther prior and after the surrounding period (on which Table 5.1 is based). From this point of view the sc-simulation is much closer to the observations. So, Figure 5.3 puts the information provided by Table 5.1 in perspective regarding longer time scales. In this manner we have selected simulations for all outstanding periods and have marked them with bold letters in Table 5.1.

During JJA and the three last outstanding summer periods (i.e. 7, 8 and 9) the parameters and figures reveal that the ECHO-G-simulations are not in good agreement with the observations and that they don't go with the temporal evolution of the observations. One possible explanation for that behaviour of the simulations could be related to the cloud cover during these periods . As elaborated in Chapter 2 homogenized GAR cloud cover is at hand. Figure 5.5 shows its temporal evolution together with GAR temperature.

Figure 5.5: Temporal evolution of the observed JJA cloud cover and temperature anomalies spatially averaged over GAR. The curves are plotted together with their time dependent standard deviation (dark grey: cloud cover, light grey: temperature). Outstanding periods are indicated by shaded bars. Note the contrary behaviour of temperature and cloud cover during the three last outstanding JJA periods.

The curves are station-averages and the time dependent standard deviations have been plotted on either side of the curves. The most prominent feature of Figure 5.5 appears the opposite behavior of temperature and cloud cover during the three last outstanding JJA periods. These periods are: 1911–1924, 1942–1951 and 1956–1985. In this succession they are cool, warm and cool again. In general the course of GAR cloud cover and temperature is not anti-correlated, the correlation over the total observation period is about zero. Hence, the opposite behavior of cloud cover and temperature in those periods may give evidence that temperature evolution may be affected by the cloud cover. A possible explanation for the disagreement in the correlations between temperature and cloud cover in the simulation and the observation could be shortcomings of ECHO-G in simulating temperature dependence on cloud cover. In wintertime, however, other processes may be responsible for a large part of the temperature variability, e.g. the temperature advection by anomalous atmospheric circulation. In this case

Table 5.2: Simulations whose 2m-temperature averaged over EU are in reasonable agreement with the observations.

DJF					JJA					YAR				
	a0	sc	ng	nv		a0	sc	ng	nv		a0	sc	ng	nv
1		×			1			×		1		×		
3	×		×		2	×	×			2	×	×		
5		×			3	×	×	×		3	×	×	×	
6	×				5	×	×		×	4	×			
7	×			×	7					5	×			
8				×	8			×		9		×		
9		×			9		×							

the anti-correlation between simulated temperature and cloudiness may be brought about by atmospherics circulation patters, such as the NAO, that are associated to milder temperatures in Western Europe and to lower winter precipitation and therefore possibly also lower cloud cover. This relationship may be simulated too strong in the model, as it is known that ECHO-G overestimates zonal atmospheric circulation in winter in the North Atlantic-European sector (see e.g. Section 6.1). A third hypothesis is that this anticorrelation in the model arises just by chance, due to the shortness of the investigated period. To investigate this third hypothesis additional simulations should be carried out, started from slightly different initila conditions but driven by the same forcing. This investigation, however will not be done within the present study but will be the subject of further investigations.

Simulations that show proper parameters (Table 5.1) *and* reasonable temporal behaviour (Figures 5.3, 5.4 or those in the Appendix A) are selected for further analysis. Table 5.2 lists them more clearly than Table 5.1. The ao- and sc-simulations go more often along with the observed temperature than the ng- and nv-simulations. This 'skewness' is mostly caused by YAR, as YAR has mainly contributions from a0 and sc.

Chapter 6

Objective analysis of atmospheric circulation over NAEU

This Chapter is devoted to the investigation of circulation over NAEU based on monthly Sea Level Pressure (SLP) fields as simulated by ECHO-G. The investigation period extends from 1756 up to 1990. At first ECHO-G SLP is compared to ERA40 SLP for all seasons. This is done for the period 1958–1990 because ERA40 starts in 1958 and the ECHO-G simulations, used in this study, ends in 1990. The comparison should point up seasons in which SLP is simulated satisfactory to a greater or lesser extent. This is followed by an objective classification of SLP patterns, based on rotated EOFs (e.g. von Storch and Zwiers 1999 or Chapter 2). In order to assess the contributions of the patterns the corresponding time coefficients are summed over the outstanding periods. Tables containing these contributions for DJF, JJA and YAR are the outcome of this chapter.

6.1 Comparison of ECHO-G and ERA40 SLP

In the following a brief comparison between the modelled SLP in the ECHO-G HIST simulation and the ERA40 reanalysis data in the period 1958–1990 will be given. This will be done separately for each season.

In winter (DJF) the mean SLP distribution shows high pressure over southern Europe, centered over the western Mediterranean region, and low pressure over the Icelandic region for both, the ECHO-G and ERA40 data. This leads to a (south) westerly advection of air masses into Europe. However, the model shows a bias towards high pressure over the Mediterranean and towards low pressure over the northeastern North Atlantic. This results in a mean westerly circulation in ECHO-G that is stronger than in ERA40.

During spring (MAM) the centre of high pressure over the subtropics is shifted westward over the subtropical eastern Atlantic in both, the ECHO-G and the ERA40 data. The pressure gradients are not so pronounced than in DJF. Here the model shows a bias towards high pressure over the Mediterranean and towards low pressure over eastern Europe. This results again in a stronger zonal circulation over Central Europe in ECHO-G compared to ERA40.

The summer (JJA) situation shows distinct differences between the ECHO-G and the ERA40 data concerning the Azores ridge extending into Central Europe that is too weakly simuated. Thus, the pressure in ECHO-G is too low over western and Central Europe and too high over the northern North Atlantic.

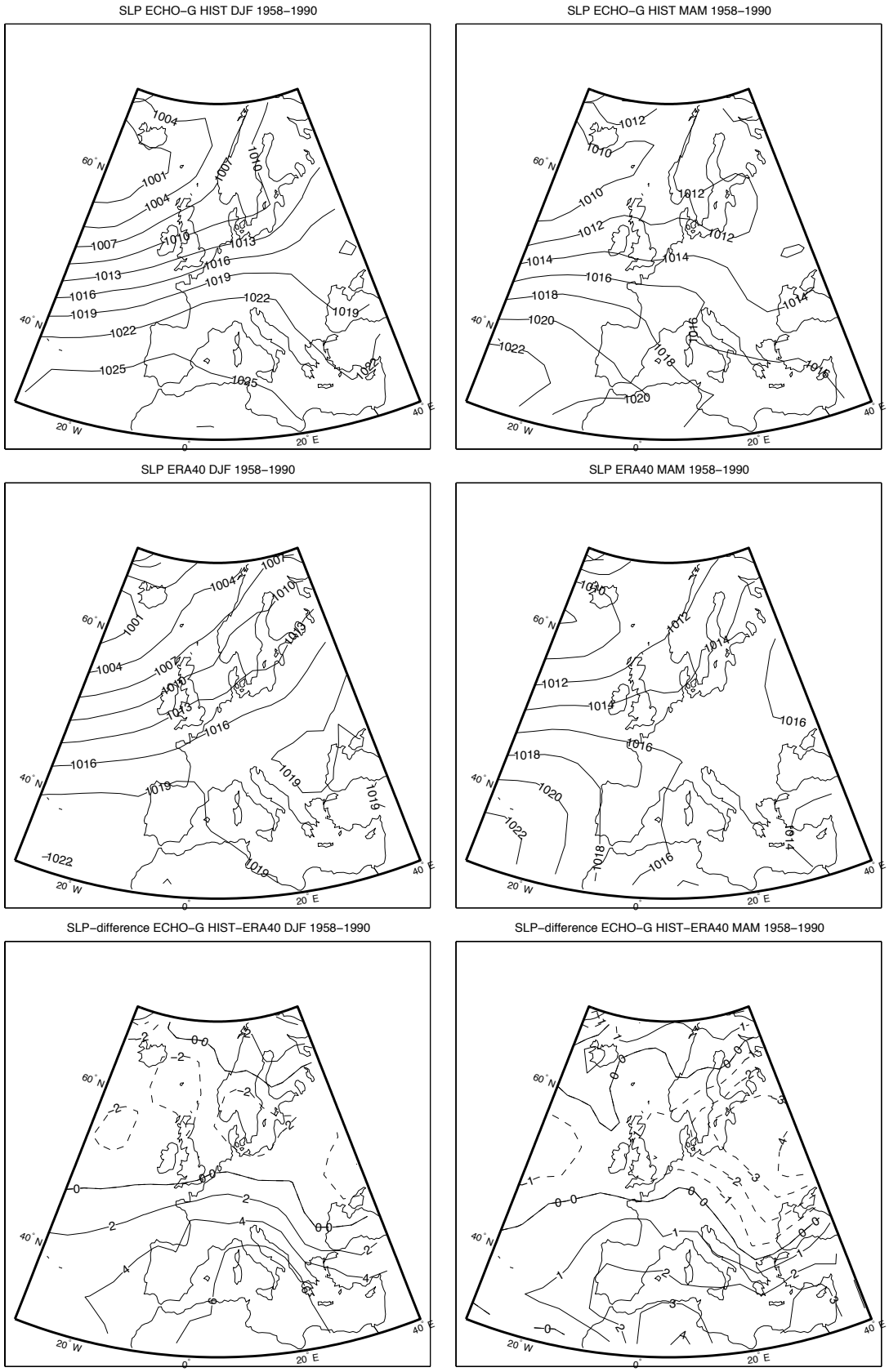

Figure 6.1: Mean SLP during winter (DJF) and spring (MAM) over the North Atlantic-Europe for ECHO-G HIST (upper panels) and ERA40 (middle panels); the lower panels shows the differences ECHO-G HIST-ERA40.

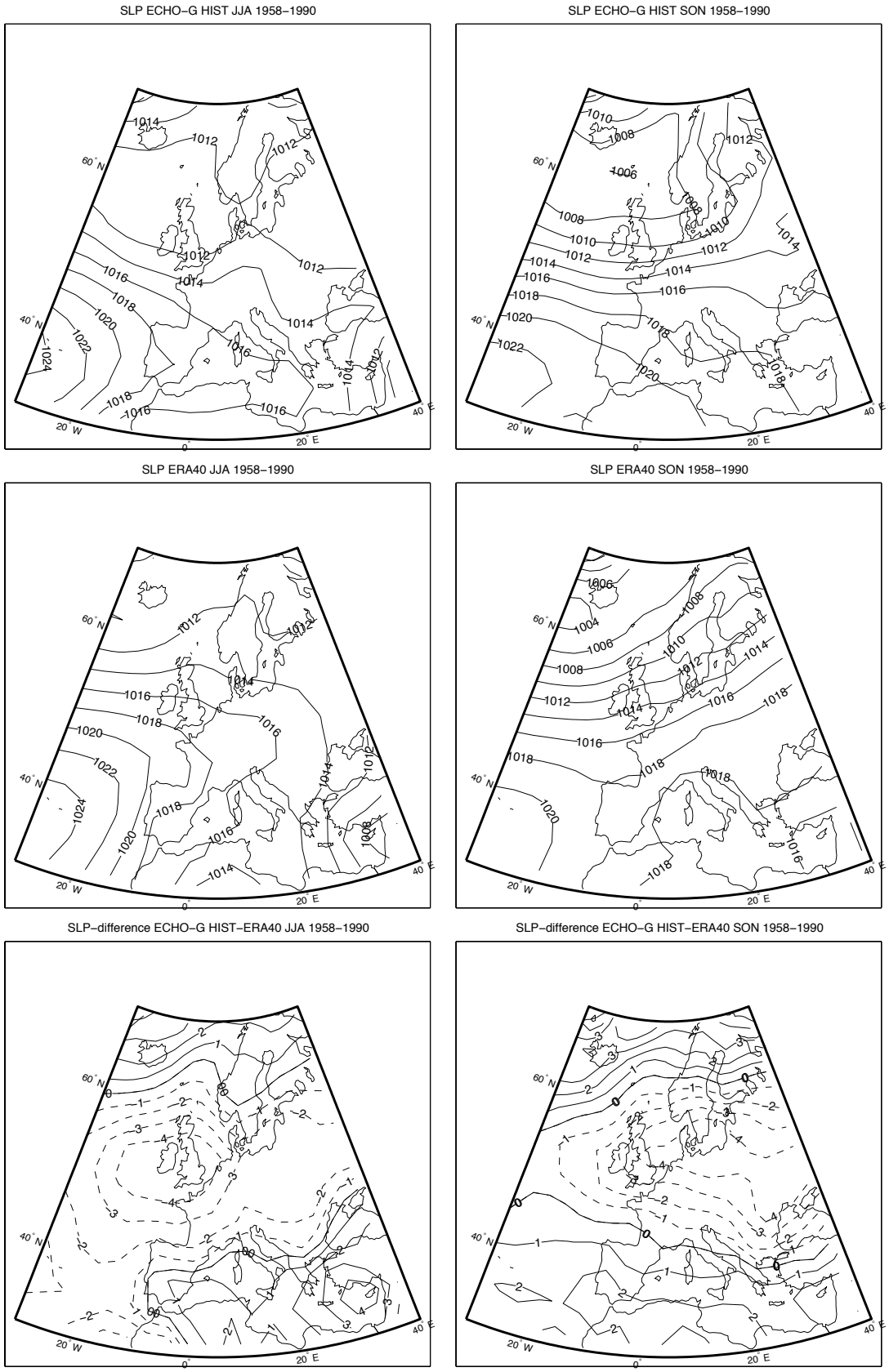

Figure 6.2: Mean SLP during summer (JJA) and autumn (SON) over the North Atlantic-Europe for ECHO-G HIST (upper panels) and ERA40 (middle panels); the lower panels shows the differences ECHO-G HIST-ERA40.

Accordingly ECHO-G shows a (cyclonic) northwesterly stream component over Central Europe, whereas ERA40 shows an (anticyclonic) westerly component over Central Europe.

During autumn (SON) the pressure gradients over the northeastern North Atlantic increase with respect to MAM and JJA. The model shows a bias towards low pressure over central and eastern Europe and high pressure over the northern North Atlantic. This results in a pure westerly stream in ECHO-G over central Europe, whereas the ERA40 data show a southwesterly stream component over Central Europe.

Recapitulatory, during autumn, winter and spring SLP is reasonably simulated by ECHO-G, although in general the strength of the circulation in particular the zonal component is overestimated. In summer SLP agrees to the reanalysis data to a lesser extent signifying a reduced reliability.

6.2 Objective classification of atmospheric circulation

Detection of weather patterns over the North Atlantic and Europe has its roots somewhere around the middle of the 20th century. Baur et al. (1944) and Hess and Brezowsky (1952) have strongly influenced the development of the so called 'Grosswetterlagen' in Europe and up to now the catalogue of Grosswetterlagen that trace back to them is continuously updated (Gerstengarbe et al. 1999) at the German Weather Service (DWD). Primarily, the classification was based upon meteorological fields given at the earth's surface (1881–1938) but later on also information about the circulation at 500 hPa were included. For the Alpine region, more precicely the Eastern Alps Lauscher (1986) introduced a classification based on air pressure at the earth's surface. In Swizerland and for the western part of the Alps Schüpp (1985) is most frequently used.

Such subjective schemes often rely upon subjective decisions and circulation patterns that stem from meteorological experience. On one hand this is of advantage because the interpretation is straight ahead but on the other hand the results can not be reproduced easily by different researchers. The disadvantage can be overcome by the definition of objective rules for these schemes that allow for automatic detection. Jenkinson and Collison (1977), for instance, developed an objective scheme to classify daily circulation according to the Lamb weather typing scheme. This objective method has been compared to the original subjective Lamb scheme by Jones et al. (1993).

Besides subjective methods, there exist a number of objective techniques. Objective methods are often based on multivariate statistical methods, are repeatable and effective. Objective methods, based on Empirical Orthogonal Functions (EOF, see e.g. von Storch and Zwiers 1999), for instance, allow for the reduction of high dimensional fields to just a small number of patterns that ideally describe the variance structure of the original field. A drawback of such methods is that mathematical constraints that ensure the efficiency of the method are often not to be found in nature.

One way to enhance interpretation may be the rotation of EOFs (Preisendorfer 1988). The purpose of rotation is to replace the patterns or the time coefficients by 'simpler', structures that allow a physical interpretation. The result of a rotation depends on the length of the EOFs that are entered into the analysis, and the measure of simplicity, which defines the spatial/temporal behaviour of the rotated patterns and time coefficients (see also Section 2.2). The new patterns and time coefficients should be easier to interpret, however, they are no longer orthogonal and uncorrelated at the same time. Barnston and Livezey 1987, for instance, have investigated

northern hemispherical geopotential height at 700hPa over a period of 35 years on a monthly base. They found rotated EOFs to be a more effective tool to analyze atmospheric circulation than 'teleconnection' analysis (Wallace and Gutzler 1981).

Within the present study rotated EOFs are used to isolate circulation patterns over the North Atlantic European sector (NAEU; see Figure 5.1). The approach is discussed in some detail in Section 2.2, where rotation is used to detect temperature regions within GAR. The analysis is based on monthly SLP fields as simulated by ECHO-G within different forced climatic simulations. Following Barnston and Livezey 1987 we renormalize the EOFs before rotation takes place (right arm in the flow chart shown in Figure 2.3). Figures 6.3, 6.4 and 6.5 show the results of the analysis for winter (DJF).

Figure 6.3 contains the so called LEV (Craddock and Flood 1969) plots for all four ECHO-G simulations. LEV plots display the logarithm of the eigenvalue against its number, when arranging the eigenvalues in a successive monotonically decreasing order. They constitute a decision guidance to identify the proper number of eigenvectors to be retained for further statistical treatment. The number is indicated by a major break in the range of values. In all panels contained in Figure 6.3 the first such break can be found between the fourth and fifth eigennumber. This indicates that, no matter which forcing is actually used to drive the ECHO-G simulation, four EOFs are sufficient to describe a large fraction of the signal contained in the winter data. This is even the case for the year as a whole (YAR), however, during summer (JJA) six EOFs have to be taken into account to achieve about the same amount of explained variance (see Appendix A for further details). Besides the LEV plot there are many other criteria how to determine the proper amount of eigenvectors (e.g. Preisendorfer 1988). von Storch and Hannoschöck (1985) showed that the variance of the eigenvalue estimates is large and biased. In general large eigenvalues are overestimated and small ones are underestimated. These errors become considerably large if the degree of freedom exceeds the sample size. However, the quality of the EOFs (as estimates for the 'real' principal vectors of the actual population) declines with increasing eigennumber and hence, if possible, a restriction to a small number of eigenvectors is recommended. Hence, for winter and the whole year rotation takes place within the 4 dimensional spaces spanned by the first four EOFs, respectively. For summer the dimension of the space that contains approximately the same amount of explained variance (see Table 6.1) is six.

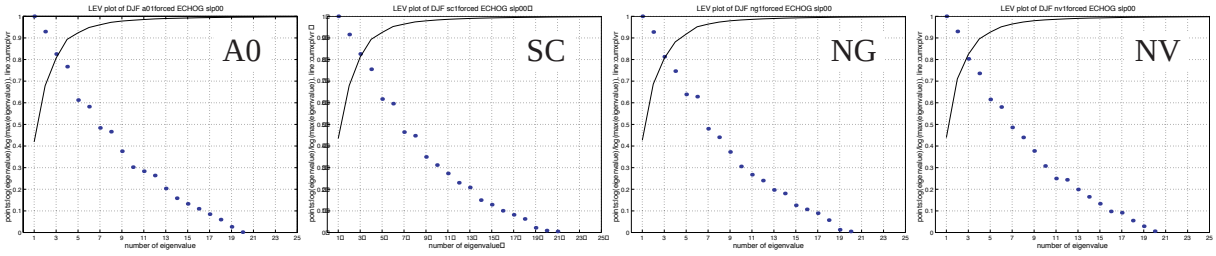

Figure 6.3: LEV plots of all simulations for SLP during NAEU winter. Logarithm of eigenvalue as fraction of Logarithm of largest eigenvalue; *x-axis*: number of eigenvalue in order of magnitude; the curve shows the summed explained variances; Different panels refer to differently forced ECHO-G simulations from left to right: hist, sc, ng, nv-simulations (for abbr. see Chapter 3 or Table 8).

Figures 6.4 and 6.5 display the first and second as well as the third and fourth rotated, renormalized DJF-EOFs (REOF$^+$) together with the appendant time coefficients (RPC$^+$), respectively. Similar figures for JJA and YAR can be found in Appendix A. The first and third rows of Figures 6.4, 6.5 show REOF$^+$s of the different ECHO-G simulations. It can be seen, that

Table 6.1: Explained variances during NAEU winter, summer and the whole year (xplvr= explained variance).

xplvr %	season		
simulation	DJF	JJA	YAR
	4EOFs	6EOFs	4EOFs
ECHO-G a0	89.6	88.1	85.9
ECHO-G sc	89.5	88.6	87.3
ECHO-G ng	88.3	86.4	85.3
ECHO-G nv	89.8	87.9	85.9

their shape is very much alike for different simulations. This indicates that the main circulation patterns during the last 250 years do not strongly depend on different simulations. With other words – although e.g. volcanic eruptions do have an impact on climate on short time scales it does not cause the circulation on a time scale of centuries to change its main features. Again, that does not mean that there is no impact on shorter timescales as for instance decades and that is exactly what the second and forth rows in the figures show. Even through the rotated patterns look alike the corresponding time coefficients are fairly dissimilar. Panels containing the time coefficients display the time coefficients as a function of time. Vertical bars indicate outstanding periods and thin, medium and bold lines pertain to yearly and filtered (Gaussian low pass 11-years and 31-years) curves, respectively.

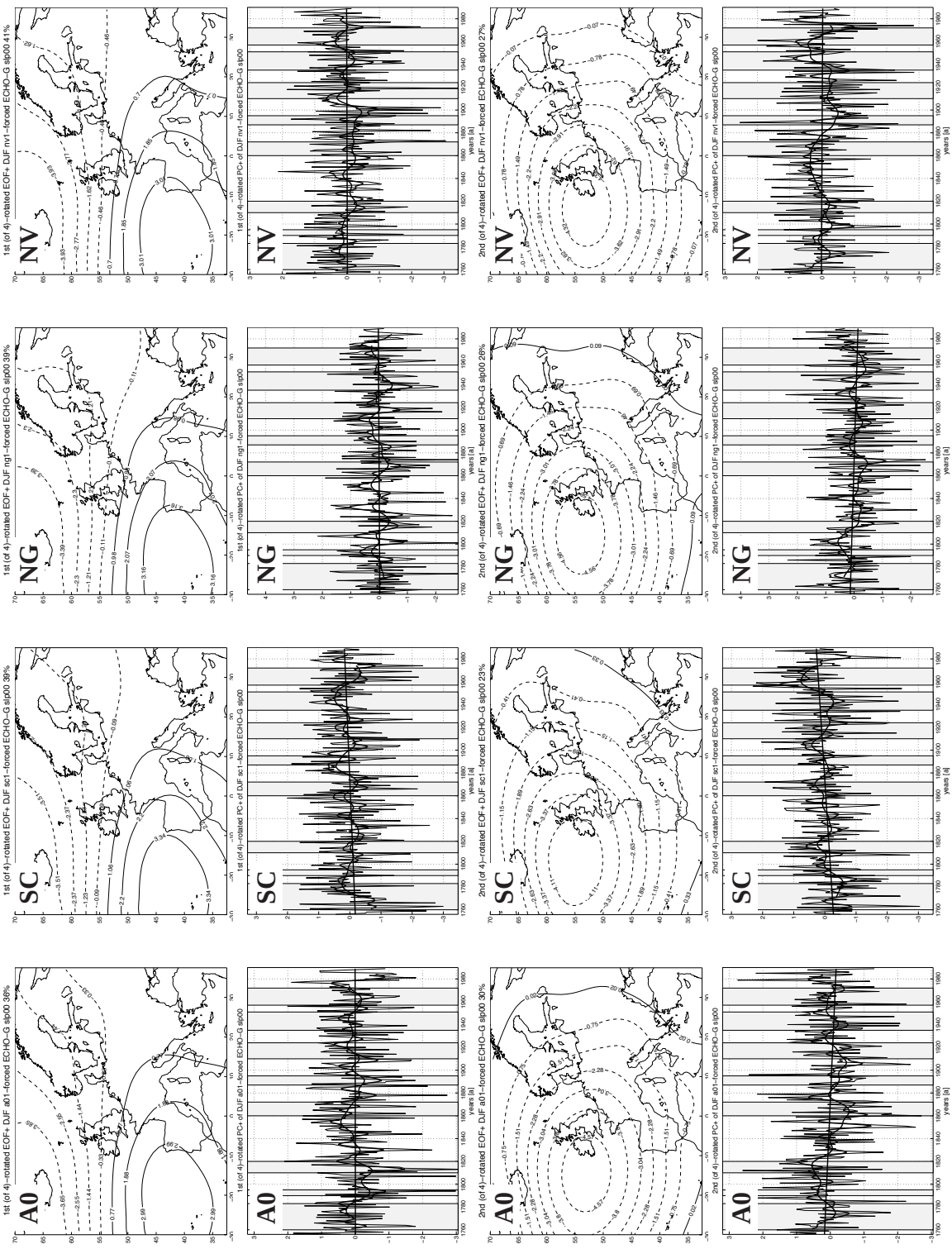

Figure 6.4: The first two rotated EOFs and the corresponding time coefficients derived from NAEU winter SLP (DJF; 1756–1990). Columns pertain to different forced ECHO-G simulations. From left to right: a0, sc, ng, nv (for abbr. see Table 8). Shaded bars indicate outstanding periods, curves display unfiltered data, 11 yr and 31 yr Gaussian low pass filtered data.

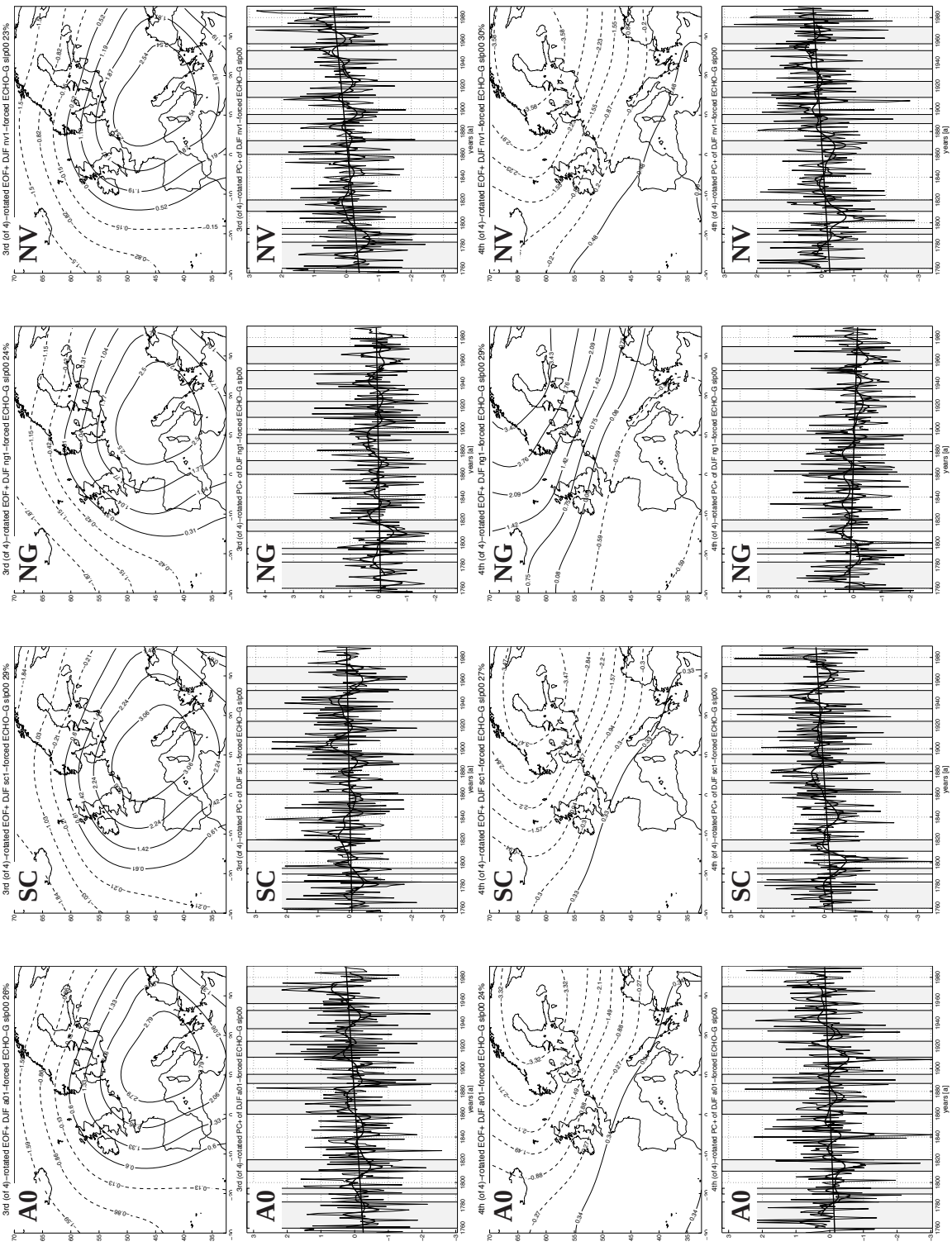

Figure 6.5: The same as Figure 6.4 but for the third and forth rotated EOFs. Note that for further statistical treatment patterns are arranged according to the a0 simulation.

Below, the SLP patterns are shortly described with respect to their circulatory relevance. The dipole structure of REOF$^+$1 with centers over Iceland and the Azores is similar to the North Atlantic Oscillation pattern (NAO; Lamb and Peppler 1987). It stands for a zonal flow from the Atlantic into Europe and hence, if its time coefficient reaches high values, it yields to warm conditions during winter but relative cool conditions in summer. If its time coefficient takes on negative values, continental air masses are carried towards Central Europe. These lead to warm conditions in summer and cool conditions in winter. The second REOF$^+$ is a monopole with the lowest values somewhat West to Ireland. Positive values of RPC$^+$2 point to advection of mild maritime air masses from the South-West toward Central Europe while negative values indicate air-transport from Fennoscandia. REOF$^+$3 shows high pressure centered over Central Europe. This pressure distribution blocks the way for cyclones to sweep in Central Europe and causes the storm track to be deflected around. Positive values of RPC$^+$3 describe a meridional flow from the Mediterranean and North Africa north-westwards over the Iberian Peninsula into the North Atlantic region near the continent. Negative values indicate a meridional air-flow from the North Sea. REOF$^+$4 at last captures variability centered around Fennoscandia and positive values of RPC$^+$4 stand for air mass advection from northern North Atlantic south-eastward into Central Europe. Note that REOF$^+$4 of the ng-simulation exhibits compared to the other simulations the opposite orientation. This can be also found in the trend of RPC$^+$4 – unlike the trends from the other simulations it is decreasing. As the EOFs are unique up to a constant this does not matter, however, to simplify matters of further statistical treatment quantities involving this REOF will be multiplied by -1.

Table 6.2: Averaged DJF and YAR time coefficients in outstanding periods. The first column refers to the period while the others to the rotated EOFs of the ECHO-G simulations.

	$\overline{\text{RPC+1}}$	$\overline{\text{RPC+2}}$	$\overline{\text{RPC+3}}$	$\overline{\text{RPC+4}}$	$\overline{\text{RPC+1}}$	$\overline{\text{RPC+2}}$	$\overline{\text{RPC+3}}$	$\overline{\text{RPC+4}}$	$\overline{\text{RPC+1}}$	$\overline{\text{RPC+2}}$	$\overline{\text{RPC+3}}$	$\overline{\text{RPC+4}}$	$\overline{\text{RPC+1}}$	$\overline{\text{RPC+2}}$	$\overline{\text{RPC+3}}$	$\overline{\text{RPC+4}}$
DJF	a0	a0	a0	a0	sc	sc	sc	sc	ng	ng	ng	ng	nv	nv	nv	nv
1	2	-1	0	4*	-1	-2	-2$^\times$	2	-1	1	-1	0	2	0	0	5*
3	-4*	6*	-5*	-5*	3$^\times$	5*	4*	2	-3	-2	-2	-2	-3	-2	4*	-3
5	3$^\times$	-9*	2	-1	-1	2	0	1	-2	-2	1	1	0	3	1	-4*
6	-5*	-5*	-2	2	2	-1	-3	-1	2	3	3	2	-3	-4$^\times$	-2	-2
7	3	-2	2	-1	2	-3	0	1	1	0	-1	1	1	-2	-2	1
8	2	0	-3$^\times$	1	3$^\times$	-3*	2	3*	-4*	0	2$^\times$	0	-1	0	0	2
9	-2	1	3*	0	-3*	6*	-5*	-3*	0	0	-3$^\times$	4*	3*	1	-2	-2
YAR	a0	a0	a0	a0	sc	sc	sc	sc	ng	ng	ng	ng	nv	nv	nv	nv
1	2$^\times$	-2$^\times$	0	2$^\times$	0	-1	-1	2	-2	2$^\times$	2	2	1	-1	1	2*
2	3$^\times$	1	2	-1	3*	2	2	-3$^\times$	2	3*	-3*	0	4*	-5*	1	-6 *
3	-5*	2	-3	-7*	-3	-2	-3	1	-4*	2	-8*	-3$^\times$	-5*	0	4$^\times$	0
4	0	0	1	-1	-4*	2	6*	2	-1	0	0	1	-7*	0	2	5*
5	2	-7*	3	2	0	4*	2	1	-1	-3$^\times$	2	4*	3$^\times$	2	-2	-5 *
9	-2	0	3*	2	0	3*	-4*	-3*	-1	1	0	2$^\times$	1	0	2*	0

Summer and whole year are treated in the same way as winter and corresponding figures can be found in Appendix A. The next step is the quantification of the frequency with which different circulation patterns (REOF+s) occur during outstanding periods. In doing so we investigate DJF and YAR at the same time, because SLP variability in winter dominates the variability of the

whole year too. This is caused by the (compared to summer and near-summer seasons) relative undisturbed succession of cyclones moving along the storm track from the North Atlantic to Europe. The similarity becomes apparent when comparing Figures 6.4 and 6.5, which depict DJF, to Figures A.6 and A.7 pertaining to YAR, shown in Appendix A. Summer (JJA), because circulation is quite different, will be treated subsequently.

The weighted frequency of circulation patterns during outstanding periods is calculated by averaging the appendant time coefficients over the periods. Table 6.2 contains just these averages. Negative values indicate contributions of opposite orientated circulation patterns. A negative contribution of the first DJF-pattern, for instance, stands for air mass transport from the continent out to the North Atlantic ocean. Cruxes in Table 6.2 signify samples whose means are at least one standard deviation away from the population average. Stars brand values that are significantly different at critical values of 0.2/0.1, depending if the accomplished statistical test are one or two-sided, respectively.

For summer the analysis is entirely the same as for winter and the year as a whole except for the fact that there are now six REOF$^+$s (see Figure 6.6) instead of four as hitherto.

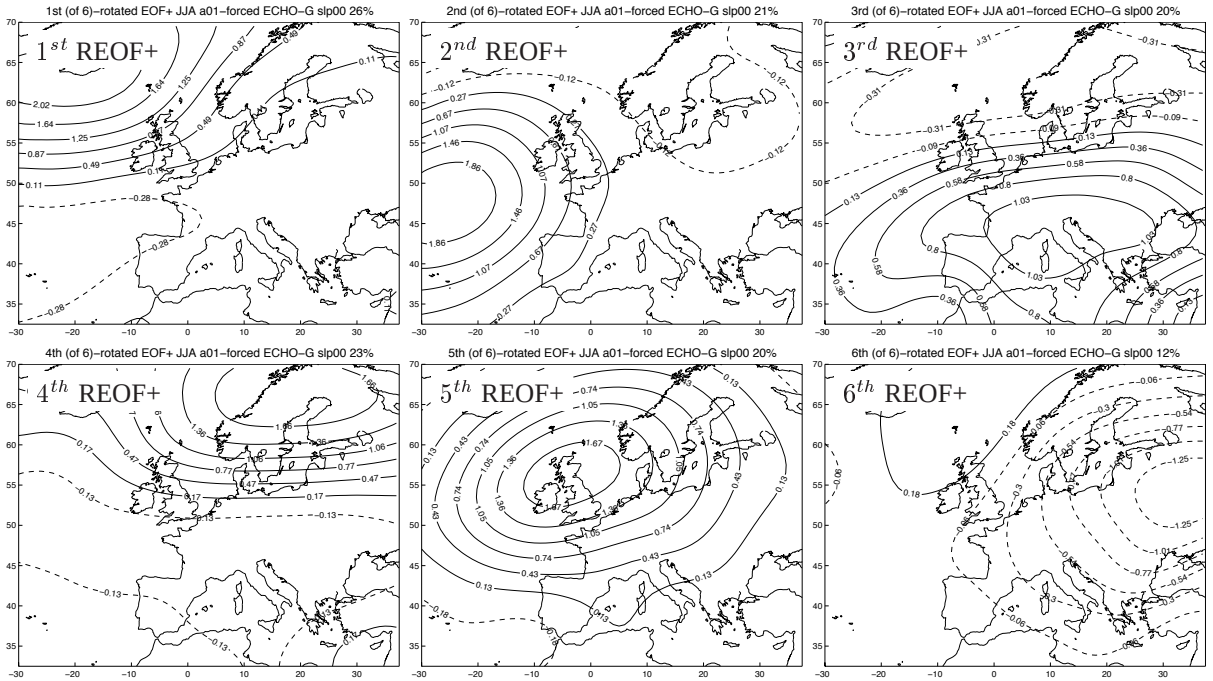

Figure 6.6: Summer REOF$^+$s over NAEU summers derived from the a0 simulation (1756–1990). Corresponding time coefficients can be found in the appendix, Figures A.8, A.9 and A.10. For abbreviations see Table 8.

The patterns in the left column of the first and second line of Figure 6.6 as well as the pattern in the right column of the first line may stand for warm conditions in Central Europe. This is because the first two patterns show flat pressure distributions and the third pattern indiceat air mass advection from northern Africa. Flat pressure distributions cause relative calm coditions and hence incoming short wave radiation can heat up the land mass and the atmosphere. Air mass advection from northern Africa, on the other hand, usually brings warm air masses to Europe. The other patterns are more related to air mass transport originating from areas cooler than the Central European landmass.

Table 6.3: Time coefficients of JJA-REOFs+ averaged over outstanding periods. The first column refers to the period while the others to the rotated EOFs of the ECHO-G simulations. The upper half of the table refers to a0 and sc simultion while the lower half to ng and nv simulations.

	$\overline{\text{RPC+1}}$	$\overline{\text{RPC+2}}$	$\overline{\text{RPC+3}}$	$\overline{\text{RPC+4}}$	$\overline{\text{RPC+5}}$	$\overline{\text{RPC+6}}$	$\overline{\text{RPC+1}}$	$\overline{\text{RPC+2}}$	$\overline{\text{RPC+3}}$	$\overline{\text{RPC+4}}$	$\overline{\text{RPC+5}}$	$\overline{\text{RPC+6}}$
JJA	a0	a0	a0	a0	a0	a0	sc	sc	sc	sc	sc	sc
1	0	2	-1	-1	$3^{\times}$	-2	$3^{\times}$	2	$-3^{\times}$	0	1	1
2	$3^{\times}$	1	-1	0	$-8^{\star}$	2	$-3^{\star}$	-1	0	$-3^{\star}$	2	$4^{\star}$
3	$4^{\times}$	$-5^{\star}$	$5^{\star}$	$3^{\times}$	2	$-5^{\star}$	$3^{\times}$	$4^{\star}$	3	3	$-3^{\times}$	-2
5	$-2^{\times}$	2	0	-1	$3^{\times}$	$-4^{\star}$	1	$-5^{\star}$	0	-2	1	-1
7	2	-1	0	$-3^{\times}$	-1	2	1	-2	1	1	-1	-2
8	$4^{\times}$	0	3	$6^{\star}$	-1	3	2	$-8^{\star}$	$-4^{\times}$	-2	2	$7^{\star}$
9	0	1	-1	0	2	0	1	$3^{\star}$	-1	0	-2	0
	ng	ng	ng	ng	ng	ng	nv	nv	nv	nv	nv	nv
1	0	2	0	$5^{\star}$	$-5^{\star}$	$3^{\star}$	2	$5^{\star}$	-2	-1	1	-1
2	-2	0	1	$-6^{\star}$	0	0	$-3^{\star}$	-1	2	$-3^{\times}$	-1	$-5^{\star}$
3	$10^{\star}$	$-4^{\star}$	0	$4^{\star}$	-2	$-6^{\star}$	-1	-3	1	0	-1	-2
5	-1	$3^{\times}$	0	-1	-2	$5^{\star}$	-2	$3^{\star}$	1	-1	-1	$3^{\times}$
7	$3^{\times}$	2	$4^{\star}$	$-5^{\star}$	1	$-4^{\star}$	1	1	1	1	-3	$5^{\star}$
8	-2	$-5^{\star}$	-2	3	$-4^{\times}$	1	1	3	$7^{\star}$	2	3	-2
9	2	-1	$2^{\times}$	0	2	0	0	1	-1	$-2^{\times}$	0	0

Table 6.3 contains the summed contributions of the JJA-PC^{+}s, just as in Table 6.2 for DJF and YAR. Based (i) on Table 5.2, which contains the selected simulations and (ii) on the sign of the summed contributions pertaining to the selected simulations (Table 6.3) the impcat of a particular REOF^{+} is assessed by counting its apperance in different modes.

Now we have gained a decomposition of the circulation over NAEU into objective patterns for DJF, YAR and JJA. Moreover we have achieved a measure for the appearance of these patterns in outstanding periods and attached levels of significance to them.

Chapter 7

Conclusions

This chapter is devoted to a comprehensive look at the results derived so far and to the interpretation of the findings gained. First, we will concern ourselves with the tables that accompanied our way so far. Findings, kept in these tables, will join cool or warm GAR conditions to different NAEU circulation patterns. Second, the detected patterns will be interpreted in terms of their climatological impact and third the external forcings' regional scale effects will be discussed.

7.1 Winter and the whole year

Based on Table 5.2, which identifies ECHO-G simulations that reasonably trace the run of GAR temperature observations, the contributions of the time coefficients are counted and attached to the corresponding outstanding periods (as given in e.g. Table 6.2). These results are now aggregated in Tables 7.1 and 7.2 below, which consist of two main-lines and two main columns. The lines refer to outstanding periods that are either cool (1st line) or warm (2nd line). Each of the two main-lines are cut into three sub-lines that in turn stand for an increasing degree of significance. The main two columns refer to negative (left) or positive (right) contributions of the time coefficients and are further cut into four or six parts depending on the season (four in case of DJF and YAR, six in case of JJA). In case of DJF and YAR, each part is devoted to one of the circulation patterns (shown in Figures 6.4 and 6.5).

To enhance the readability of the tables and their coaction among each other we state an example: Let us select the first DJF circulation pattern (REOF$^+$1, see Figure 6.4). Then Table 4.1 tells that there is a total of 8 outstanding periods during winter. Together with the special period from 1810 to 1820 (which is also included) there is a total of 9 periods. However, as the second period persists for only 5 years and the last period, that starts 1990, is outside of the simulated period (1756–1990) only seven periods are actually taken into account. Five of these are cool periods (1, 3, 6, 8, 9) and two are warm (5, 7; see Table 4.1). As said above, cool periods belong to the first main-line and warm periods to the second main-line.

Table 5.2 tells that, during period 1 observations are reasonably traced by the sc-simulation. This simulation exhibits negative contributions for the first three patterns and a positive contribution for the fourth (as it can be seen in Table 6.2, first line, column 6 to 9). Thus, three marks are drawn in the first sub-line, left half of Table 7.1, right into the columns that stand for the 1st, 2nd and 3rd circulation pattern and one mark is made in the right half, where the positive contributions of the 4th pattern are counted. During a warm period the approach is the same but we would draw the marks into the second main-line.

Table 7.1 contains the marks for all periods and for all three levels of significance (the three

Table 7.1: Counting of positive or negative occurrences of RPC+s in warm or cool outstanding DJF periods. Positive or negative contributions are indicated by $\not\circ$. Cruxes indicate values that are farther than one σ away from the population average and stars correspond to averages that are significantly different at critical values of 0.2/0.1 (two/one-tailed tests).

			1^{st} main column				2^{nd} main column			
	DJF	sig	-				+			
			RPC+1	RPC+2	RPC+3	RPC+4	RPC+1	RPC+2	RPC+3	RPC+4
1^{st} m. line	cool	$\not\circ$	~~///~~ /	////	////	///		//		///
		$\times$	///	/	///	//		//		
		$\star$	///	/	//	//		//		
2^{nd} m. line	warm	$\not\circ$	/	//	/	/	//	/	/	//
		$\times$								
		$\star$								

sub-lines of the two main-lines). Thereby, $\not\circ$ stands for the the averaged time coefficients being above or below zero, $\times$ stands for values being at least one σ away from the population means and $\star$ for values being different at critical values of 0.2 for two tailed tests. Briefly, Table 7.1 shows the attribution of circulation patterns to cool and warm outstanding periods.

Now we make use of the following assumption, which will assist in interpreation: The occurrence of negative contributions during outstanding cool periods is put together with occurrences of positive contributions during outstanding warm periods. This assumption can be formulated in another way too: We do not distinguish between the occurrence of a particular circulation pattern in a cool GAR episode and the occurrence of its inverse pattern in a warm periode and vice versa. We count such cases as the same. We have pictured that with blue and red lines in the central columns of the table which are a 'score sheet'. Practically, this means that we put the marks contained in the upper left/right boxes together with the corresponding marks in the lower right/left boxes (in Tables 7.1, 7.2 and 7.3).

For DJF all that yield the following results: RPC+1 contributes 8 times positively to warm or negatively to cool outstanding periods, while it contributes one time to the opposite case (i.e. negatively to warm or positively to cool outstanding periods). The result of RPC+3 is somewhat similar. It can be found 5 times contributing positively to warm or negatively to cool outstanding periods while the other way around appears just once. The other RPC+s show a more balanced picture: 5 to 4 in both cases.

When averages are tested on their dissimilarity from the population average the sample size shrinks (i.e. there are fewer contributions) but the main message remains with a slight alteration regarding RPC+4. For RPC+1 the result is 3 to 0 (for $\times$ as well as for $\star$) and for RPC+3 it is 3 to 0 and 2 to 0, depending on $\times$ or $\star$, respectively. RPC+2 remains balanced: 1 to 2 in both cases ($\times$ and $\star$) but RPC+4 turns out to contribute 2 times positively to warm periods and no longer positively to outstanding cool periods.

Table 7.2 corresponds to YAR and is composed analog to Table 7.1. As already elaborated, the patterns for DJF and YAR are similar and hence, results shown in Table 7.2 may be used as another sample to investigate the assignment of the patterns to warm and cool outstanding periods. Some of the outstanding periods occur in both 'seasons', DJF *and* YAR and hence,

Table 7.2: The same as Table 7.1 but for YAR.

YAR	sig	-				+			
		RPC+1	RPC+2	RPC+3	RPC+4	RPC+1	RPC+2	RPC+3	RPC+4
cool	⌀ × ⋆	/// // //	//	~~///~~ // //	/// /// //		/// / /		//
		RPC+1	RPC+2	RPC+3	RPC+4	RPC+1	RPC+2	RPC+3	RPC+4
warm	⌀ × ⋆		/ / /		/// /	/// // /	//	////	/

such samples are not really independent. However, Table 7.2 works as an addendum that helps to get a clearer picture of the patterns' regional scale impact. As for DJF, REOF$^+$1 and REOF$^+$3 contribute more frequently positively/negatively to warm/cool outstanding periods than the other way around (REOF$^+$1: 6 times to 0 times and REOF$^+$3: 9 times to 0 times). Again, the other REOF$^+$s appear more balanced. However, similar as for DJF, on a higher level of significance, REOF$^+$4 appears to provide positive contributions during outstanding warm periods, while REOF$^+$2 tends to contribute to the opposite case.

Summing up DJF and YAR findings, the resulting picture may be described in the following way: Occurence of REOF$^+$1, REOF$^+$3 and somewhat less pronounced of REOF$^+$4 seem to cause warm conditions in GAR, when being orientated in accordance to Figures 6.4 and 6.5, and cool conditions in the reverse case. REOF$^+$2 seems to work in the opposite direction. This outcome agrees to the physical meaning of the patterns (Figures 6.4 and 6.5). REOF$^+$1 stands for transport of relatively warm, maritime air masses from the Atlantic into Europe. REOF$^+$2 blocks the way for westerlies to enter Europe and can be related to cool, continental conditions in DJF. REOF$^+$3 signifies advection of tropical air masses across the Iberian Peninsula out to the North Atlantic. REOF$^+$4 indicates meridional air transport from the area around Iceland south-eastward into Europe. And because the North Atlantic ocean in DJF around Iceland is warmer than the continent (Reynolds and Smith 1995) it causes warm GAR conditions.

The arising question is: 'Is this result trivial?'. The answer is: 'No'. Even if, from a meteorological point of view, the physical meaning of the patters is almost obvious, it is not an essential consequence that this is actually achieved here. There is no guarantee that ECHO-G, even if it reasonably reproduces temperature evolution during outstanding periods, produces meaningful circulation at the same time in a comparably small part of the Northern Hemisphere. This result tells that the investigated simulations, carried out with ECHO-G, show meaningful features of the atmosperic circulation in NAEU during outstanding DJF and YAR periods in case that their temperature evolution is in agreement with the observations.

Table 5.2 still contains another finding. It shows that GAR temperature in DJF and YAR is more often similarly modeled when forced historically or with a constant solar constant than when forced with no increasing greenhouse gases or without volcanoes. Simulations forced historically and with constant solar constant are found to appropriately describe the observed temperature evolution during outstanding periods seven times whereas the ng- and nv-simulations

are two times applicable. Figure 7.1 shows the historical forcings in terms of effective solar constant (see Chapter 3) and the DJF (long term subset) GAR detrended temperature. The blue curve shows the year to year variability, the red and black curves the 11- and 31-year low-pass filtered temperature, respectively. The effective solar constant is plotted in pink. As explicitely discussed in Chapters 2 and 4, two trends corresponing to different subperiods (1760–1890, 1891–2000) have been removed from the long term temperature subset. This causes the jump discontinuity at 1890/1891. Of corse, things should not been overrated, but one may conclude that the run of the effective solar constant and those of GAR temperature are not independent. Especially, volcanic activity seems to be related to GAR temperature. This appears even more palpable in the right panel, which shows the temperature evolution on a yearly base and hence includes effects on summer temperature caused by volcanic activity. The 1810s may act as an example where pronounced volcanic eruptions occur together with low GAR temperatures. Therefore, it appears plausible that ECHO-G simulations, driven by forcings that include volcanic activity are able to simulate GAR temperature somewhat more similar than simulations that let them out. From another point of view this could be said in another way: The external forcings shown in Figure 7.1 exhibt similarities to GAR temperature. And hence, the fact that ECHO-G simulations based on volcanic forcings are more similar to the observations during outstanding temperature periods may indicate ECHO-G's ability to reasonable represent the climate system in the investigated area.

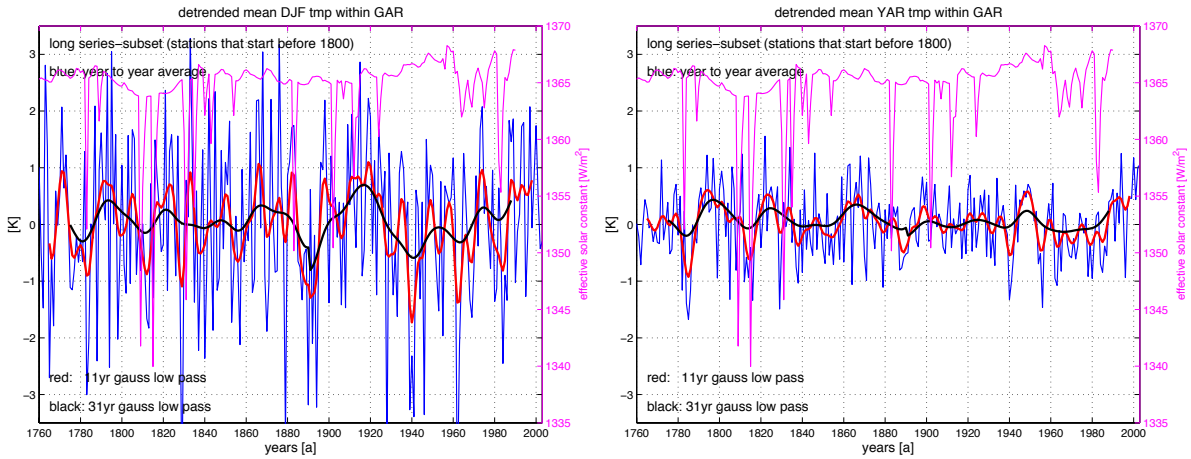

Figure 7.1: Historical forcings in terms of effective solar constant (W/m^2, pink) and GAR detrended temperature (K; blue, red and black) for DJF and YAR. *abszissa*: years from 1760 to 2000; *left ordinate*: degree Kelvin; *right ordinate*: W/m^2.

7.2 Summer

Table 6.3 contains the averaged contributions of the JJA-PC$^+$s, just as in case of Table 6.2 for DJF and YAR. Based (i) on Table 5.2, which comprises the selected simulations and (ii) on the sign of the averaged contributions of the time coefficients pertaining to the selected simulations that reasonably traces the observed temperature run (given in Table 6.3) the impact of a particular REOF$^+$ is assessed by counting its apperance in different modes (postitive or negative – i.e. in accordance to Figure 6.6 or mirrored, respectively). The approach is exactly the same as for DJF and YAR but the outcome is more difficult to interpret (see Table 7.3). Cool

Table 7.3: Counting of positive or negative occurrences of selected RPC$^+$s in warm or cool outstanding JJA periods. Cruxes indicate values that are more than $\pm\sigma$ away from the population average and Stars correspond to averages that are significantly different at critical values of 0.2/0.1(two/one-tailed tests). Note, we have abbreviated REOF$^+$s here as R$^+$s to manage with the width of the page.

JJA	sig	-						+					
		R$^+$1	R$^+$2	R$^+$3	R$^+$4	R$^+$5	R$^+$6	R$^+$1	R$^+$2	R$^+$3	R$^+$4	R$^+$5	R$^+$6
cool	⌀		//	//		////	///	////	///	//	////	/	/
	×		//			//	///	///	//	/	///		/
	⋆		//			/	//	/	//	/	//		/
		R$^+$1	R$^+$2	R$^+$3	R$^+$4	R$^+$5	R$^+$6	R$^+$1	R$^+$2	R$^+$3	R$^+$4	R$^+$5	R$^+$6
warm	⌀	////	///	//	////	///	//	//	///	/	/	///	////
	×	//	//		/	//	/	/	/			/	//
	⋆	/	//		/	/	/		/				/

conditions are more closely related to REOF$^+$1, REOF$^+$3 (very weakly) and REOF$^+$4, warm GAR conditions contingently to REOF$^+$6. The other patterns appear balanced.

The outcome, achieved for summer is, in contrary to the findings related to winter and the year as a whole, somewhat unexpected. REOF$^+$1, REOF$^+$3 and REOF$^+$4 contribute positively to cool conditions. Taking them together, the proportions of the 'cool to warm contributions' are 20 to 6 ($\not\varnothing$), 1 to 10 ($\times$) and 0 to 6 ($\star$), in order of increasing levels of significance as shown in Table 7.3. Hence, one may conclude that occurrence of these patterns (REOF$^+$1,3,4) when orientated as shown in Figure 6.6 is more likely to cause cool conditions in JJA than the other way around. The other REOF$^+$s show an unclear picture. Putting the countings of these patterns together leads to: 19 times to 13 times (positive contributions to outstanding warm episodes or negative ones in outstanding cool periods $\not\varnothing$), 11 to 8 ($\times$) and 7 to 7 times ($\times$). This would mean that the occurrence of patterns REOF$^+$1,5,6 do not yield a clear local scale reaction in the sense of cool or warm conditions.

However, this result should not be overrated. There are several reasons making the JJA findings more questionable than those achieved for DJF and YAR. First, the sample size is considerably smaller and so the results are more unstable. Second, weather conditions during summer-near seasons in the midlatitudes are much more triggered by small scale conditions than the synoptic scale weather producing systems of the winter season. This is reflected by e.g. the fact that six summer-EOFs are needed to explain about the same fraction of variance than four DJF- or YAR-EOFs. Third, the assumption about the impact caused by the occurrence of the patterns resp. it's inverse which was made in case of DJF and YAR and applied to summer too, may not hold for summer. The argument that, if a particular circulation pattern causes a particular local scale temperature reaction, it's inverse causes the opposit local scale reaction should work when large scale evolution happens by jumping from one state (i.e. pattern) to the other, not taking on two or more at the same time. (A coherent temporal appearance of two or more pattern will work too.) Although the statement is incomplete, one would intuitively expect it to work better in the case of just a few states (patterns), each explaining a comparable large part of circulation variation, than in the case of many patterns that carry only small fractions of explained varinaces.

So, conclusions drawn for summer are even more arguable than those derived for winter because of the smaller sample size, the more patchy atmospheric conditions and the succsessional more uncertain application of the classification statement.

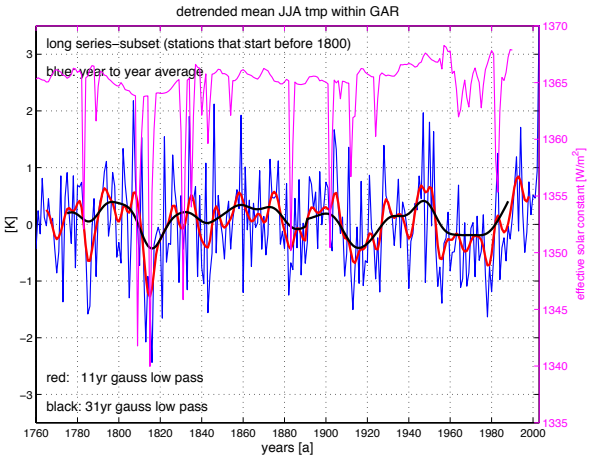

Figure 7.2: Historical forcings in terms of effective solar constant (W/m^2, pink) and GAR detrended temperature (K; blue, red and black) for JJA. *abszissa*: years from 1760 to 2000; *left ordinate*: degree Kelvin; *right ordinate*: W/m^2.

Another newsworthy detail is shown in Figure 5.2 (first line) where the summers of period 3 (1810–1820) are depict. This periode was characterized by pronounced volcanic activities and GAR temperature was, in partucular during the warm season, significanlty low. All ECHO-G simulations that account for volcanoes show low temperature values compared to the surrounding period. The nv-simulation in contrast shows distinct high temperatures.

Chapter 8

Summary and Outlook

This chapter is devoted to the question 'what is new?' or 'what are the contributions made to the current body of knowledge?' on one hand and to the question: 'what is left and worth for further investigations?' on the other hand.

For the first question: We believe that the generation of HISTALP, a homogenized instrumental dataset that consists of a number of climate elements (temperature, precipitation, pressure, hours of sunshine, cloudiness, ...) and spans a long period of about 250 years is of enormous value. It contributes in many ways to the ongoing discussion about climate change and variability and it constitutes a solid basis for model studies and estimating possibe future changes. This is mainly because (i) the sample size is large and (ii) non-climatic information as, for instance, changes in the measuring instruments or sites are removed. Parts of this exhausting procedure, which is described in Chapter 2, were done within the scope of this study. Compared to other leading datasets, HISTALP adds another 50 (precipitation) to 100 (temperature) years to the "instrumental period". This brings a new quality into the early instrumental period of the late 18th to mid-19th century which is usually covered by indirect climate information only.

The detailed evaluation of temperature variability and trends in Chapter 2 revealed interesting new climatological aspects and puts several common opinions in perspective. Some of the astonishingly different monthly temperature trends, see for examples Figure 2.7, deserve further analysis. Other features like the seasonal variation of sub-regional differences (e.g. Figures 2.11, 2.12) are planned to be further analyzed. The detection and quantifying of homogeneous GAR temperature regions and the subsequent analysis of the corresponding temperature evolutions show that there are significant differences on the seasonal and yearly timescale, which will be further investigated in following studies, but that differences become small on larger (decadal) timescales. This finding was central for the present study, because it is a good argument for GAR temperature to be on a mulit-annual to decadal timescale representative for an even larger region. For such a region of e.g. European scale it is reasonable to expect climate models to generate meaningful results for temperature.

The detection of outstanding temperature periods in GAR during the past 250 years is a new contribution. It is less centennial climatic trends which are recognized in real life. It is much more the variations at multi-annual to decadal scale that better correspond to the public awareness. A time span of 100 years and more may be of intellectual interest but it does not relly touch our minds and has problems to interfere with the public opinion. Therefore, dealing with the timescale of the "outstanding periods" of our study may help to reduce the mentioned recognition problem of slow long-term evolutions of climate. These periods are detected by objective methods and evaluated also by the use of Alpine glacier records. Although glaciers

are among the leading means to visualize long-term climate warming, a second closer look reveals an additional glacier variability component that corresponds to the time scale of the OPs of our study. The reason of this ”detrending” of glacier variability towards long-term features is the (more or less time lagged) tendency of glaciers to find a balance with climate by removing/descending to higher/lower altitudes to answer climate warming/cooling. We could show that, although advancing and retreating of glaciers is triggered by more parameters than temperature alone there is a rather good agreement with the outstanding periods and those few cases where glacial behavior does not go along with temperature can be understood by the help of precipitation.

Four of the nine isolated outstanding periods were detected in the early instrumental period, being for the first time systematically documented now at satisfying quality by HISTALP. Two of them stand for immediately successive interesting periods. The first (near 1800) with high spring-summer temperatures still is a matter of discussion among instrumental- and proxy climatologists. It was followed by a sudden temperature decrease (the most extreme ”sudden climate event” in the study period) in the 1810s, the ”Volcanic Years without Summers”. The climate deterioration in the latter period has caused severe impacts on crops and also astonishingly fast glacier advances. Also the following series of OPs each had specific impacts for which thoseon glaciers are exemplarily discussed in the study. Of special interest in terms of the current climate change discussion is the pre-last - the cooling (strongest in summer months) in the 1960s and 70s. Here, typically for the erronious mixing of different time scales, a widespread discussion about a possible and disastrous future cooling took place. Although the stronger impact of anthropogenic greenhouse gases increase on future climate (at centennial scale) was clear already within the scientific community, the respective transport of this message towards the public opinion had no chance in a time of (decadal scale) summer cooling.

Over a large scale sector, that covers the North Atlantic and Europe, we have objectively investigated atmospheric circulation as simulated by ECHO-G by means of Rotated Empirical Orthgonal Functions. It was found that the circulation patterns corresponding to differently forced simulations are similar but the time coefficients, showing the patterns’ appearance, are quite diverse. This may reflect the impact of different external forcings on atmospheric circulation and forms the basis of further analysis.

For all outstanding periods we selected ECHO-G simulations, that reasonably trace the observed temperature run, and caluclated the corresponding contributions of the circulations patterns. Thereby it is possible to relate different circulation patterns to outstanding warm or cool European conditions.

Circulation of the whole year is mainly dominated by winter conditions. This is well known and expressed in the circulation patterns found by REOF-analysis, which are similar. So, winter and the year as a whole were joined together, whereby the sample size is enhanced. Findings assign a pronounced zonal airflow, advection of subtropical air and air mass transport from northern North Atlantic to warm conditions in Europe, while blockings over Central Europe are attached to cool conditions. This agrees to the physical understandings of the atmospheric processes and is likely to show some ability of ECHO-G in consistently simulating temperature and circulation during outstanding periods.

The assignment of differently forced simulations to outstanding periods may also be used to relate forcings to regional scale impacts. Summers of the 1810s may serve as an example. Simulations that do account for volcanic activities show low temperatures compared to the surrounding period. This is in accordance with the observations. The only simulation that does not fit is the one driven without volcanic forcings. This may admit of the conclusion that

volcanic activities were responsible for the cool summers of the 1810s in Europe.

Findings derived for summer are clearly more indistinct. In contrary to winter and the whole year, which is dominated by large scale atmospheric processes, summer exhibits processes that are in general smaller in space and shorter in duration. This is well known and can be seen by the objective analysis of the summer-criculation over NAEU. Because of this and the small sample size on which conclusions are based summer findings should not be overrated.

Anyway, in the course of the study we came up against some open questions or needs which will be shortly adressed in the following.

There is a need of multi-centennial spatially high resolved model runs. This is, up to our mind, necessary to allow for a better comparison of measured and modeled climate. One way to circumvent expensive simulations would introduce statistical downscaling (von Storch et al. 1993). This approach would even permit to investigate the stability of empirical transferfunctions, as the period that provides measurements is quite large.

Closly linked to the above is the regional scale need. It is desireable to have spatially high resolved and well homogenized measured time series with European coverage. Such a dataset does not exist so far. HISTALP (covering 7% of Europe) may serve as an example.

Furthermore the inclusion of other climatic elements like, for instance, cloudiness, sunshine and humidity is reasonable for sure. In this study we have shortly used cloudiness to formulate a hypothesis that cold serve as en explanation for pronounced differences between modeled and measured temperature evolutions during three summer outstanding periods. We consider a much more intensive use of the complete bandwidth of climate elements as essential for a better understanding of climate variability. This would also bring a new quality and extended possibilities into combined model-data analysis. Today's concentration on temperature narrows the view and fails to use the overwhelming part of the capacity of climate modelling. The cloudiness-example in this study hinted at the respective potential.

This study strongly benefited from the teamwork of two 'species' of climate researchers – the 'modellers' and the 'data-specialists'. Often there is not much of an intersection between their 'worlds' in the sense of a real understanding of mutual abilities – strengths and enervations. 'data-specialists' often do not have an idea of how to interpret model output (spatial and temporal scales) whereas 'modellers' often take measurements as they are although pertaining errors can be in the range of the signal or even larger (homogenisation, outlayer-elimination, etc.).

Such cases of 'interdisziplinary' teamwork should become more usual.

Appendix A

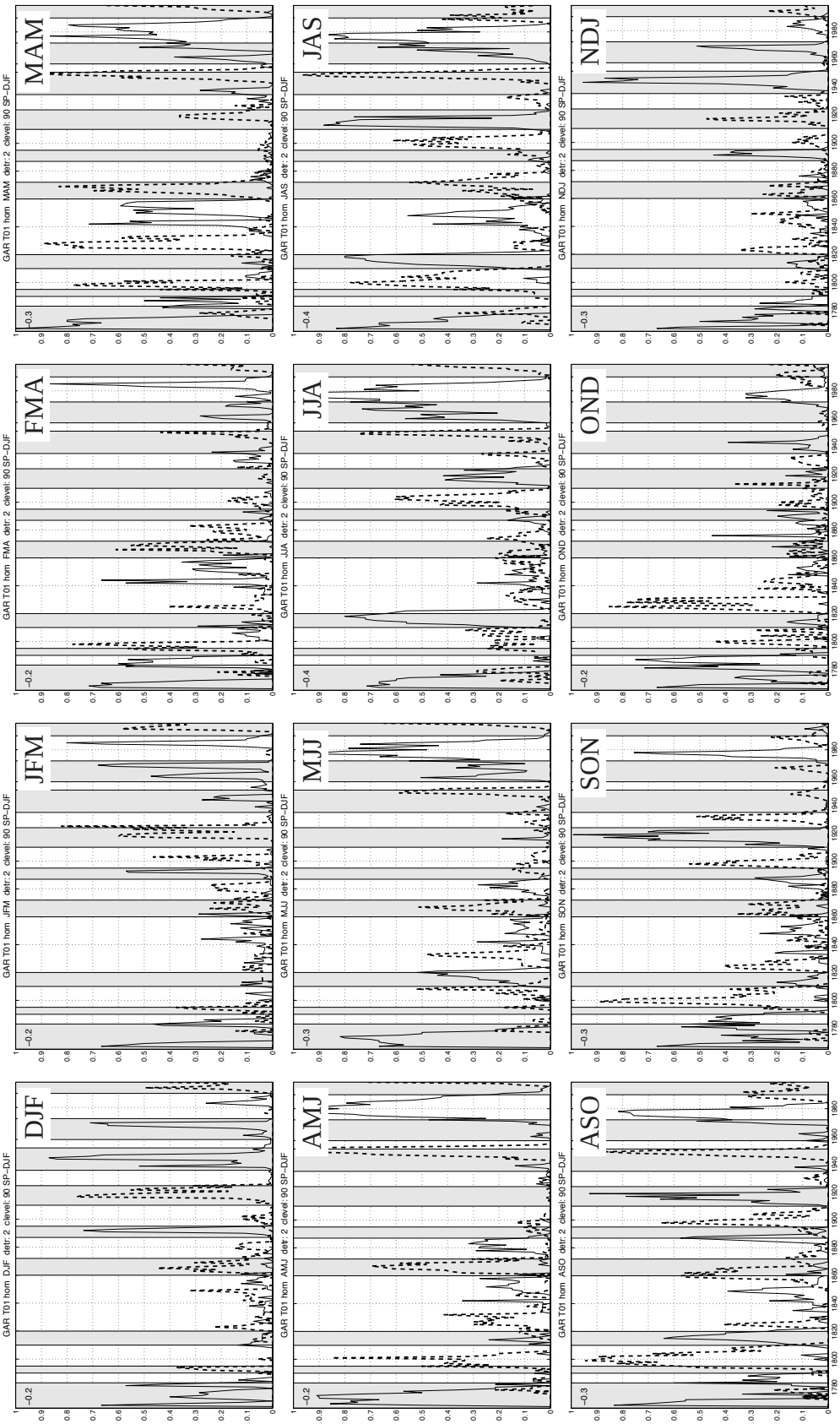

Figure A.1: Fraction of stations with significant temperature-anomalies for classical and moving seasons (1760–2003). Vertical shaded bars indicate outstanding JJA periods, dashed/solid lines refer to positive/negative anomalies. Note the relative large fraction of stations that show significant (α=0.9) anomalies in the 1860s (fourth shaded bar from left), lasting from AMJ (left panel, second row) to ASO (left panel, third row). This is mentioned in the discussion on page 52. Another noteworthy period is the warm one located prior to 1800, which is most pronounced from SON to AMJ (with breaks). This period is known as the 'Josefinische Wärmeinsel' and refered to on page 54.

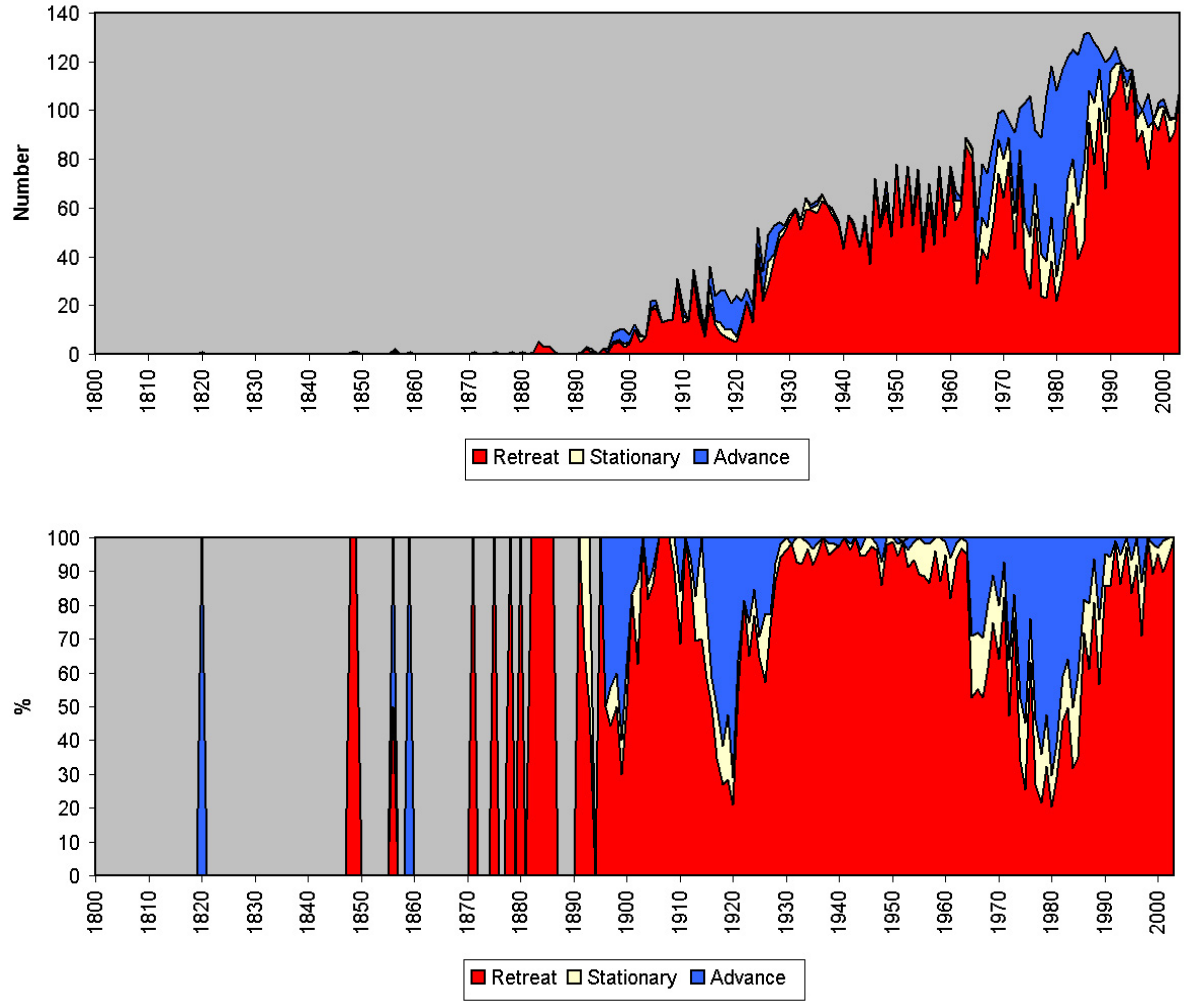

Figure A.2: Advances and retreats of Austrian glaciers; orange indicates glacier retreats, blue: advances and yellow: no change; grey: no data; *upper panel*: actual number of glaciers contributing to the analysis against time; *lower panel*: percentage of the total number of contributing glaciers against time. Note: the listing on page 56 refers to the advances of the 1810s and the retreats of the 1860s.

Figure A.3 (Page 96) shows the comparison between ECHO-G temperature simulated within outstanding periods and simulated within surrounding periods in °K. The Figure contains three main columns – the first for winter (DJF), the second for summer (JJA) and the third for the year as a whole (YAR). Each of these columns is split into four subcolumns for the different ECHO-G simulation, i.e. a0, sc, ng and nv, respectively. The lines refer to all outstanding periods listed in Table 4.1. Note, for instance, the cool summers of the 1810s (enhanced vulcanic activity), which can be found in all simulations besides the nv-simulation, which does not account for volcanic activity – the mild 1860s (end of LIA) or the 1910s (Alpine glaciers advanced), a maritime GAR period, etc.

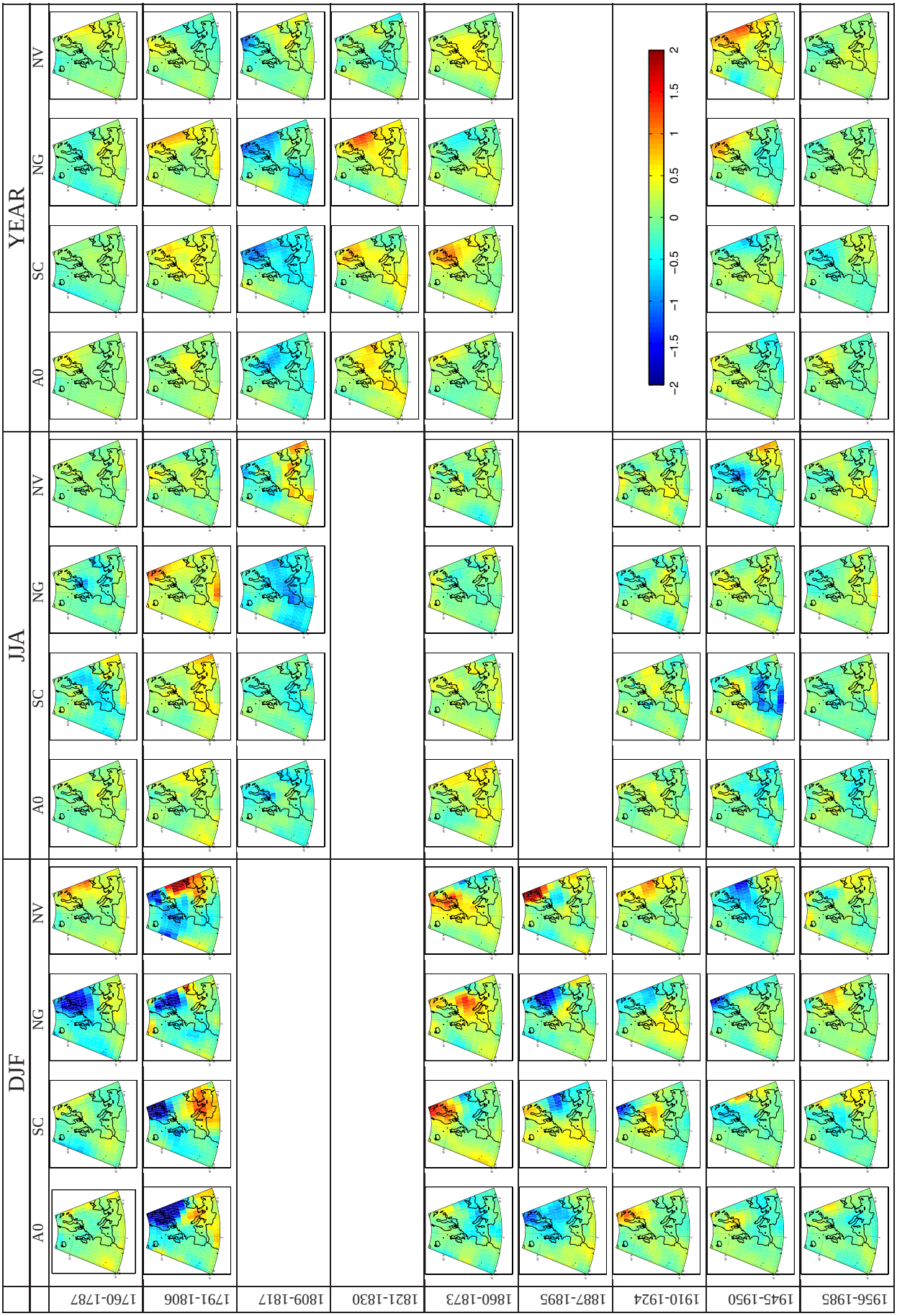
YEAR
JJA
DJF
A0
SC
NG
NV
1760-1787
1791-1806
1809-1817
1821-1830
1860-1873
1887-1895
1910-1924
1945-1950
1956-1985
−2
−1.5
−1
−0.5
0
0.5
1
1.5
2

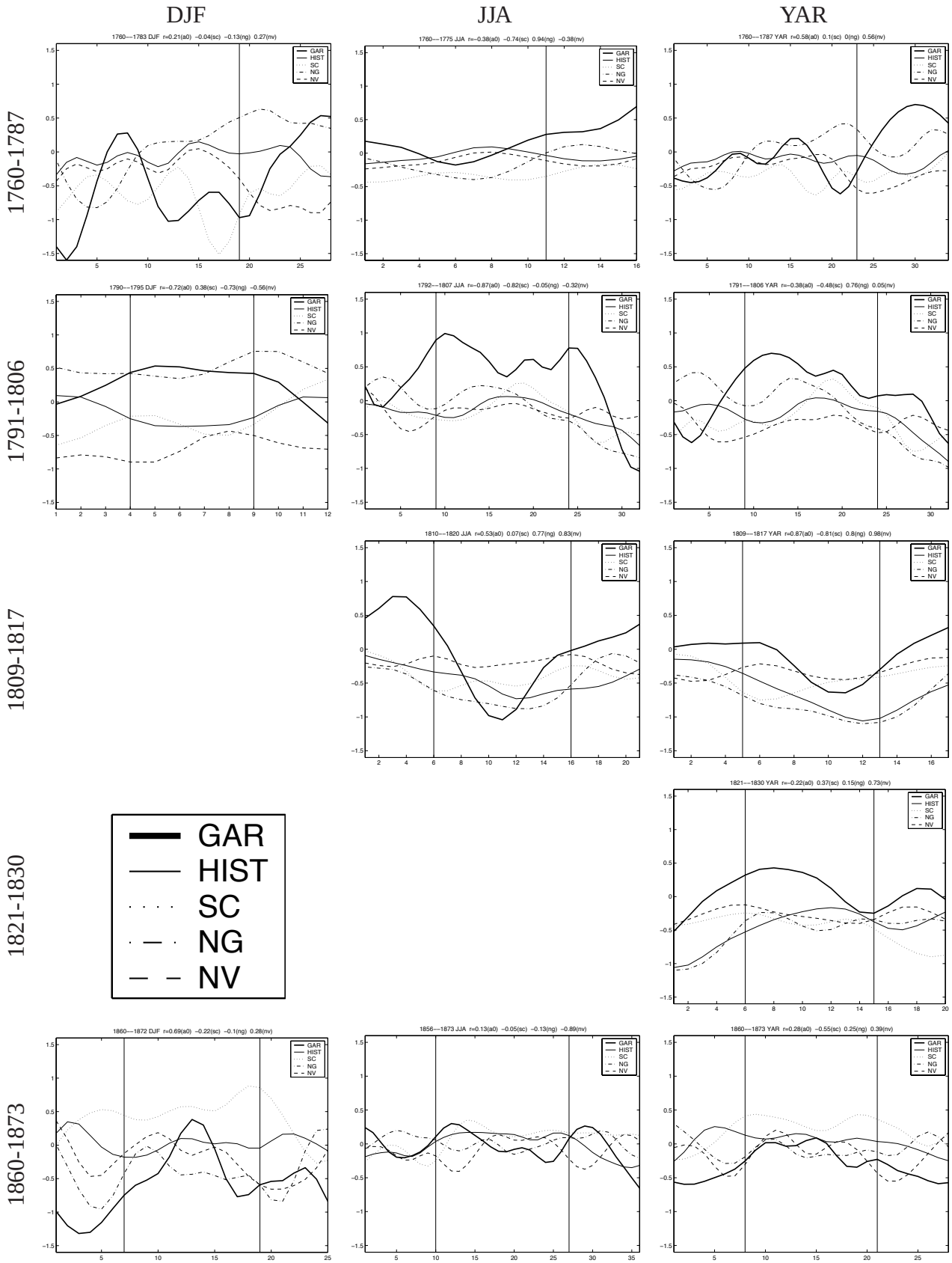

Figure A.4: Comparison of spatially averaged ECHO-G simulations and homogenized observations for DJF JJA and YAR (periods 1 to 5); bold, drawn through line: historical GAR series; thin, drawn through line: a0; dotted: sc; dashed-dotted: ng; dashed: nv.

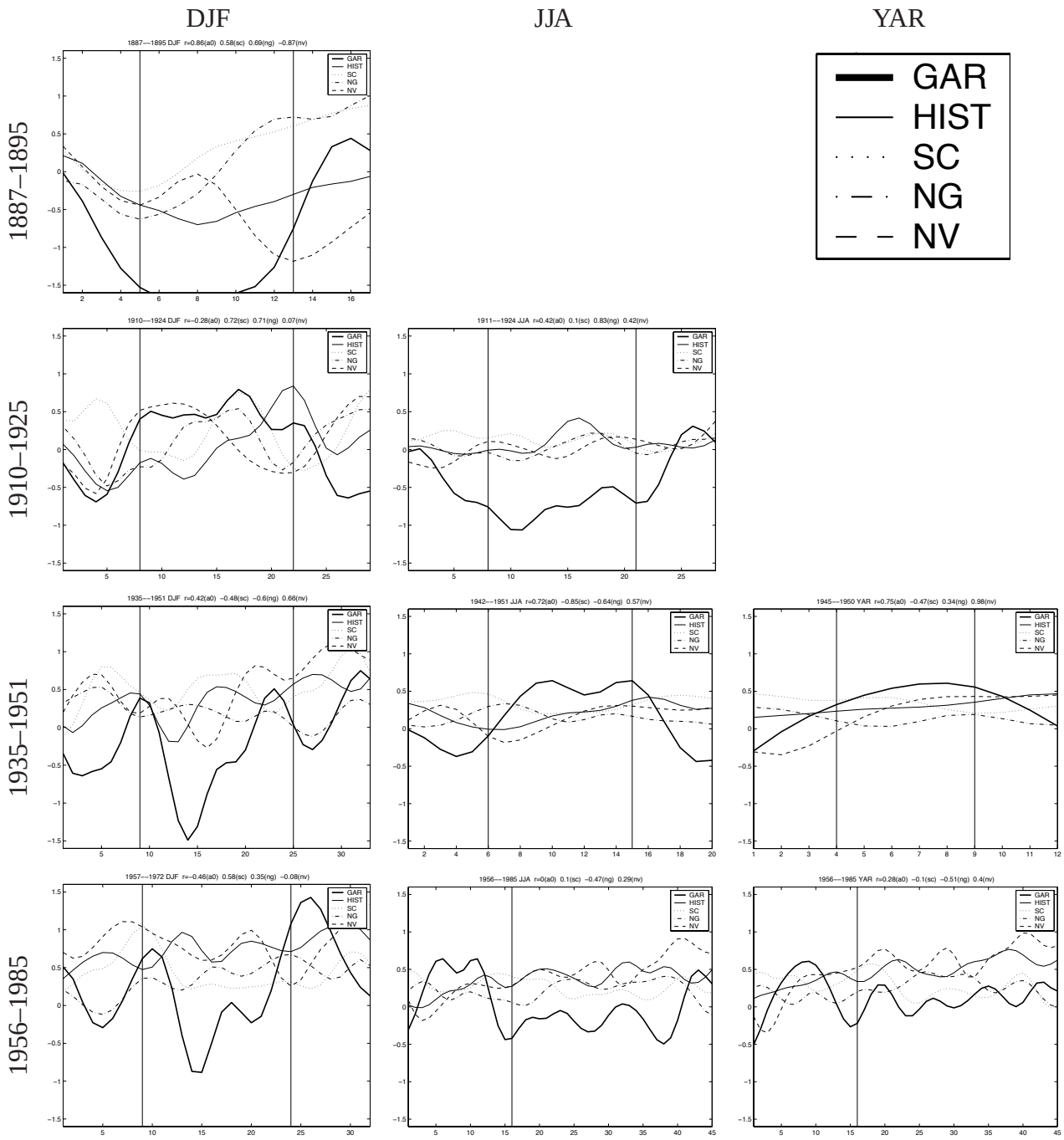

Figure A.5: Comparison of ECHO-G of spatially averaged simulations and homogenized observations for DJF JJA and YAR (periods 6 to 9); bold, drawn through line: historical GAR series; thin, drawn through line: a0; dotted: sc; dashed-dotted: ng; dashed: nv.

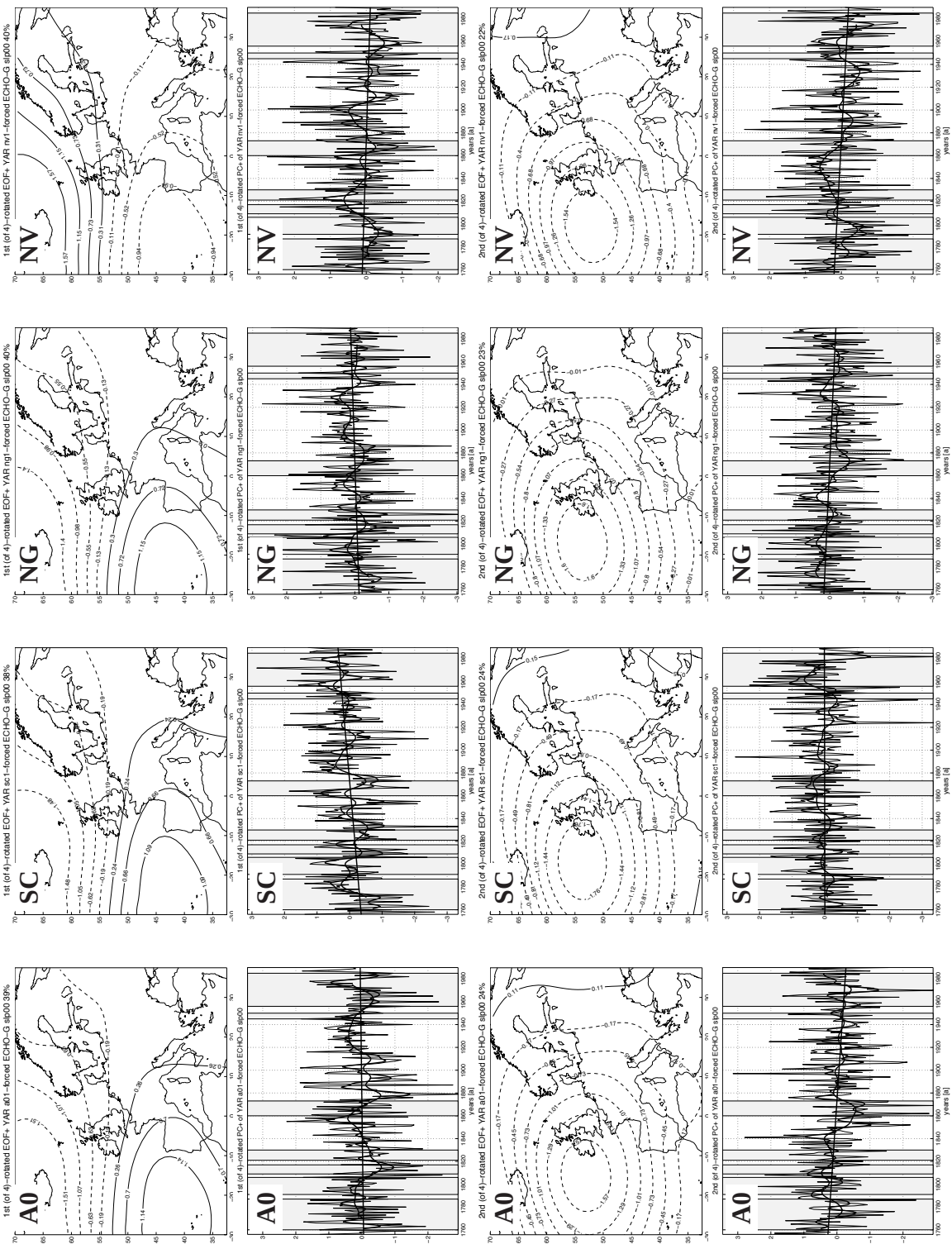

Figure A.6: The first two rotated EOFs and the corresponding time coefficients derived from NAEU years (YAR; 1756–1990). Columns pertain to different forced ECHO-G simulations. From left to right: a0, sc, ng, nv (for abbr. see Section 3). Shaded bars indicate outstanding periods; Curves display unfiltered data, 11 yr and 31 yr Gaussian low pass filtered data.

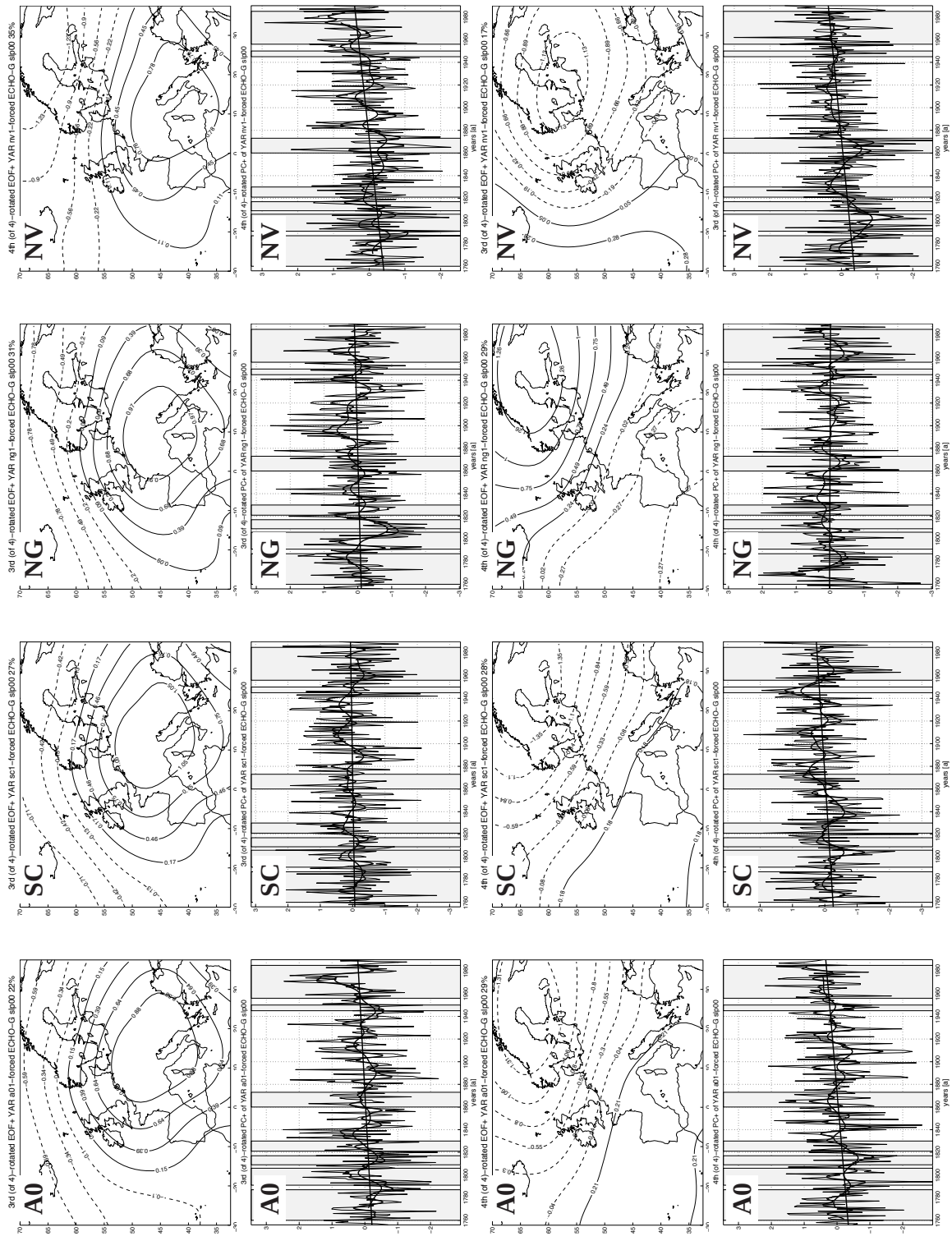

Figure A.7: The same as Figure A.6 but for the third and forth rotated EOFs. Note that patterns are arranged according to the arrangement given by the a0 simulation. For further analysis orientation of (sc, ng, nv) patterns are adjusted to agree with the a0 patterns.

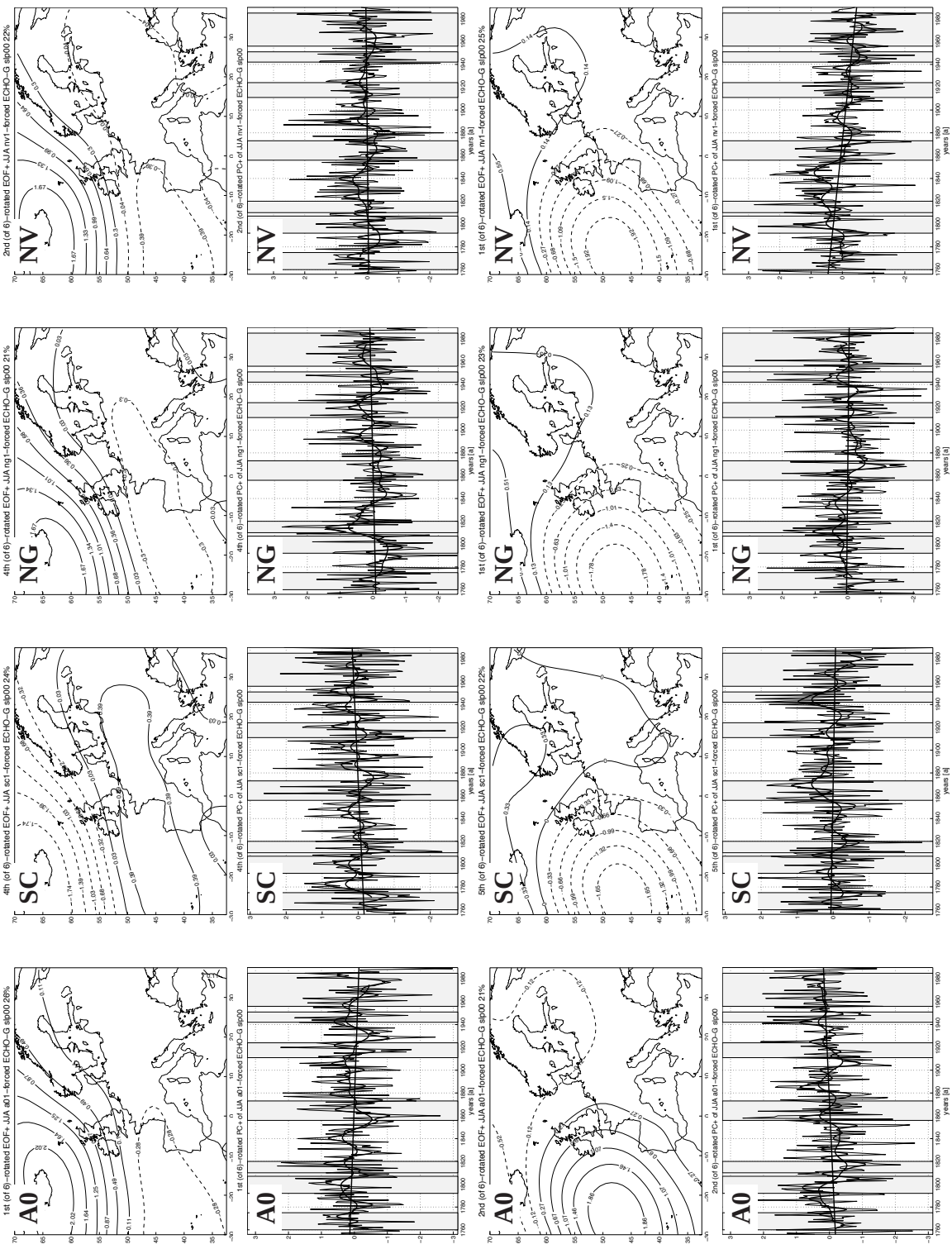

1^{st} REOF+ 1^{st} RPC+ 2^{nd} REOF+ 2^{nd} RPC+

Figure A.8: The first two rotated EOFs and the corresponding time coefficients derived for NAEU summers (JJA; 1756–1990). Columns pertain to different forced ECHO-G simulations. From left to right: a0, sc, ng, nv (for abbr. see Section 3 or Table 8). Shaded bars indicate outstanding periods, curves display unfiltered data, 11 yr and 31 yr Gaussian low pass filtered data.

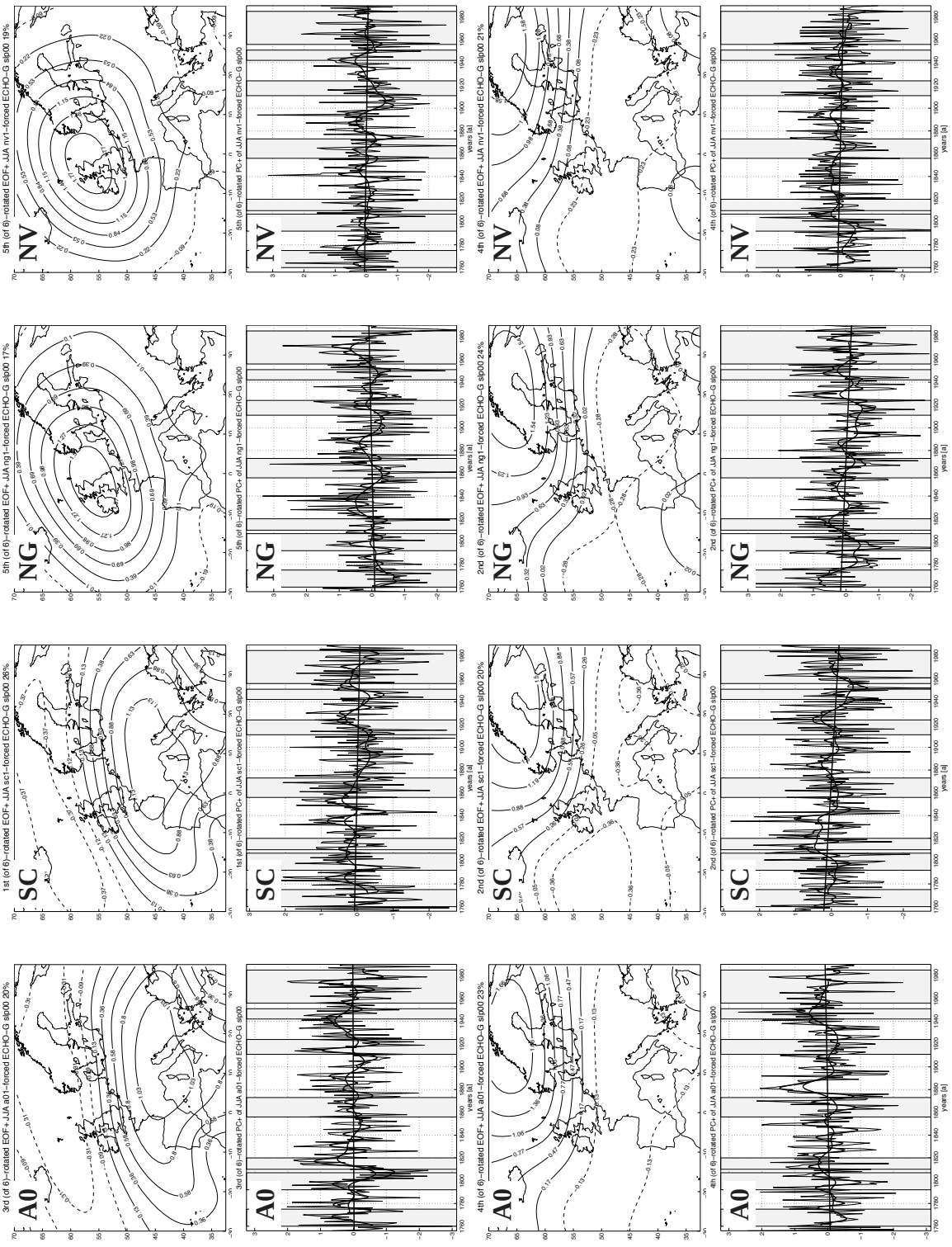

Figure A.9: The same as Figure A.8 but for the third and forth rotated EOFs. Note that patterns are arranged according to the arrangement given by the a0 simulation. For further analysis orientation of (sc, ng, nv) patterns are adjusted to agree with the a0 patterns.

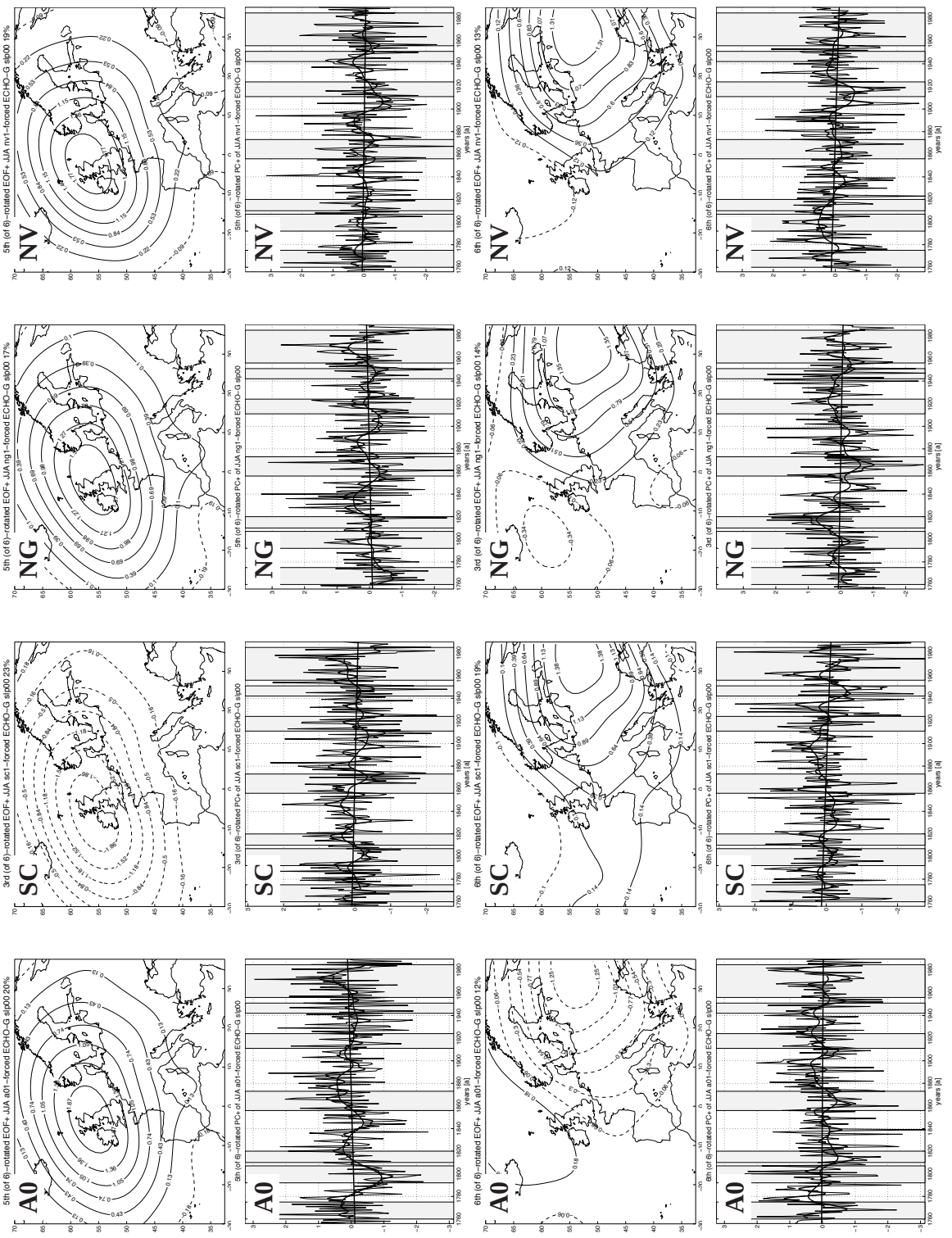

Figure A.10: The same as Figure A.9 but for the fourth and fifth rotated EOFs. Note that patterns are arranged according to the arrangement given by the a0 simulation. For further analysis orientation of (sc, ng, nv) patterns are adjusted to agree with the a0 patterns.

a0 or HIST	ECHO-G simulation driven by the reconstructed forcings
ALOCLIM	Austrian LOngterm CLIMate
ALP-IMP	EU=FP5 RTD project (2003–2006)
AOGCM	Atmospheric Ocean General Circulation Model
CLIVALP	Austrian Science Fund (FWF) RTD project (2002–2005)
DM	Dalton Minimum
ECHO-G	AOGCM developed at MPI Hamburg
ECMWF	European Centre of Medium Range Forecasting
EOF	Empirical Orthogonal Functions
ERA40	ECMWF Re-Analysis
EU	EUrope
GAR	Greater Alpine Region (43N4E to 49N19E)
Hist or a0	ECHO-G simulation driven by the reconstructed forcings
HISTALP	Database of historical, monthly, long-term, spatially dense, multiple climate time series in different modes – two station modes (original and homogenized) and two grid modes (1deg, 10min lat-lon)
IPCC	Intergovernmental Panel on Climatic Change
LEV	Logarithm of EigenValue
LIA	Little Ice Age
LLM	Late Mounder Minimum
MPI	Max Planck Institute for Meteorology
NAEU	North Atlantic EUrope
NAO	North Atlantic Oszillation
NG or ng	as a0 but with CO_2 concentration kept as 280 ppm
NV or nv	as a0 but without the effect caused by volcanic activities
REOF	Rotated normalized EOF
REOF+	Rotated re-normalized EOF
RPC	time coefficient of REOF
RPC+	time coefficient of REOF+
SC or sc	as a0 but with solar forcing kept at DM average
SLP	Sea Level Pressure
xplvr	eXPLained VaRiance

References

Aguilar, E., I. Auer, M. Brunet, T.C. Peterson, and J. Wieringa, 2003: Guidelines on Climate Metadata and Homogenization. World Meteorological Organization (WMO), Geneva. WCDMP-No. 53; WMO-TD No. 1186.

Aschwanden, A., M. Beck, C. Häberli, G. Haller, M. Kiene, A. Roesch, R. Sie, and M. Stutz, 1996: Bereinigte Zeitreihen – Die Ergebnisse des Projekts Klima90, Band.2: Methoden. Klimatologie der Schweiz (Jahrgang 1996). Schweizerische Meteorologische Anstalt, Zürich.

Auer, I., 1993: Niederschlagsschwankungen in Österreich. Österreichische Beiträge zu Meteorologie und Geophysik 7, Central Institute for Meteorology and Geodynamics, Hohe Warte 38, Vienna, Austria. pp. 73.

Auer, I., R. Böhm, A. Jurković, A. Orlik, R. Potzmann, W. Schöner, M. Ungersböck, M. Brunetti, T. Nanni, M. Maugeri, K. Briffa, P. Jones, D. Efthymiadis, O. Mestre, J. Moisselin, M. Begert, R. Brazdil, O. Bochnicek, T. Cegnar, M. Gajic-Capka, K. Zaninivic, Z. Majstorovic, S. Szalai, and T. Szentimrey, 2005: A new instrumental precipitation dataset in the Greater Alpine Region for the period 1800-2002. *Int. J. Climatol.*, **25**, 139–166. Published online in Wiley InterScience (www.interscience.wiley.com). DOI: 10.1002/joc.1135.

Auer, I., R. Böhm, and W. Schöner, 2001: Austrian long-term climate 1767–2000 – Multiple instrumental climate time series from Central Europe. Central Institute for Meteorology and Geodynamics, Hohe Warte 38, Vienna, Austria. pp. 147.

Bard, E., G. Raisbeck, F. Yiou, and J. Jouzel, 2000: Solar irradiance during the last 1200 years based on cosmogenic nuclides. *Tellus*, **52B**, 985–992.

Barnston, A., and R. Livezey, 1987: Classification, seasonality and persistance of low-frequency atmospheric circulation patterns. *Mon. Wea. Rev.*, **115**, 1825–1850.

Baumgartner, A., E. Reichel, and G. Weber, 1983: *Der Wasserhaushalt der Alpen – Niederschlag, Verdunstung, Abfluß und Gletscherspende der Alpen für die Normalperiode 1931–1960*. R. Oldenburg Verlag München, Wien.

Baur, F., P. Hess, and H. Nagel, 1944: Kalender der Großwetterlagen Europas 1881–1939. Bad Homburg v. d. H.

Begert, M., G. Seiz, T. Schlegel, M. Musa, G. Baudraz, and M. Moesch, 2003: Homogenisierung von Klimamessreihen der Schweiz und Bestimmung der Normwerte 1961-1990 – Schlussbericht des Projekts NORM90. Veröffentlichungen MeteoSchweiz 67, MeteoSchweiz.

Beniston, M., 2004: The 2003 heat wave in europe: A shape of things to come? *Geophysical Research Letters*, **31**. L02202.

Blüthgen, J., and W. Weischet, 1980: *Allgemeine Klimageographie*. de Gruzer.

Böhm, R., 1992: Lufttemperaturschwankungen in Österreich seit 1775. Österreichische Beiträge zu Meteorologie und Geophysik 5, Central Institute for Meteorology and Geodynamics, Hohe Warte 38, Vienna, Austria.

Böhm, R., 2004: Systematische Rekonstruktion von zweieinhalb Jahrhunderten instrumentellem Klima in der größeren Alpenregion – ein Statusbericht. In: *Alpenwelt – Gebirgswelten. Inseln, Brücken, Grenzen. Tagungsbericht und wissenschaftliche Abhandlungen*, W. Gamerith, P. Messerli, P. Meusburger, and H. H. Wanner (Eds.), Heidelberg, Bern, pp. 121–131. 54. Deutscher Geographentag.

Böhm, R., I. Auer, M. Brunetti, M. Maugeri, T. Nanni, and W. Schöner, 2001: Regional temperature variability in the European Alps: 1760-1998 from homogenized instrumental time series. *Int. J. Climatol.*, **21**, 1779–1801.

Breuer, G., 2005: 154 Tage Schnee – Wie ein Vulkanausbruch in Island zur französischen Revolution beitrug. Presse (Austrian daily Newspaper).

Brunetti, M., 2005: REOF-based regionalisation of the HISTALP T01-station mode dataset. Personal communication.

Brunetti, M., M. Maugeri, and T. Nanni, 2000: Variations of temperature and precipitation in Italy from 1866 to 1995. *Theor. Appl. Climatol.*, **65**, 165–174.

Craddock, J., and C. Flood, 1969: Eigenvectors for representing the 500 mb geopotential surface over the Northern Hemisphere. *Quart. J. Roy. Meteor. Soc.*, **95**, 576–593.

Crowley, T., 2000: Causes of climate change over the past 1000 years. *Science*, **289**, 270–277.

Cubasch, U., B. Santer, and G. Hegerl, 1995: Klimamodelle - wo stehen wir? *Physikalische Blätter*, **51**, 269–276.

Cubasch, U., and R. Voss, 2000: The influence of total solar irradiance on climate. *Space Science Reviews*, **94**, 185–198.

Cubasch, U., R. Voss, G. Hegerl, J. Waszkewitz, and T. Crowley, 1997: Simulation of the influence of solar radiation variations on the global climate with an ocean-atmosphere general circulation model. *Climate Dynamics*, **13**, 757–767.

Eddy, J., 1976: The Maunder Minimum. *Science*, **192**, 1189–1202.

Efthimiadis, D., P. Jones, K. Briffa, I. Auer, R. Böhm, and W. Schöner, 2005: Construction of a 10-min gridded precipitation dataset fort he Greater Alpine Region 1800–2003. in preparation.

Ehrendorfer, M., 1987: A regionalization of Austria's precipitation climate using principal component analysis. *J. Climatology*, **7**, 71–89.

Etheridge, D., L. Steele, R. Langenfelds, R. Francdey, J. Barnola, and V. Morgan, 1996: Natural and anthropogenic changes in atmospheric CO_2 over the last 1000 years from air in Antarctic ice and firn. *Journal of Geophysical Research*, **101**, 4115–4128.

Fliri, F., 1974: Niederschlag und Lufttemperatur im Alpenraum. *Wiss. Alpenv.*, **24**, 111–125.

FOWG, 2004: Hydrologischer atlas der schweiz. ISBN 3-9520262-0-4.

Frei, C., and C. Schär, 1998: A precipitation climatology of the alps from high-resolution rain-gauge observations. *Int. J. Climatol.*, **18**.

Gajic-Capka, M., M. Percec Tadic, and M. Patarcic, 2003: Digitalna godisnja oborinska karta hrvatske (a digital annual precipitation map of croatia). *Hrvatski meteoroloski casopis (Croatian Meteorological Journal)*, **38**, 21–33.

Gerstengarbe, F.W., P. Werner, and U. Rüge, 1999: Katalog der Großwetterlagen Europas (1881–1998) Nach Paul Hess und Helmuth Brezowsky. Potsdam-Institut für Klimafolgenforschung.

González-Rouco, J.F., H. von Storch, and E. Zorita, 2003: Deep soil temperature as proxy for surface air-temperature in a coupled model simulation of the last thousand years. *Geophysical Research Letters*, **30**, doi:10.1029/2003GL018264.

Graf, H.F., I. Kirchner, A. Robock, and I. Schult, 1993: Pinatubo eruption winter climate effects: model versus observations. *Climate Dynamics*, **9**, 81–93.

Haeberli, W., 2004: *Mass Balance of the Cryosphere*, Chapter 15, pp. 559–578. Cambridge University Press.

Haeberli, W., H. Bösch, K. Scherler, G. Østrem, and C. Wallén, 1989: World Glacier Inventory Status 1988, A contribution to the Global Environment Monitoring System (GEMS) and the Intenational Hydrologial Programme. IAHS(ICSI)-UNEP-UNESCO, World Glacier Monitoring Service.

Haeberli, W., and H. Holzhauser, 2003: Alpine glacier mass changes during the past two millenia. *Pages News*, **11**, 13–15.

Harington, C. (Ed.), 1992: *The Year Without A Summer? World Climate in 1816*. Canadian Museum of Nature, Ottawa, 576 pp.

Hegerl, G., T. Crowley, S. Baum, K.Y. Kim, and W. Hyde, 2003: Detection of volcanic, solar and greenhouse gas signals in paleo-reconstructions of Northern Hemispheric temperature. *Geophysical Research Letters*, **30**, doi:10.1029/2002GL016635.

Herzog, J., and G. Müller-Westermeier, 1998: Homogenitätsprüfung und Homogenisierung klimatologischer Meßreihen im Deutschen Wetterdienst. Berichte des Deutschen Wetterdienstes 202, Selbstverlag des Deutschen Wetterdienstes, Offenbach am Main,Deutschland.

Hess, P., and H. Brezowsky, 1952: Katalog der Großwetterlagen Europas. Ber. Dt. Wetterd. in der US-Zone.

Hibler, W., 1979: A dynamic-thermodynamic sea-ice model. *Journal of Physical Oceanography*, **9**, 815–846.

Houghton, J., Y. Ding, D. Griggs, M. Noguer, P. van der Linden, X. Dai, K. Maskell, and C. Johnson (Eds.), 2001: *Intergovernmental Panel on Climate Change Third Assessment Report Climate Change 2001: The Scientific Basis*. Cambridge University Press.

Hurrell, J.W., 1995: Decadal trends in the North Atlantic Oscillation: Regional Temperatures and Precipitation. *Science*, **269**, 676–679.

HZRS, 1995: Klimatographija slovenije 1961–1990.

IPCC, 2001: *Climate Change 2001 - The Scientific Basis*, Chapter 10. Cambridge University Press.

Jenkinson, A., and F. Collison, 1977: An initial climatology of gales over the North Sea. Meteorological Office, Bracknell.

Jones, P., K. Briffa, T. Barnett, and S. Tett, 1998: High-resolution palaeoclimatic records for the last millennium: interpretation, integration and comparision with General Circulation Model control-run temperatures. *The Holocene*, **8**, 455–471.

Jones, P., M. Hulme, and K. Briffa, 1993: A comparison of Lamb circulation types with an objective classification scheme. *Int. J. Climatol.*, **113**, 655–663.

Kasser, P., 1993: Längenänderungen der Schweizer Gletscher 1782/83 bis 1990/91 geschätzt aufgrund der Sommertemperaturen und der Jahresniederschläge von Genf. In: *Aktuelle Aspekte in der Hydrologie (Currrent Issues in Hydrology)*, D. Grebner (Ed.), Volume 53 of *Züricher Geographische Schriften*, pp. 153–168. Verlag Geographisches Institut ETH Zürich.

Katušin, 1994: Meteorological stations network in Croatia. *Hrv. meteor. časopis (Croatian Meteorological Journal)*, **29**, 47–56.

Köppen, W., 1918: Klassifikation der Klimate nach Temperatur, Niederschlag und Jahresverlauf. *Peterm. Mitt.*, **64**, 193–203 und 243–248.

Kuhn, M., 1980: Die Reaktion der Schneegrenze auf Klimaschwankungen. *Zeitschrift für Gletscherkunde und Glacialgeologie*, **16**, 241–254.

Lamb, H., 1989: *Klima und Kulturgeschichte, Der Einfluß des Wetters auf den Gang der Geschichte*. rororo, Rowohlts Enzyklopädie, 449 pp.

Lamb, P., and R. Peppler, 1987: North Atlantic oscillation: Concept and an application. *Bull. Amer. Meteorol. Soc.*, **68**, 1218–1225.

Lauscher, F., 1980: Die Wärmeinsel des österreichischen Donauraumes zur Regierungszeit Kaiser Josephs II. *Annalen der Meteorologie (Neue Folge)*, **16**, 199–200.

Lauscher, F., 1986: Klimatologische Synoptik Österreichs mittels der ostalpinen Wetterlagenklassifikation. *Arbeiten aus der Zentralanstalt für Meteorologie und Geodynamik*, **302**, pp. 65.

Lean, J., and D. Rind, 1999: Evaluating sun-climate relationships since the Little Ice Age. *Journal of Atmospheric and Solar-Terrestrial Physics*, **61**, 25–36.

Legutke, S., and R. Voss, 1999: The Hamburg atmosphere-ocean coupled model ECHO-G. German Climate Computer Center (DKRZ).

Mann, M.E., R.S. Bradley, and M.K. Hughes, 1998: Global-scale temperature patterns and climate forcing over the past six centuries. *Nature*, **392**, 779–787.

Marsland, S., M. Latif, and S. Legutke, 2003: Antarctic circumpolar modes in a coupled ocean-atmosphere model. *Ocean Dynamics*, **53**, 323–331.

Matulla, C., 2005: Regional, seasonal and predictor-optimized downscaling to provide groups of local scale scenarios in the complex structured terrain of Austria. *Meteorol.Z.*, **14**, 33–47.

Matulla, C., E.K. Penlap, P. Haas, and H. Formayer, 2003: Multivariate techniques to analyse precipitation in Austria during the 20th century. *Int. J. Climatol.*, **23**, 1577–1588.

Matulla, C., and S. Wagner, 2004: SLP + relative Topography: ECHAM4 compared to ERA40 (German). COSREM 18. internal report, available from the Institute of Meteorology, University of Natural Resources and Applied Life Sciences, Vienna, Institute of Meteorology, Türkenschanzstr. 18, A-1180 Vienna, Austria.

Mercalli, L., C. Berro, S. Montuschi, C. Castellano, M. Ratti, G. DiNapoli, G. Mortara, and N. Guindani, 2003: Atlante climatic della Valle d'Aosta.

Moisselin, J., M. Schneider, C. Canellas, and O. Mestre, 2002: Changements climatiques en france au 20ème siècle. Étude des longues séries de données homogénéisées françaises de précipitations et températures. *La Météorologie*, **38**, 45–56.

Oerlemans, J., 2000: Holocene glacier fluctuations: is the current rate of retrate exceptional? *Annals of Glaciology*, **31**, 39–44.

Patzelt, G., 1970a: Die Längenmessungen an den Gletschern der österreichischen Ostalpen 1890–1969. *Zeitschrift für Gletscherkunde und Glacialgeologie*, **6**, 151–159.

Patzelt, G., 1970b: Die neuzeitlichen Gletscherschwankungen in der Venedigergruppe (Hohe Tauern, Ostalpen). *Zeitschrift für Gletscherkunde und Glacialgeologie*, **9**, 5–57.

Penlap, K.E., C. Matulla, H. von Stroch, and M.F. Kamga, 2004: Downscaling of GCM scenarios to assess possible changes of precipitation in Cameroon. *Clim. Res.*, **26**, 85–96.

Peterson, T.C., D.R. Easterling, T.R. Karl, P. Groisman, N. Nicollis, N. Plummer, S. Torok, I. Auer, R. Böhm, D. Gullett, L. Vincent, R. Heino, H. Tuomenvirta, O. Mestre, T. Szentimrey, J. Salinger, E.J. Førland, I. Hanssen-Bauer, H. Alexandersson, P. Jones, and D. Parker, 1998: Homogeneity adjustments of in situ atmospheric climate data: a review. *Int. J. Climatol.*, **18**, 1493–1517.

Preisendorfer, R.W., 1988: *Principal Component Analysis in Meteorology and Oceanography*. Seattle: Elsevier, 425pp.

Reynolds, R.W., and T.M. Smith, 1995: A high resolution global sea surface temperature climatology. *J. Climate*, **8**, 1571–1583.

Richman, M., 1986: Rotation of principal components. *International Journal of Climatology*, **6**, 239–235.

Robertson, A., J. Overpeck, D. Rind, E. Mosley-Thompson, G. Zielinski, J. Lean, D. Koch, J. Penner, I. Tegen, and R. Healy, 2001: Hypothesized climate forcing time series for the last 500 years. *Journal of Geophysical Research*, **106**, 14783–14803.

Robock, A., 2000: Volcanic eruptions and climate. *Reviews of Geophysics*, **38**, 191–219.

Robock, A., and M. Free, 1996: The volcanic records in ice cores for the past 2000 years. In: *Climatic variations and Forcing Mechanisms of the Last 2000 years*, pp. 533–546. Springer-Verlag.

Robock, A., and J. Mao, 1995: The volcanic signal in surface-temperature observations. *Journal of Climate*, **8**, 1086–1103.

Roeckner, E., J. Oberhuber, A. Bacher, M. Christoph, and I. Kirchner, 1996: ENSO varability and atmospheric response in a global coupled atmosphere-ocean GCM. *Climate Dyn.*, **12**, 737–745.

Schär, C., P. Vidale, D. Lüthi, C. Frei, C. Häberli, M. Liniger, and C. Appenzeller, 2004: The role of increasing temperature variability in european summer heat waves. *Nature*, **427**, 332–336.

Scheifinger, H., and R. Böhm, 2005: Spatial decorrelation and homogenisation of climate time series. *Int. J. Climatol.*. submitted.

Schöner, W., I. Auer, and R. Böhm, 2000: Climate variability and glacier reaction in the Austrian eastern Alps. *Annals of Glaciology*, **31**, 31–38.

Schönwiese, C.D., T. Staeger, and S. Trömel, 2004: The hot summer 2003 in germany. some preliminary results of a statistical time series analysis. *Meteorol.Z.*, **13**, 323–328.

Schüpp, 1985: Alpenwetterstatistik – Witterungskalender.

Schwarb, M., C. Daly, C. Frei, and C. Schär, 2001: *Hydrologischer Atlas der Schweiz*. Bundesamt für Landestopographie, Wabern - Bern.

Slupetzky, H., and N. Slupetykz, 1995: Betreff des Wachsthums der Kletscher und Kälterwedung des Klimas. Institut für Geographie der Universität Salzburg, Salzburg.

Szalai, S., 2004: Proceedings of the 4th seminar for homogenisation and quality control in climatological data bases. WCDMP 56, WMO-TD 1236, Budapest.

Szalai, S., and T. Szentimrey, 1999: Proceedings of the second seminar for homogenisation of surface climatological data. WCDMP 41, WMO-TD 962, Budapest. WMO, Geneva.

Szolgála), H.M.S.O.M., 1996: Proc. of the First Seminar for Homogenisation of Surface Climatological Data. Budapest, Hungary.

Tahvonen, O., H. von Storch, and J. von Storch, 1994: Economic efficiency of CO_2 reduction programs. *Climate Research*, **4**, 127–141.

Terray, L., S. Valcke, and A. Piacentini, 1998: The oasis coupler user guide. Version 2.2. CERFAS.

Ungersböck, M., I. Auer, and R. Böhm, 2002: First results of project CLIVALP–CLimate Variability studies in the ALPine region. In: *4th Conference on Applied Climatology, ECAC-2002*, Abstract Volume, Brussles.

Ungersböck, M., A. Orlik, and A. Jurkovič, 2003: HISTALP – eine Datenbank zur kombinierten Erfassung von historischen Klimazeitreihen und deren Metadaten. In: *6. Deutsche Klimatagung Klimavariabilität*, J. F. W. Negendank (Ed.), Volume 6 of *Terra Nostra*, pp. 450–452. Alfred-Wegener-Stiftung.

Uppala, S., 2003: ECMWF ReAnalysis 1957–2001, ERA-40. *Proceedings of the Workshop on Reanalysis 5–9 Nov. 2001*, ECMWF. 1–10.

Vasold, M., 2004: Die Eruptionen des Laki von 1783/84 – Ein Beitrag zur deutschen Klimageschichte. *Naturwissenschaftliche Rundschau*.

von Storch, H., 1995: Inconsistencies at the interface of climate impact studies and global climate research. *Meteorol. Z., N.F.*, **4**, 72–80.

von Storch, H., and G. Hannoschöck, 1985: Statistical aspects of estimated principal vectors (EOFs) based on small sample sizes. *J. Clim. Appl. Meteor*, **24**, 716–724.

von Storch, H., E. Zorita, and U. Cubasch, 1993: Downscaling of global climate change estimates to regional scales: An application to Iberian rainfall in wintertime. *J. Climate*, **6**, 1161–1171.

von Storch, H., E. Zorita, J. Jones, Y. Dimitriev, F. González-Rouco, and S. Tett, 2004: Reconstructing past climate from noisy data. *Science*, **306**, 679–682.

von Storch, H., and F. Zwiers, 1999: *Statistical Analysis in Climate Research*. Cambridge University Press, 528 pp.

Wagenbach, D., R. Böhm, H. Cachier, W. Haeberli, M. Hoelzle, M. Legrand, V. Maggi, , and T. Stocker, 1998: Environmental and climate records from high elevation alpine glaciers (ALPCLIM). In: *Proceed. of ECSC*. European Commission's Science Conference. CD-Rom.

Wagner, S., 2004: *The role of different forcings on the historical climate variability, with special consideration of the Dalton Minimum (1790–1830): A model study*. Phd-Thesis, available as GKSS report 2004/13, University of Hamburg, Germany.

Wallace, J., and D. Gutzler, 1981: Teleconnections in the geopotential height field during the Northern Hemisphere winter. *Mon. Wea. Rev.*, **109**, 784–812.

Widmann, M.L., 1996: *Mesoscale variability and long-term trends of Alpine precipitation and their relation to the synoptic-scale flow*. Ph. D. thesis, ETH Zürich.

Wolff, J., E. Maier-Reimer, and S. Legutke, 1997: The Hamburg Primitive Equation Model HOPE. German Climate Computer Center (DKRZ).

Woth, K., 2001: Abschätzung einer zukünftigen Niederschlagsentwicklung mit statistischen Methoden unter Einbezug räumlicher Differenzierungsverfahren am Beispiel des südwesteuropäischen Raums. Master's thesis, GKSS-Report 2001/28 - University of Trier, 101 pp.

Zorita, E., H. von Storch, J. González-Rouco, U. Cubach, J. Luterbacher, S. Legutke, I. Fischer-Bruns, and U. Schlese, 2004: Transient simulation of the climate of the last five centuries with an atmosphere-ocean coupled model: Late Maunder Minimum and the Little Ice Age. *Meteorol.Z.*, **13**, 271–289.

Zumbühl, H., 1980: *Die Schwankungen der Grindelwaldgletscher in den historischen Bild- und Schriftquellen des 12. bis 19. Jahrhunderts*, Volume 92 of *Denkschriften der Schweizerischen Naturforschenden Gesellschaft*. Verlag Birkhäuser, Basel, Boston, Stuttgard, 1–279 pp.

Acknowledgements

This study and the creation of the HISTALP database were conducted within the research project CLIVALP – Climate Variability Studies in the Alpine Region (P16076-N06), funded by the FWF (Austrian Science Fund). Homogenized air temperature and precipitation were provided by the EU-project ALP-IMP (EVK2-CT-2002-00148).

Professor Hans von Storch has enabled and raised this cooperation. Sincere thanks are given to him.

We want to address special thanks to Dr. H. Kuhn (system-administrator at the GKSS) who helped to overcome serious problems concerning computational facilities. Roland Potzman was in charge of computational facilities at ZAMG.

Many thanks go to Dr. J.F. Gonzales-Rouco who provided a compiled ECHO-G version and helped a lot to keep the model running.

We are thankful to Sophie Debit and Beate Gardeike for skillfully preparing Figures and to H. Matulla for critically commented on the manuscript.

CM wants to thank his beloved wife Ewa for her moral support and for Johannes and Patrick (see Figure A.11). Without her patience and encouragement many things would not have happened.

Figure A.11: Johannes K. Matulla together with Patrick L. Matulla in paschal mood.